NASA/TM–20210017474

A Summary of ATD Results from a Full-Scale F28 Crash Test

Justin D. Littell, Jacob B. Putnam
Langley Research Center, Hampton, Virginia

June 2021

NASA STI Program Report Series

Since its founding, NASA has been dedicated to the advancement of aeronautics and space science. The NASA scientific and technical information (STI) program plays a key part in helping NASA maintain this important role.

The NASA STI program operates under the auspices of the Agency Chief Information Officer. It collects, organizes, provides for archiving, and disseminates NASA's STI. The NASA STI program provides access to the NTRS Registered and its public interface, the NASA Technical Reports Server, thus providing one of the largest collections of aeronautical and space science STI in the world. Results are published in both non-NASA channels and by NASA in the NASA STI Report Series, which includes the following report types:

- TECHNICAL PUBLICATION. Reports of completed research or a major significant phase of research that present the results of NASA Programs and include extensive data or theoretical analysis. Includes compilations of significant scientific and technical data and information deemed to be of continuing reference value. NASA counterpart of peer-reviewed formal professional papers but has less stringent limitations on manuscript length and extent of graphic presentations.

- TECHNICAL MEMORANDUM. Scientific and technical findings that are preliminary or of specialized interest, e.g., quick release reports, working papers, and bibliographies that contain minimal annotation. Does not contain extensive analysis.

- CONTRACTOR REPORT. Scientific and technical findings by NASA-sponsored contractors and grantees.

- CONFERENCE PUBLICATION. Collected papers from scientific and technical conferences, symposia, seminars, or other meetings sponsored or co-sponsored by NASA.

- SPECIAL PUBLICATION. Scientific, technical, or historical information from NASA programs, projects, and missions, often concerned with subjects having substantial public interest.

- TECHNICAL TRANSLATION. English-language translations of foreign scientific and technical material pertinent to NASA's mission.

Specialized services also include organizing and publishing research results, distributing specialized research announcements and feeds, providing information desk and personal search support, and enabling data exchange services.

For more information about the NASA STI program, see the following:

- Access the NASA STI program home page at http://www.sti.nasa.gov

- Help desk contact information:

https://www.sti.nasa.gov/sti-contact-form/
and select the "General" help request type.

NASA/TM–20210017474

A Summary of ATD Results from a Full-Scale F28 Crash Test

Justin D. Littell, Jacob B. Putnam
Langley Research Center, Hampton, Virginia

National Aeronautics and
Space Administration

Langley Research Center
Hampton, Virginia 23681-2199

June 2021

Available from:

NASA STI Program / Mail Stop 148
NASA Langley Research Center
Hampton, VA 23681-2199
Fax: 757-864-6500

Table of Contents

List of Figures v
List of Tables vii
Abstract viii
Introduction 1
Aircraft Buildup and Layout 2
Seating Configuration 3
ATD Layout 8
ATD Instrumentation 22
Airframe Result Summary 23
ATD Result Summary – 50th Percentile ATDs 26
ATD 1 – Pilot 27
ATD 3 – Seat 6A 29
ATD 4 – Plinth Seat 1B 31
ATD 5 – Seat 12A 32
ATD 6 – Seat 10C 33
ATD 8 – Plinth Seat 1A 36
ATD 13 – Seat 6D 38
ATD 14 – Seat 3D 41
ATD 18 – Seat 9D 44
ATD 20 – Seat 6B 46
ATD 23 – Seat 3A 49
ATD Results – Other Adult ATDs 51
ATD 10 – Seat 5B 52
ATD 11 – Seat 5A 56
ATD 16 – Seat 8B 60
ATD 22 – Seat 3E 62
ATD Results – Child ATDs 66
ATD 9 – Seat 9B 66
ATD 12 – Seat 4E 67
ATD 15 – Seat 10E 68
ATD 17 – Seat 5E 69
ATD 19 – Seat 10D 71
ATD 24 – Seat 9A 74
ATD 25 – Seat 4D 75

ATD Results – Comparative Analyses 77
Lumbar Load Response vs. Cabin Location 77
Lumbar Load Response vs. Seat Location 78
Head Injury Criteria (HIC) Response vs. Cabin Location 79
Lap Belt Load vs. Cabin Location 80
Braced Position vs. Non-Braced Position 81
Hybrid III 5th vs. Hybrid III 95th 82
THOR vs. Hybrid II 84
CARES Restraint vs. Standard Lap belt 86
Hybrid III 10 YO vs. LODC 10 YO 88
Post-Test ATD Position 91
Conclusion 92
References 94

List of Figures

Figure 1. Landing and Impact Research Facility (LandIR) 2
Figure 2. Fokker F28 Tail # C-GCRN taxi into LaRC (2001) 3
Figure 3. Original F28 seating configuration from the F28 Weight and Balance Manual. Reprinted from [12] 4
Figure 4. Installed seat configuration 5
Figure 5. Plinth seat configuration 6
Figure 6. Seat rows with underfloor structure identified 6
Figure 7. Forward section subfloor structure. Cavity prior to luggage foam install (left) and luggage foam (right) 7
Figure 8. Wingbox stiffened structure 7
Figure 9. Aft fuselage structure 8
Figure 10. Hybrid II ATD (left) and Hybrid III ATD (right) 9
Figure 11. Non-standard size ATDs. 95th percentile, background, and 5th percentile, foreground 10
Figure 12. Hybrid II 50th percentile, foreground, and THOR-K, background 11
Figure 13. Obese ATD seated in Seat 8B 12
Figure 14. ARL WIAMan, foreground, and FAA HIII, background 13
Figure 15. ATD 17, Q-1 with CARES configuration 14
Figure 16. ATD 25 configuration 15
Figure 17. LODC ATD, foreground, and Hybrid III 10 YO, background 16
Figure 18. ATD layout 17
Figure 19. Lap belt load cell locations 18
Figure 20. ATD starboard side layout 19
Figure 21. ATD port side layout 20
Figure 22. Laser scan of starboard side ATDs 20
Figure 23. Laser scan of port side ATDs 21
Figure 24. Laser scan detail of ATD 7 and 3 21
Figure 25. ATD (left) and Aircraft (right) coordinate system reference 23
Figure 26. Impact motion sequence 24
Figure 27. Cabin port side accelerations 25
Figure 28. Starboard side accelerations 26
Figure 29. 50th percentile ATD locations 27
Figure 30. ATD 1 28
Figure 31. ATD 1 Accelerations 29
Figure 32. ATD 1 Lumbar loads and moment 29
Figure 33. ATD 3 Image sequence 30
Figure 34. ATD 3 Accelerations 31
Figure 35. ATD 3 Lumbar load and moments 31
Figure 36. ATD 5 Image sequence 32
Figure 37. ATD 5 Accelerations 33
Figure 38. ATD 5 Lumbar loads and moment 33
Figure 39. ATD 6 Accelerations 34
Figure 40. ATD 6 Head rotation rates 34
Figure 41. ATD 6 Upper neck loads and moment 35
Figure 42. ATD 6 Lumbar loads and moment 35
Figure 43. ATD 6 Belt load 36
Figure 44. ATD 8 Accelerations 37
Figure 45. ATD 8 Lumbar loads and moment 37
Figure 46. ATD 8 Belt load 38

Figure 47. ATD 13 Image sequence 39
Figure 48. ATD 13 Accelerations 39
Figure 49. ATD 13 Head rotations 40
Figure 50. ATD 13 Upper neck loads and moment 40
Figure 51. ATD 13 Lumbar loads and moment 41
Figure 52. ATD 13 Belt load 41
Figure 53. ATD 14 Image sequence 42
Figure 54. ATD 14 Accelerations 43
Figure 55. ATD 14 Lumbar loads and moment 43
Figure 56. ATD 14 Belt loads 44
Figure 57. ATD 18 Image sequence 45
Figure 58. ATD 18 Accelerations 46
Figure 59. ATD 18 Lumbar loads and moment 46
Figure 60. ATD 20 Image sequence 47
Figure 61. ATD 20 Accelerations 48
Figure 62. ATD 20 Lumbar loads and moment 48
Figure 63. ATD 20 Belt load 49
Figure 64. ATD 23 Accelerations 49
Figure 65. ATD 23 Head rotations 50
Figure 66. ATD 23 Upper neck loads and moment 50
Figure 67. ATD 23 Lumbar loads and moment 51
Figure 68. Non-standard sized and type ATD locations 51
Figure 69. ATD 10 Image sequence 53
Figure 70. ATD 10 Accelerations 54
Figure 71. ATD 10 Head rotation rate 54
Figure 72. ATD 10 Upper neck loads and moment 55
Figure 73. ATD 10 Lumbar loads and moment 56
Figure 74. ATD 10 Belt load 56
Figure 75. ATD 11 Image sequence 57
Figure 76. ATD 11 Accelerations 58
Figure 77. ATD 11 Head rotation 58
Figure 78. ATD 11 Upper neck loads and moments 59
Figure 79. ATD 11 Lumbar loads and moments 59
Figure 80. ATD 11 Belt load 60
Figure 81. ATD 16 Accelerations 60
Figure 82. ATD 16 Belt loads 61
Figure 83. ATD 16 Post-test position (left), and pelvic to femur joint separation (right) 62
Figure 84. ATD 22 Image sequence 63
Figure 85. ATD 22 Accelerations 64
Figure 86. ATD 22 Head rotation rate 64
Figure 87. ATD 22 Neck loads and moments 65
Figure 88. ATD 22 Lumbar loads and moment 65
Figure 89. Child ATD locations 66
Figure 90. ATD 9 Accelerations 67
Figure 91. ATD 9 Belt loads 67
Figure 92. ATD 15 Accelerations 68
Figure 93. ATD 15 Upper neck load and moment 69
Figure 94. ATD 15 Lumbar load and moment 69
Figure 95. ATD 17 Accelerations 70
Figure 96. ATD 17 Upper neck loads and moments 70
Figure 97. ATD 17 belt loads 71

Figure 98. ATD 19 Accelerations 72
Figure 99. ATD 19 Neck loads and moments 72
Figure 100. ATD 19 Rotations 73
Figure 101. ATD 19 Pressures 73
Figure 102. ATD 24 Accelerations 74
Figure 103. ATD 24 Upper neck loads and moment 75
Figure 104. ATD 24 Belt load 75
Figure 105. ATD 25 belt load 76
Figure 106. ATD 25 configuration at load cell loss of signal 77
Figure 107. Lumbar load as a function of row position 78
Figure 108. Lumbar load as a function of seat location 79
Figure 109. HIC36 as a function of row position 80
Figure 110. Belt load as a function of row position 80
Figure 111. Head kinematic response – Upright vs. Braced position 81
Figure 112. Lumbar response – Upright vs. Braced position 82
Figure 113. Head kinematic response – 95th vs. 5th 82
Figure 114. Upper neck response – 95th vs. 5th 83
Figure 115. Lumbar response – 95th vs. 5th 84
Figure 116. Head kinematic response – Hybrid II vs. THOR 84
Figure 117. Chest kinematic response – Hybrid II vs. THOR 85
Figure 118. Lumbar response – Hybrid II vs. THOR 86
Figure 119. ATD 9 to 24 Head horizontal acceleration comparison 87
Figure 120. ATD 9 to 24 Head Vertical Acceleration Comparison 87
Figure 121. ATD 9 to ATD 24 Lap belt load comparisons 88
Figure 122. ATD 19 and ATD 15 Image sequence 89
Figure 123. Head kinematic response – Hybrid III 10 YO vs. LODC 10 YO 90
Figure 124. Pelvis kinematic response – Hybrid III 10YO vs. LODC 10 YO 90
Figure 125. Upper neck response – Hybrid III 10YO vs. LODC 10 YO 91
Figure 126. Post-test interior laser scan – Starboard side: Row 1–6 (Top) & 8–12 (Bottom) 91
Figure 127. Post-test interior laser scan – Port side: Row 1–6 (Top) & 9–10 (Bottom) 92

List of Tables

Table 1 - ATD layout 17
Table 2 – Measured Impact Conditions 23
Table 3 – Major post-impact events 25
Table 4 – 50th Percentile ATD locations 27
Table 5 - Non-standard sized and type ATDs 51
Table 6 – Child ATD locations 66

Abstract

On June 20, 2019, a full-scale crash test was conducted on a Fokker F28 aircraft as a part of a joint National Aeronautics and Space Administration (NASA) / Federal Aviation Administration (FAA) effort to investigate crashworthiness of transport category aircraft, as defined by 14 Code of Federal Regulations, Part 25. This aircraft was tested at NASA Langley Research Center's Landing and Impact Research Facility in a combined horizontal and vertical impact condition. The aircraft contained 24 Anthropomorphic Test Devices (ATDs, a.k.a. crash test dummies) of various types, sizes, and builds instrumented to collect data on occupant response and injury prediction under controlled aircraft (simulated) crash conditions. The ATDs were provided by four government agencies including NASA, FAA, the National Highway Transportation Safety Administration (NHTSA), and the Army Research Laboratory (ARL), and one commercial manufacturer, Humanetics.

The majority of the ATDs were seated within twelve rows of seats in the main cabin which were arranged in a triple/double configuration, with triple place seats configured on the starboard side of the cabin and the double place seats configured on the port side. The layout of the cabin contained three distinct regions: the Cargo Hold, the Wingbox, and the Aft Fuselage, which are delineated due to differences in their subfloor structure. Due to the deterioration of the original seats in the aircraft, the seats used in the test were removed from an in-service aircraft and modified to match the F28 seat track spacing and configuration. A single ATD was seated in the cockpit in order to measure cockpit loads and was seated in the original pilot's chair.

The aircraft impacted a soil surface with 65.3 ft/s horizontal and 31.8 ft/s vertical velocities and with slight roll and yaw. Aircraft accelerations ranged between 12 and 16 g in the vertical direction to approximately 10 g in the horizontal directions, with peak values achieving 25 g in some locations. After the initial impact, the aircraft plowed through the soil, sliding a total distance of 32.5 ft, and experienced a secondary "slap down" impact almost 1 second after initial ground contact. The entirety of the impact event lasted 1.62 s.

The majority of the ATDs typically used in certifications demonstrated lumbar loads higher than the limits defined for certification, indicating potential for lumbar spine injury. No correlation between location within the cabin and injury risk was identified since ATDs seated in all three regions of the cabin experienced similar results. When in a seat with a forward seatback, all adult ATDs were shown to experience head strike with that seatback. Additionally, the loads measured in the ATDs were higher than those of similarly conducted vertical drop tests of F28 hardware. A full set of ATD results will be presented along with some comparisons made between seated location, seated position, ATD type, and ATD size. There will also be discussions on the various child and non-standard ATDs that were included in the test.

Introduction

Transport category aircraft (TCA), as defined by 14 Code of Federal Regulations (CFR) Part 25, have been utilized to transport people around the world for almost 100 years. These aircraft, which were first developed in the early 1900s, have evolved into high-tech ultra-efficient airplanes that are now using advanced materials such as composites for their construction.

Through a collaborative research effort between the National Aeronautics and Space Administration (NASA) and the Federal Aviation Administration (FAA), a series of tests was conducted for the investigation of TCA crashworthiness. TCA crashworthiness originated with an FAA Aviation Rulemaking Advisory Committee (ARAC) formed to evaluate crashworthiness characteristics of TCA [1]. A partial recommendation from the resultant ARAC document [2] proposes conducting a vertical drop test of a partial airframe section in order to investigate items such as occupant injury, egress characteristics, and overhead mass stability. In order to provide data to the ARAC committee, a series of tests using Fokker F28 hardware, which is currently located at NASA Langley Research Center (LaRC), was utilized. The test series consisted of two F28 partial fuselage sections (commonly called "barrels") and a full-scale retired F28 Mark 1000 aircraft.

The first of the tests was of the Forward Section, which was tested in a pure vertical impact condition onto soft soil in March 2017. The second of the barrel tests was of the Wingbox Section which was tested under a pure vertical drop; however, the orientation of the section was a pitched down condition and the soil surface was sloped forward in an attempt to introduce a forward velocity component resulting from the rotation of the section at impact. A full summary of airframe results from both sections can be found in [3].

The third test in the test series was a full-scale impact test. One of the reasons for conducting the full-scale test was to capture the deformation of the seats and ATDs as a result of the added forward motion which would not be present in a pure vertical test. Presumably, results such as ATD head flail, seat disengagement, and other types of results that are not seen in a pure vertical test that would be present in a full-scale test would allow for investigations into the effect and comparisons to a pure vertical test.

There have been two notable full-scale impact tests occurring on actual flying aircraft. The first, which was a joint NASA/FAA effort, was conducted on a Boeing 720 aircraft in 1984, and was known as the Controlled Impact Demonstration [4]. The main objective of this test was to study a fuel additive known as anti-misting kerosene (AMK) and its effect on fuel fire suppression during a crash. A second objective of the test, which was led by a team at NASA LaRC, was to evaluate the survivability for a handful of onboard ATDs [5]. The second test was more recent and occurred in 2012 on a Boeing 727-200 [6]. Conducted for the Discovery channel show *Curiosity*, the airplane was intentionally crashed for investigation on airframe loads and occupant survivability.

As a part of the current certification efforts for TCA, a set of two dynamic tests is required for the seats in order to assess occupant injury [7]. The tests utilize seats mounted onto horizontal sleds which then provide an impact pulse into the seat. Standardized ATD injury metrics are used to determine whether the seat will provide adequate protection for an occupant, which are thereby considered certified. There is almost no data, outside of actual mishap events, which show the performance of a seat and restraint system under realistic crash conditions. This gap is due to a number of factors, but foremost is the time, cost, and ability to conduct full-scale crash tests of TCA under realistic crash conditions which include a forward velocity component.

Fortunately, the Landing and Impact Research (LandIR) facility at LaRC provides the opportunity to study full-scale aircraft crash tests under controlled conditions. LandIR provides the capability of lifting and pendulum-swinging full-scale aircraft up to 64,000 lb in weight. The LandIR facility is shown in figure 1.

Figure 1. Landing and Impact Research Facility (LandIR)

This report will present the data obtained from the onboard occupants of a full-scale Fokker F28 TCA crash test which was conducted at NASA LaRC in 2019. Partial sets of test and computational analyses results have been published in [8], [9], and [10], and additionally, the complete test buildup details and airframe results are discussed in detail in [11]. It is the intent of this report to provide a complete summary of all of the ATD test data which was obtained from the crash test along with comparative analyses of the various ATD sizes, types, and locations in order to provide a complete picture of the occupant loading environment.

Aircraft Buildup and Layout

A brief summary of test buildup is provided in this section for completeness. The test article was a Fokker F28 Mark 1000, tail number C-GCRN, purchased by NASA in 2000. Figure 2 shows the aircraft as it taxied into LaRC in 2001 after landing at Joint Base Langley-Eustis (LFI). The aircraft was then placed into outside storage until the test campaign began in late 2018.

Figure 2. Fokker F28 Tail # C-GCRN taxi into LaRC (2001)

In placing the aircraft into outside storage, the engines, fluids, majority of the avionics, and some fairings were removed. During the buildup for test campaign, partial ballast was reinstalled in the engine areas in order to shift the aircraft center of gravity (CG) into realistic limits; however, many of the other components were not reinstalled to save on weight. In the cabin, the aircraft did not include hat rack hardware, and all of the plastic interior moldings were removed. In addition, the items in the galley, lavatory, and rear crew areas were also removed.

The aircraft build-up included installing the necessary lifting hardware at the wingbox attachment locations in order to lift and swing the aircraft for the test. Underfloor luggage in the Cargo Hold section was simulated using several layers of foam of varying density. Hat rack hardware and ballast was simulated through the mounting of aluminum c-channels and brackets and then attaching ballast lead into the c-channel. Finally, a new set of seats was installed in order to accommodate the ATD experiments. The original floors were used, as they remained in the aircraft during storage.

The weight and balance of the test article provided a test weight of 33,306 lb, with a CG at aircraft station (ST) 11553.8, centered along the lateral axis, and at waterline (WL) –80. This weight was below the take-off weight of the F28. However, the CG was within realistic limits according to the F28 Weight and Balance Manual [12].

Seating Configuration

The original seats were removed due to their deteriorated condition from being stored in outside storage. In their place, a set of triple seats that have been 14 CFR §25.562 certified were used. These seats were removed from an in-service Boeing 737 aircraft and modified to interface into the F28 aircraft for the full-scale test. The original seat leg configuration positioned the two seat legs underneath the junction between the middle and window seat for the outboard leg, and between the middle and aisle seats for the inboard seat legs. Reconfiguring these tests essentially shifted both seat legs outboard, creating a cantilevered

overhung seat in the starboard aisle seat location. Additionally, since the seat configuration for the F28 was a triple-double configuration, the new triple seats located on the port side of the aircraft were made into a double place seats by removing the original window seat and then shifting the seat legs inboard, thus making the original middle seat the new window seat, and the legs mimicking the starboard window and middle seat. This procedure was identical to that completed during the F28 vertical barrel drop tests and allowed for direct comparisons between the vertical and full-scale tests. The seat pitch was set at 32 inches between seats, primarily to allow for the ease of ATD install. The cabin of the aircraft was capable of holding 65 passengers, which amounted to 13 rows of 3+2 seating for each row. However, with the necessity of adding large amounts of instrumentation, cabling and sensors, not all seat rows were installed. Figure 3 shows the F28 seating configuration, reprinted from the Fokker F28 Weight and Balance Manual [12], with notable dimensions included. The modifications to the B737 seats gave an actual aisle width of 16.5 inches, and not the 17 inches as called out in the manual. All other modifications to the seats were as close to the original F28 configuration as possible. Figure 4 shows the actual F28 cabin with seats installed, starting at Row 2.

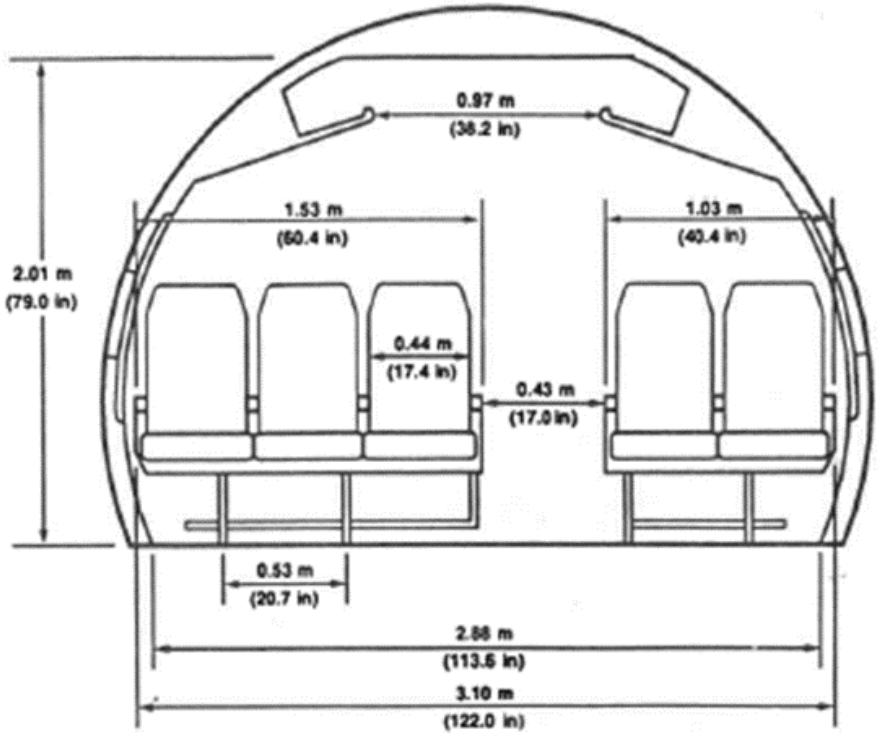

Figure 3. Original F28 seating configuration from the F28 Weight and Balance Manual. Reprinted from [12]

Figure 4. Installed seat configuration

A “plinth seat” configuration was utilized in starboard Row 1. The plinth seat configuration consisted of an aluminum plate mounted on six load cells which interfaced with the starboard seat tracks with three on the inboard seat track locations and three on the outboard seat track locations. An additional seat track utilizing the same F28 spacing was fixed to the top of the plate which provided a way to install a double place seat on top of the plate. However, the seat tracks were shifted to be centered on the plate, shifting the double place seat to match more of a port side configuration. The subsequent illustrations show the plinth seat positioned in this centered position. The purpose of the plinth seat was to examine the interface loads between the seat base and the seat track, and the inclusion of the plate and load cells raised the seats approximately 4 inches above the cabin floor. The plinth seat is not pictured in figure 4, which starts at Row 2, but is shown in figure 5.

Figure 5. Plinth seat configuration

In both sides of the aircraft Row 13 was left vacant to allow for test personnel to move equipment and other items within the cabin. On the starboard side, Row 7 was removed to allow for the full range of motion to be gained from the oversized "Obese" ATD seated in Row 8. On the port side, Rows 1, 7, and 11 were removed to allow for the install of all of the data acquisition system (DAS) racks, Row 8 was removed to allow for the install of all of the onboard camera controllers, and Row 12 was removed to allow the umbilical cable bundles to be assembled before exiting the aircraft. The configuration of the seat rows, without ATD labels, and with aircraft underfloor structure defined is shown in figure 6.

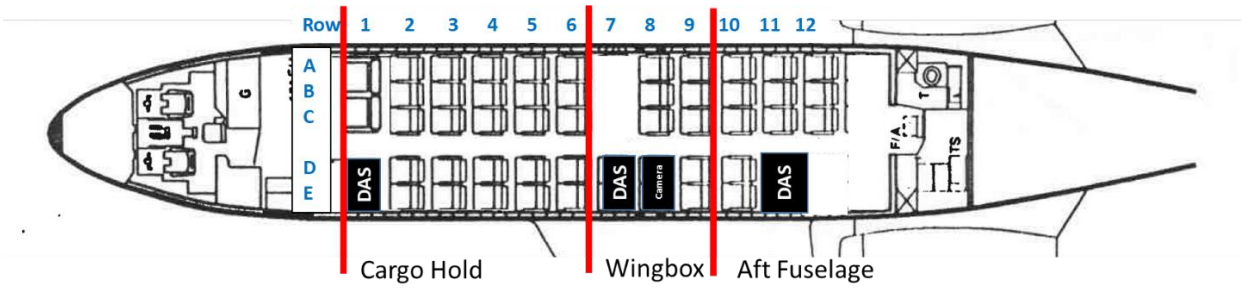

Figure 6. Seat rows with underfloor structure identified

As figure 6 shows, the first six rows of the aircraft were located in the Cargo Hold portion of the cabin, which has a hollow cavity in the subfloor and is where the luggage was stowed. As previously mentioned, this hollow cavity was filled with layers of foam to simulate a full luggage load, and the only aircraft structure capable of providing support besides the luggage foam was stanchions going between the seat track and the bottom frames. Figure 7 shows the empty Cargo Hold (left) and the foam luggage simulant (right).

Figure 7. Forward section subfloor structure. Cavity prior to luggage foam install (left) and luggage foam (right)

The Wingbox section was located beneath Rows 7–9. Unfortunately, due to the circumstances of the test, there were only two rows on the starboard side and one on the port side available for ATD placement. The wingbox itself had a stiffened truss structure in the subfloor region to distribute the wing loads from the aircraft during flight. It was the stiffest part of the aircraft due to these features. Figure 8 shows the internal wingbox truss stiffeners.

Figure 8. Wingbox stiffened structure

The Aft Fuselage section near the rear of the cabin ran between the aft portion of the wingbox and the rear pressure bulkhead, which encompassed Rows 10–12. This area contained critical aircraft systems, along with two keel beams and a cavity for the landing gears to retract. It was the only area of the aircraft structure which contained the two keel beams which made it structurally different than the other two sections. Figure 9 shows an internal view of the Aft Fuselage structure, noting that the prominent feature is the vertical keel beam, and the void in the foreground is the landing gear compartment.

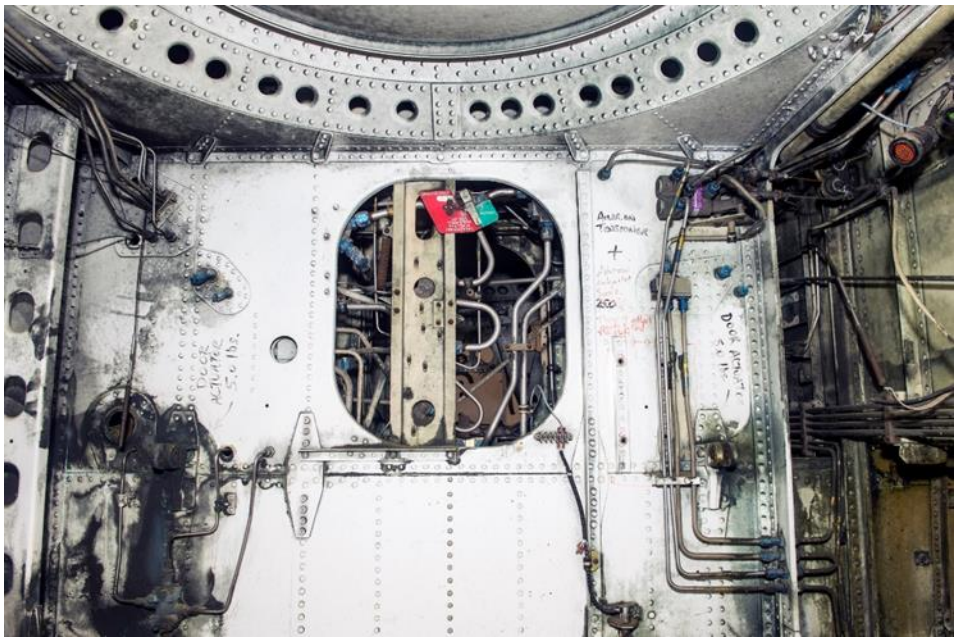

Figure 9. Aft fuselage structure

ATD Layout

With the exception of the pilot location, all ATDs were seated in the cabin section of the aircraft. There were 12 rows of seats installed, which gave a total of 60 possible seats; however, with the various rows removed for either test or other logistical reasons, a total of 47 possible locations for ATD install remained. Twenty-three of the 47 locations were used and with a pilot ATD in the cockpit gave a total of 24 ATDs ultimately used for the test.

Four government agencies provided ATDs for the test including NASA, the FAA, the National Highway Traffic Safety Administration (NHTSA), and the Army Research Laboratory (ARL), along with one commercial manufacturer, Humanetics. This section describes each ATD and its location on the aircraft. Each ATD was labeled as an experiment number for identification, and numbers ranged from 1 to 25 (ATD 7 was removed). The ATD number will be the main identifier in this report, and the label definitions will be defined in table 1. However, a general overview of each of the ATD types, sizes, and features is described herein.

There were 11 standard sized 50th percentile ATDs which are currently used in the certification regulations [7] capable of providing injury data for evaluation directly. These consisted of Hybrid II (HII) and FAA Hybrid III (FAA HIII) ATDs. The FAA HIII is a standard Hybrid III with the lumbar spine component retrofitted from a HII. The HII lumbar spine component is straight opposed to the curved spine of a standard Hybrid III. The straight spine is retrofitted within the FAA HIII in order to accurately capture the posture of a seated occupant for aerospace applications. Though the lumbar spine components are identical between ATDs, there are additional differences between the HII and FAA HIII ATDs which are noted in Pellettiere et al. [13]. A significant difference between these two ATDs is in the components which compose the ATD neck. The FAA HIII contains segmented rubber discs designed to provide improved neck biofidelity. In contrast, the HII ATD neck is a single molded rubber piece which produces a stiffer neck response. The differences in the neck components is one of the comparisons made between different ATDs.
Additionally, the FAA HIII ATDs contained sensors that the HII did not. All HII and FAA HIII ATDs contained accelerometers in the head, chest, and pelvis, along with lumbar load 3-axis load cells measuring force and moments in the horizontal and vertical directions. However, the HIII instrumentation also

included an upper neck load cell and rotational rate sensors in the head. Figure 10 shows examples of the HII and FAA HIII ATDs used in the test.

Figure 10. Hybrid II ATD (left) and Hybrid III ATD (right)

In addition to the standard-sized Hybrid III ATDs, there were two non-standard sized Hybrid III ATDs included in the test which were used to identify the effect of anthropometric size on occupant response. The two non-standard sized ATDs were a 5th percentile female and a 95th percentile male. The 5th percentile female was seated in Seat 5B, while the 95th percentile male was seated in Seat 5A. This configuration mimicked the configuration used on the vertical section drop tests, and therefore measurements obtained can be directly compared to those vertical drop test measurements. Figure 11 shows the non-standard sized 95th and 5th percentile ATDs.

Figure 11. Non-standard size ATDs. 95th percentile, background, and 5th percentile, foreground

A THOR-K [14] was recently developed for automotive certification applications, and utilized in the test to evaluate its performance under aerospace loading. The THOR ATD is grouped as one of the advanced, non-standard ATDs used on the test, which encompassed adult-sized ATDs not in the HII or HIII families. These ATDs contain higher biofidelic components and advanced sensor suites. The THOR ATD, while designed to be a primarily frontal impact ATD, has been used in previous NASA testing in both the vertical [15] and horizontal directions [16] for the evaluation of injury prediction use in NASA applications. The THOR was instrumented with head, chest, and pelvic accelerometers, along load cells in the upper and lower neck and lumbar spine. It was seated in seat 3E and positioned in the neutral position. This ATD was positioned next to a standard HII ATD so that comparisons between the two ATDs could be made. Figure 12 shows the THOR ATD in the background, with a standard HII 50th percentile ATD in the foreground.

Figure 12. Hybrid II 50th percentile, foreground, and THOR-K, background

The Obese ATD [17] was the second advanced ATD added to the test and was included in the test as an experiment to gather information on occupant responses from larger sized adults. The Obese ATD was a concept prototype provided by Humanetics and does not represent their current design. This ATD was based on the THOR platform and targeted a Body Mass Index (BMI) of 35 kg/m^2, which categorizes this ATD as Obese. Material was added to the chest jacket to simulate increased superficial tissue and abdominal fat, which put the ATD total weight at 273 lb. This ATD was seated in Seat 8B which was behind an empty Row 7 and chosen in part due to the accessibility of the seat, but also to limit the interaction between this ATD and other experiments should the ATD or seat adversely move during the impact. The distance between the front of the face to the rear seat back in Row 6 was 52 inches which allowed for this ATD to experience 52 inches of motion before contact with the seat would occur. Since it was experimental, this ATD only contained sensors to measure head, chest, and pelvic accelerations. The data collected from the ATD will be forreference use only. Figure 13 shows a picture of the Obese ATD seated in Seat 8B.

Figure 13. Obese ATD seated in Seat 8B

Two Warrior Injury Assessment Manikins (WIAMan) [18] were operated by ARL and provided a third type of advanced ATD in the test. The two WIAMan ATDs were spaced such that one was near the front of the cabin and one was near the rear to allow for positional comparisons. The WIAMan ATDs were in the 50th percentile range; however, they did not anthropometrically match up to a standard HIII 50th percentile ATD. The WIAMan ATD data acquisition systems were self contained and seated next to FAA HIII ATDs in each location. The WIAMan response and its comparisons to the standard Hybrid ATD data will be the subject of a separate report. The WIAMan is shown in the foreground of figure 14.

Figure 14. ARL WIAMan, foreground, and FAA HIII, background

There were seven child ATDs utilized for the test. These ATDs ranged between a Quarter 1 (Q-1) infant to a 10 year old (10 YO) sized child. The Q-1 infant, labeled ATD 17, was seated in Seat 5E, and secured using the Child Aviation Restraint System (CARES) device [19]. This device fastened around the seat back and provided additional shoulder harness restraints to restrict the ATD head and chest motion. This ATD contained sensors in the head measuring accelerations and an upper neck load cell measuring forces and moments. Figure 15 shows the Q-1 ATD with CARES device attached.

Figure 15. ATD 17, Q-1 with CARES configuration

The Child Restraint and Airbag Interaction (CRABI) infant, labeled ATD 25, was located in Seat 4D. This ATD was placed in a rear facing car seat which was secured by attaching the lap belt through the guides near the legs. The ATD was secured into the car seat using its standard harnessing system. The lap belt buckle was secured over the knees of the ATD. The ATD itself weighed approximately 25 lb and was uninstrumented. Only loads from the lap belt were recorded for this ATD. Figure 16 shows the ATD in the test configuration.

Figure 16. ATD 25 configuration

The test also included an experimental child ATD, named the Large Omnidirectional Child (LODC). This ATD was a prototype 10 YO sized ATD and was developed by NHTSA [20] as an improved device to measure child injuries during automotive testing. It features an improved thoracic spine, thorax, and instrumented abdomen, along with a biofidelic pelvis which gives a more realistic representation of a child occupant compared to the standard Hybrid III 10 YO ATD. Instrumentation in the ATD included accelerometers in the head, chest and pelvis, along with a rotation sensor recording rotation rate in the head. It also included upper and lower neck load cells and pressure gages for recording abdominal pressure. The LODC was seated in Seat 10D, directly next to a standard Hybrid III 10 YO ATD so that comparisons could be made. Figure 17 shows the LODC in the foreground and the Hybrid III 10 YO in the background.

Figure 17. LODC ATD, foreground, and Hybrid III 10 YO, background

The entirety of the ATD layout is shown in figure 18. Note there is a single cockpit ATD in the pilot seat while all other ATDs are seated in the cabin. There are empty rows of seats which housed instrumentation cabling and other test equipment, and some rows were removed to allow for the data and camera control systems to be installed. Additionally, only one of the ATDs (ATD 6) was seated in a C-seat location, whereas all other ATDs were seated in seats A, B, D or E. This positioning was intentional and due to the seat location C being configured with a large overhang which was a result of repositioning of the seat legs to match the F28 spacing. Previous F28 vertical testing [3] has shown that ATDs seated in seat position C experienced much lower loads due to the amounts of seat frame bending that occurred in that specific seat, and the results obtained had the potential to be artificially low. However, ATD 6 was placed in this seat position intentionally to obtain at least one data point for comparisons.

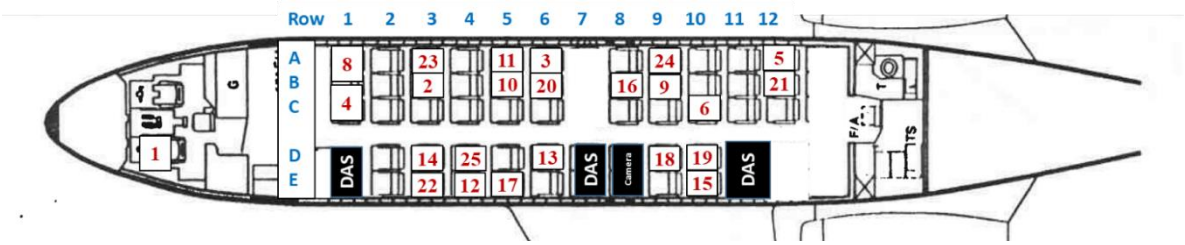

Figure 18. ATD layout

Each number in figure 18 corresponds with the experiment number used to identify each ATD throughout the report. Table 1 provides details for each experiment.

Table 1. ATD layout

ID #	ATD Type	Size	Seat	Owner	Notes
1	Hybrid II	50	Pilot	NASA	
2	WIAMan	50	3B	ARL	
3	Hybrid II	50	6A	NASA	
4	Hybrid II	50	1B	FAA	Plinth
5	FAA Hybrid III	50	12A	FAA	Internal DAS
6	FAA Hybrid III	50	10C	FAA	
8	Hybrid II	50	1A	NASA	Plinth
9	Hybrid III	3 YO	9B	NASA	
10	Hybrid III	5	5B	NASA	
11	Hybrid III	95	5A	NASA	
12	Hybrid III	6 YO	4E	NASA	
13	FAA Hybrid III	50	6D	FAA	
14	Hybrid II	50	3D	NASA	
15	Hybrid III	10 YO	10E	NASA	
16	THOR	“Obese”	8B	Humanetics	
17	Q1	Q1	5E	FAA	CARES restraint
18	Hybrid II	50	9D	NASA	
19	LODC	10 YO	10D	NHTSA	
20	Hybrid II	50	6B	NASA	Brace position
21	WIAMan	50	12B	ARL	
22	THOR	50	3E	NHTSA	
23	FAA Hybrid III	50	3A	NASA	
24	Hybrid III	3 YO	9A	FAA	CARES restraint
25	CRABI	18 mth	4D	FAA	

The majority of ATDs placed in the cabin were secured in the seats using the standard lap belts that were included on the seats. The Obese Hybrid III ATD seated in Seat 6D included a seatbelt extender since the standard belt did not reach fully around its abdomen. The only other exception was ATDs which included a CARES restraint, which provided additional support through the use of a shoulder harness system. The lap belts were secured around each ATD's waist and tightened using the "two finger" method in which the belts were tightened until no more than two fingers could fit between the belt and pelvis. The preload force in the belts was not recorded. The Hybrid II seated in the pilot seat had a 5-point belt standard for the pilot seat original to the aircraft. The 5-point belt was tightened using the same method as the lap belts. Strap load cells were used on a majority of the ATD seatbelts. There were not enough strap load cells available to be utilized on all ATDs, and care was taken in choosing the locations to instrument. For the Obese ATD, two strap load cells were used, one on the latch side and one on the buckle side to ensure the tensions were measured. All armrests were locked in the up position during the test as to not interfere with the arm motion. Finally, all ATD hands were tied to the legs with 550 lb strength parachute cord in order to prevent arm flail during the swing, but allow the arms to flail during impact. Figure 19 shows the seat locations in which strap load cells were used on the lap belts.

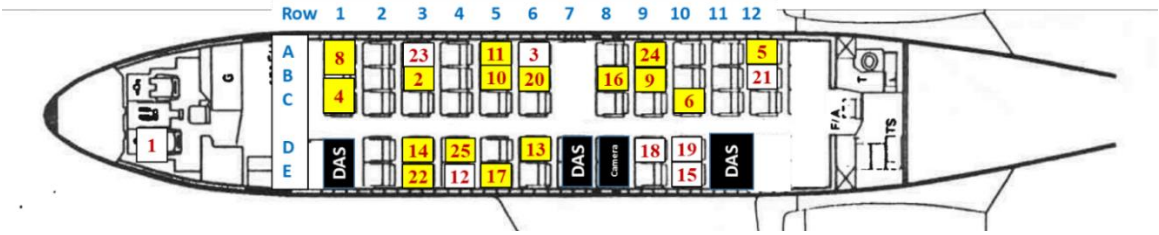

Figure 19. Lap belt load cell locations

Figure 20 and figure 21 provide an overview of all ATDs on the starboard and port sides, respectively. Additionally these figures show the three areas of the cabin section: the Cargo Hold section which contained the luggage and included Rows 1–6- the Wingbox section which contained the stiffened underfloor structure used to tie in the wings to the fuselage and included Rows 8 and 9- and finally the Aft Fuselage section which contained the aft keel beams along with other equipment in the underfloor structure and includes Rows 10–12. The three different underfloor sections were of three different overall stiffnesses, and thus were expected to provide different amounts of floor support during the crash event. Thus, comparisons can be made between ATDs over differing aircraft sections.

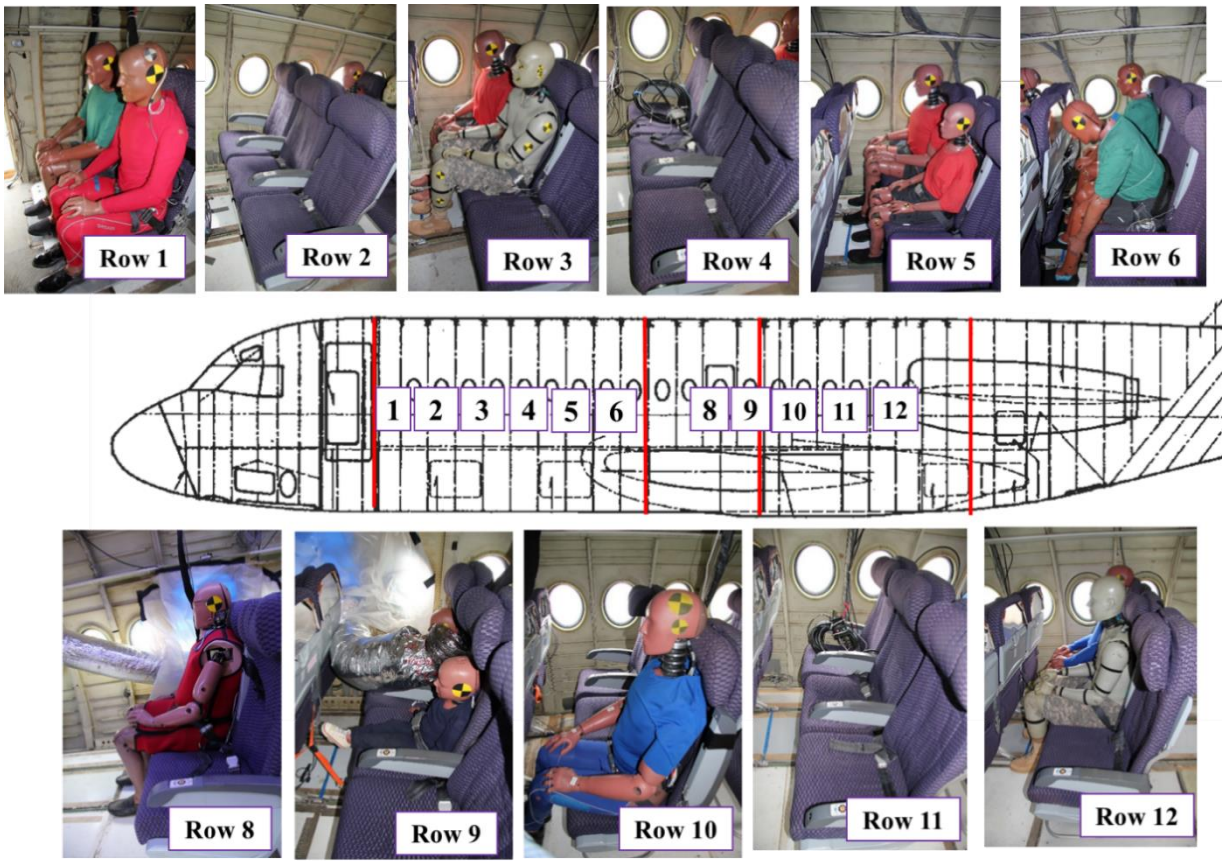

Figure 20. ATD starboard side layout

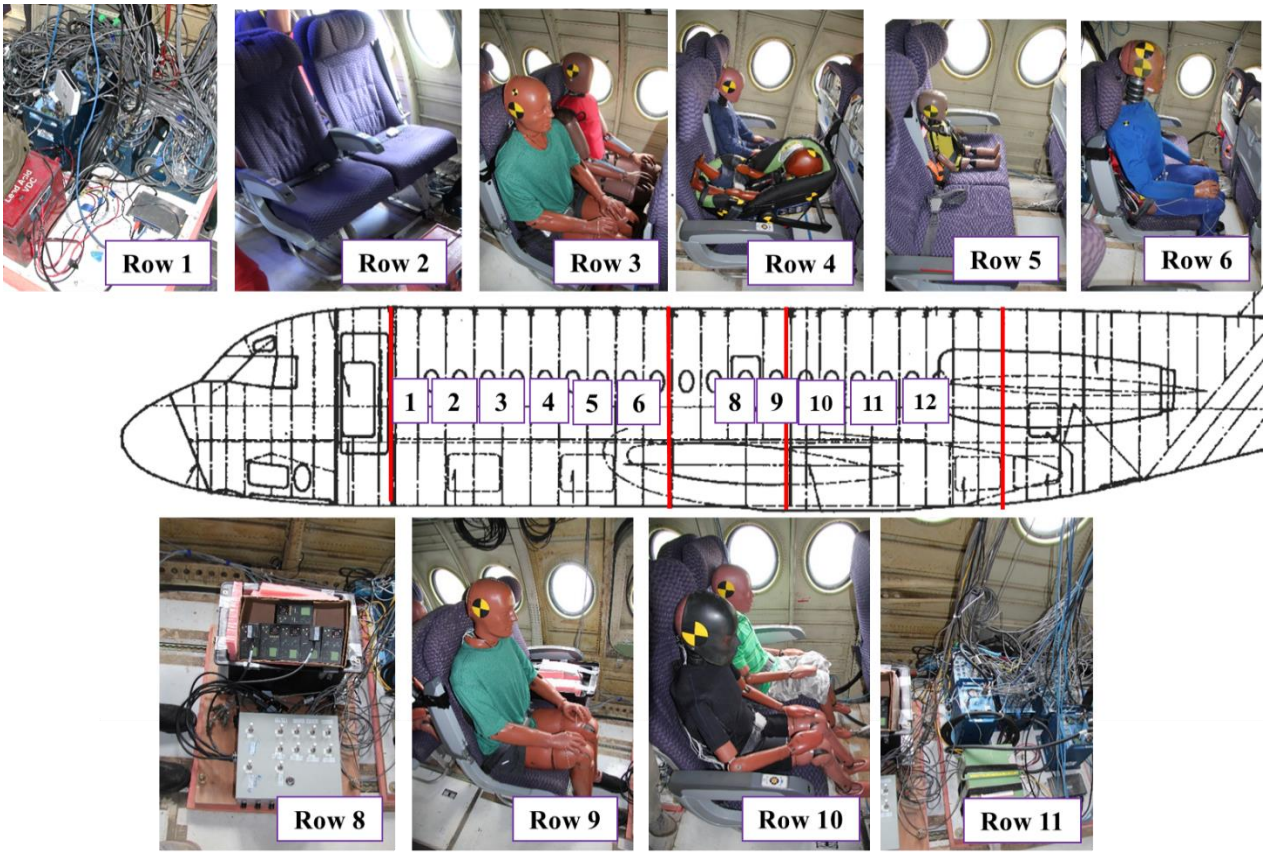

Figure 21. ATD port side layout

All ATDs were placed in a nominal position, which oriented both the upper and lower legs and the upper legs to torsos at 90° angles to each other. Finally, because H-point measurements were not taken due to the complexity of the test setup and constraints on the space available, pre-test laser scans were used to capture the overall position of all of the ATDs prior to the test. The National Transportation Safety Board (NTSB) conducted and provided all of the laser scan measurements both inside and outside the aircraft. Figure 22 shows an overview of the starboard side ATDs while figure 23 shows an overview of the port side ATDs.

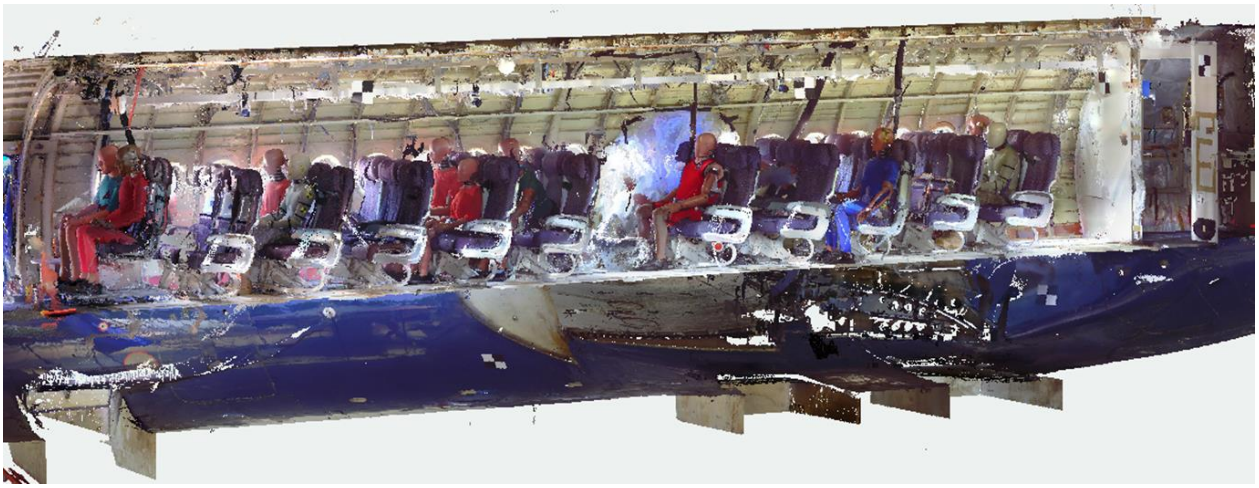

Figure 22. Laser scan of starboard side ATDs

Figure 23. Laser scan of port side ATDs

A detailed view of ATDs 3 and 7 is shown in figure 24. The detail of these scans was important because it demonstrated the laser scan technique was capable of providing detailed position measurements of all of the ATDs both pre- and post-test. This allowed for both initial and final conditions of the ATDs to be documented. Additionally, the laser scan proved to be invaluable for computer simulation efforts, wherein the ATDs in the simulations could be positioned to match the test configuration. Detailed views were available for all the ATDs onboard the aircraft.

Figure 24. Laser scan detail of ATD 7 and 3

ATD Instrumentation

A subset of the available instrumentation was placed on various components of the aircraft including numerous structural frame members throughout the aircraft cabin, seats, cockpit, engines, tail, and overhead hat rack mass ballast. The data collected from these sensors allowed for understanding of the airframe response during the impact event. The remaining instrumentation was dedicated to ATD response.

Depending on the ATD make, build, and type, various sensors were utilized within the ATDs. Most ATDs contained accelerometers in head, chest, and pelvic locations. Most standard sized ATDs also included a lumbar load cell for spinal force and moment measurements, and the majority of the HIII ATDs contained a neck load cell measuring forces and moments. A handful of ATDs had rotational rate sensors in the head and pelvis; however, most ATDs did not include these sensors. In contrast, the child ATDs typically only contained head accelerometers. The THOR, Obese THOR, and WIAMan ATDs all contained additional sensors in the arms and legs, most of which ultimately went unused due to channel availability limitations. The data collected from each ATD's specific sensor suite will be identified in that ATD's specific section of this report, and all usable data collected will be presented. Note that all data was filtered in accordance with SAE J-211 filtering guidelines [21].

The data was recorded into onboard DAS modules that were mounted on pallets in Rows 1, 7, and 11 on the port side of the aircraft. Three ATDs contained internal, stand-alone data systems and did not interface with the onboard DAS. This data was stored in memory modules internal to the ATD itself. The majority of the data was acquired at 10 kHz for a duration of 30 seconds, with the exception of the WIAMan ATDs which recorded at 200 kHz. In total, there were 711 channels of data collected from the test.

Typically, the data reported will include the ATD results, along with the acceleration at the seat base for reference. The sign convention at the seat base was the following: in the horizontal direction, positive acceleration was measured from the tail to the nose, indicating that a negative measurement was necessary to stop the aircraft, and in the vertical direction, positive acceleration was measured from the belly to the top of the aircraft, indicating a positive measurement was necessary to stop the aircraft. This sign convention is consistent throughout the report. The ATD coordinate system used coincides with the aircraft in the horizontal direction but is oriented opposite to the aircraft in the vertical direction. Instances where this system deviates from these references will be noted. For reference, the ATD and aircraft coordinate systems are shown in figure 25. Response descriptors specific to the ATDs include flexion and extension, which describe rotation directions of the ATD. Flexion refers to rotation in the forward direction (+X) while extension refers to rotation in the rearward direction (–X). Loading direction terms used within this report are described herein; tension – upward lengthening, compression – downward shrinking, shear – perpendicular with respect to load cell.

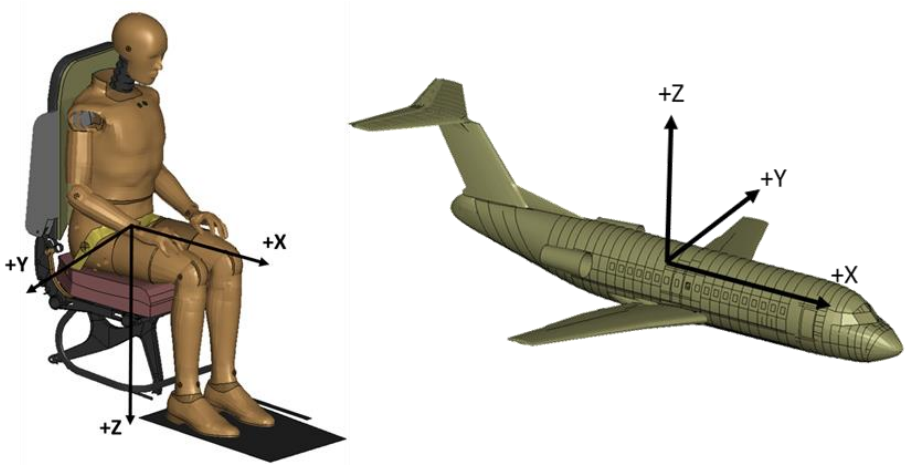

Figure 25. ATD (left) and Aircraft (right) coordinate system reference

There were nine onboard high-speed cameras in the aircraft cabin. Each camera was a 1-megapixel, monochrome ruggedized camera positioned to capture either one or two rows of seats, either on the port or starboard side. While there was a significant amount of camera coverage available, the large number of ATDs necessitated picking which ATDs would ultimately be recorded by the onboard cameras and thus a handful of ATDs did not receive camera coverage. In spots where a high-speed camera was not present, video coverage was supplemented by onboard realtime high-definition and ultra-high-definition cameras. All onboard high-speed cameras were time synced with the DAS such that examination of the video frames could be referenced to the recorded DAS values. This synchronization proved to be beneficial when determining ATD behavior at a particular point during the impact.

Airframe Result Summary

The complete set of airframe results have been reported in [11]; however, a partial set of results will be reprinted in this section for completeness. The test occurred on June 20, 2019. The aircraft was lifted to a CG height of 97.7 feet in the air and impacted into a soil bed. The measured impact conditions are shown in table 2.

Table 2. Measured Impact Conditions

Component	Measured value
Horiozntal Velocity	65.3 ft/s
Vertical Velocity	31.8 ft/s
Lateral Velocity	0.0 ft/s (assumed)
Pitch	0.38 degree nose down
Roll	4.3 degree starboard side down
Yaw	2.58 degree nose left

The motion sequence starting at impact is shown in figure 26. At impact, the aircraft was at an approximate level orientation. The next two images show first the maximum downward deflection of the airframe (upper middle) and then the maximum port side wing flexion (upper right) which occurred only 0.117 s after initial impact. The aircraft rebounded with a maximum nose pitch 0.435 s after impact. The drag chain engaged at approximately 0.751 s after impact (middle center), which occurred 0.125 s prior to the second nose impact. The aircraft experienced a second maximum displacement at 0.906 s after initial impact, and slid to motion stop at 1.62 s. The first indication of port side wing failure occurred at 0.970 s after impact, which was after both the initial and secondary nose maximum vertical deflections. Because it was well after the critical loading events, the wing attachment failure was not of consequence. Additionally, due to the use of

non-flight like fasteners in conjunction with the lifting hardware attachment, the wing failure is not representative of an actual failure, but rather an artifact of the test setup.

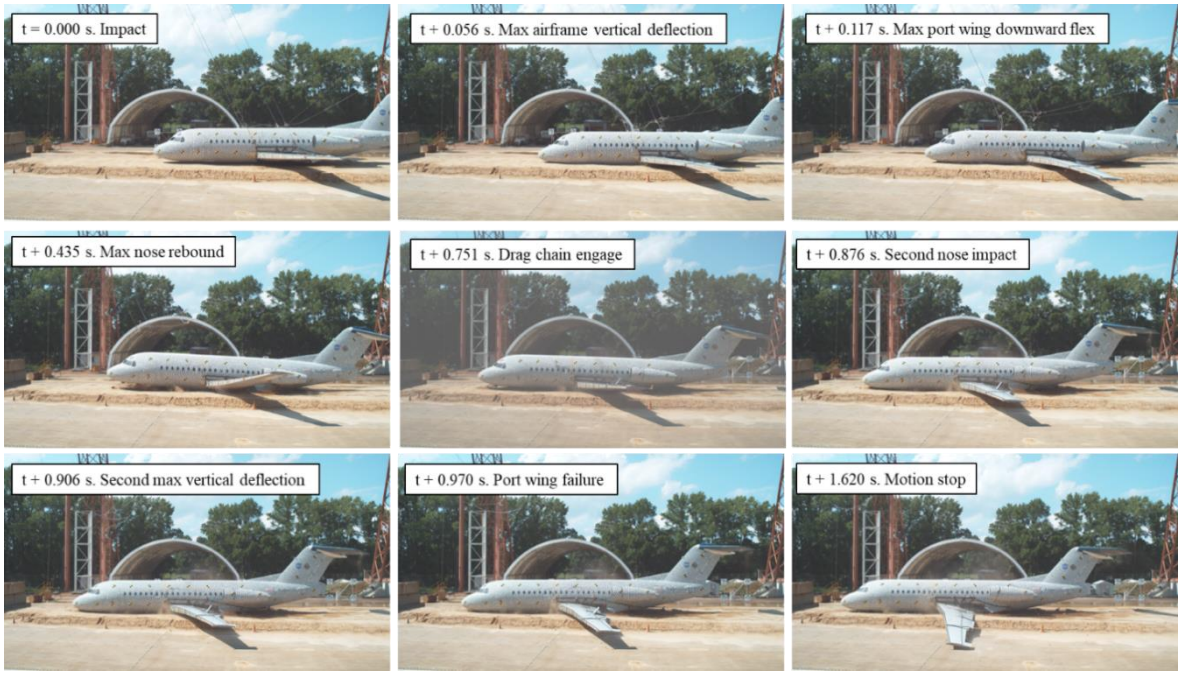

Figure 26. Impact motion sequence

One major unknown, prior to the test, was the amount of post-impact horizontal slide-out the aircraft would experience. The slide-out was a variable dependent primarily on the aircraft/soil interaction post-impact and was uncontrollable prior to the test due to the soil properties dependent on ambient conditions and test day weather. Additionally, due to LandIR facility constraints, a rigid concrete barrier had to be erected 53 feet in front of the impact location to restrict the aircraft from travelling into the Hydro Impact Basin. The barrier's location allowed the aircraft 53 feet of uncontrolled slide out/deceleration solely from the soil surface. After the 53 feet was expended, barrier impact would occur, and the nose of the aircraft would likely be crushed. In order to help slow the aircraft down prior to barrier impact, a drag chain was attached between the lifting hardware and anchor weights located approximately 200 feet aft of the tail. The drag chain system was designed to engage approximately 25 feet after initial ground contact, providing a controlled (external) deceleration due to the weight drag prior to barrier impact.

When examining the post-test position of the aircraft, it was determined the actual slide-out of the aircraft was approximately 32.5 ft, with the drag chain engaging approximately 24 feet after ground contact and 0.75 s after impact. Kinematic analysis of the tracking targets on the side of the aircraft showed little to no change in slope from the displacement values obtained, indicating drag chain engagement did not play a significant role in stopping the aircraft and the response was primarily from the aircraft/soil interaction. Additionally, the timing of the drag chain engagement at t+0.751 s was well after the time in which the primary loading of the ATDs occurred.

Major events that occurred on the airframe post-impact are shown in table 3. These events are important to capture because their influence on the ATD results should be examined. Some of the events are pictured in figure 26, while others are visible in other camera views, not included in this report.

Table 3. Major post-impact events

Event #	Time after Impact (s.)	IRIG Time (s)	Event
1	–3.504	31.226	Release
2	0.000	34.730	Impact
3	+0.056	34.786	Maximum airframe vertical deflection
4	+0.090	34.820	Maximum starboard wing downward flex
5	+0.117	34.848	Maximum port wind downward flex
6	+0.435	35.168	Maximum nose rebound
7	+0.751	35.481	Drag chain engage
8	+0.876	35.606	Second nose impact
9	+0.906	35.636	Second maximum vertical deflection
10	+0.970	35.750	First indication of wing bolt failure
11	+1.620	36.350	Motion Stop

Airframe accelerations in the horizontal and vertical locations were collected over the entire length of the cabin. The horizontal accelerations on the port side are first shown in figure 27, noting that the color of the trace in the plot corresponds to the starred cabin location on the right. Figure 27 also includes accelerations in the cockpit of the aircraft, which were collected to examine the pilot response.

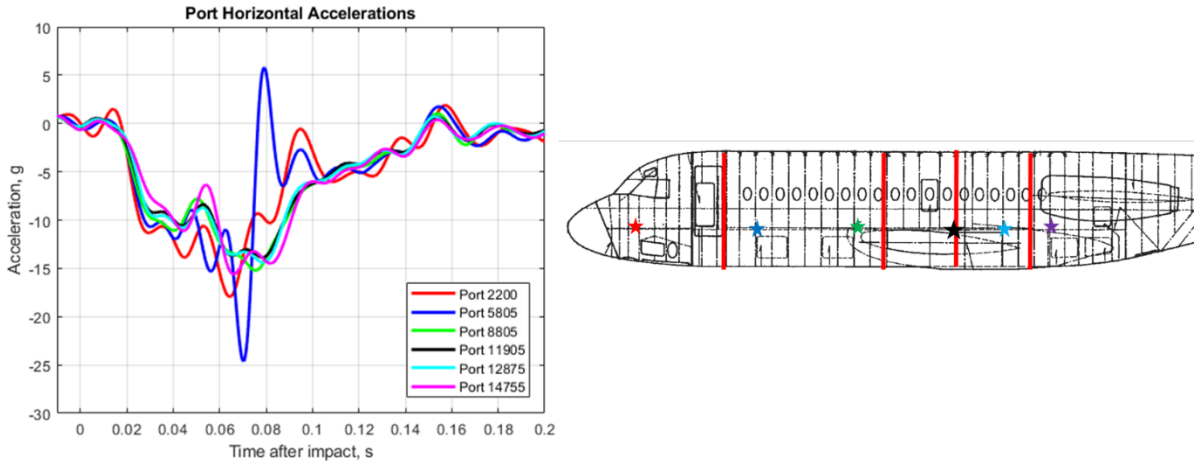

Figure 27. Cabin port side accelerations

Figure 27 also shows port side accelerations that were collected at two spots in the Cargo Hold, one spot in the Wingbox section, and one spot in the Aft Fuselage section. The plot legend includes fuselage station numbers, which are the primary way to denote each frame's location in the aircraft. As the acceleration traces show, with the exception of the one measurement at station 5805 which is at the front of the Cargo Hold portion of the cabin, all acceleration measurements were similar in magnitude, duration, and shape. The station 5805 measurement recorded two electrical spikes which saturated the signal at 0.07 s and 0.079 s. The data, along with these spikes, was filtered which caused a perceived large oscillation during these times. Further examination suggests that the location near the plinth seat and its interaction with the cabling could have been the cause of these saturations, and the signal in this sensor should be ignored during this oscillation. However, the majority of the data shows a triangular-to-trapezoidal pulse shape which was primarily uniform throughout the entire cabin section. The accelerations deviated from a zero value at approximately 0.011 s after impact and reached a plateau of approximately 10 g approximately 0.03 s after impact. During this time, the aircraft and the internal components experienced downward motion and deformation. After this short plateau, the accelerations reached their minimum values approximately 0.07 s after impact. This time was after the maximum vertical deflection of the aircraft and before the maximum

wing deflections, so it was likely that the additional downward deflection of the wings were pushing the aircraft into the soil, causing additional horizontal acceleration. After the minimum accelerations were measured, they tracked back toward zero and crossed the zero axis between 0.14 s and 0.16 s after initial contact. This time was after both of the wings achieved maximum flexure, and during the aircraft rebound. The aircraft contained horizontal motion well into motion stop at 1.62 s after impact; however, during this initial event and the second nose impact, horizontal accelerations were negligible. The second nose impact produced much smaller accelerations; however, the majority of the ATD response was a result of this initial impact. Further analysis on the horizontal acceleration measurements can be found in [11]. Next the vertical accelerations for the starboard side of the cabin are shown in figure 28.

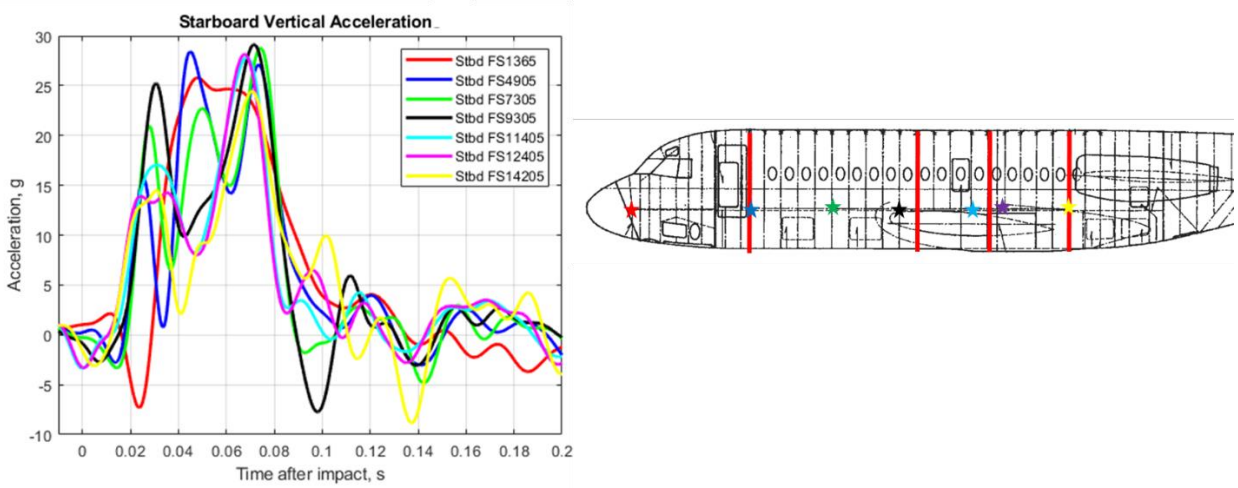

Figure 28. Starboard side accelerations

In the vertical direction, the measurements resembled a trapezoidal pulse shape with two major peak events at the end points of the plateau region. The pulse duration was approximately the same as the horizontal duration of between 0.14 and 0.16 s. Maximum acceleration values approached but did not exceed 30 g, and the varying oscillation and peak locations were attributed to the aircraft geometry with the wingbox making the initial contact with the soil, along with the impact orientation of the aircraft. As with the horizontal accelerations, there was late time vertical accelerations that occurred during the second nose impact. However, because the ATD response was primarily a function of the initial impact, those results are not shown in figure 28. Further analysis on the vertical acceleration measurements can be found in [11].

ATD Result Summary – 50th Percentile ATDs

The locations of the 50th percentile ATDs are highlighted in red in figure 29 and detailed in table 4. These ATDs included the Hybrid II and the FAA Hybrid III variants. The ATDs were positioned such that there were ATDs in the Cargo Hold, Wingbox, and Aft Fuselage sections of the cabin, on both the port and starboard sides, and in every seat with the exception of Seat E. This layout provided data points from all major locations within the aircraft.

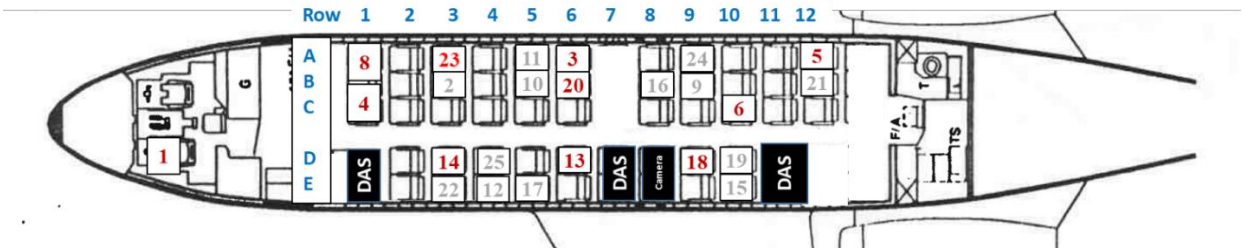

Figure 29. 50th percentile ATD locations

Table 4 – 50th Percentile ATD locations

ID #	ATD Type	Size	Seat	Owner	Notes
1	Hybrid II	50	Pilot	NASA	
2	WIAMan	50	3B	ARL	
3	Hybrid II	50	6A	NASA	
4	Hybrid II	50	1C	FAA	Plinth
5	FAA Hybrid III	50	12A	FAA	Internal DAS
6	FAA Hybrid III	50	10C	FAA	
8	Hybrid II	50	1B	NASA	Plinth
13	FAA Hybrid III	50	6D	FAA	
14	Hybrid II	50	3D	NASA	
18	Hybrid II	50	9D	NASA	
20	Hybrid II	50	6B	NASA	Brace position
23	FAA Hybrid III	50	3A	NASA	

The next sections will present the data from each ATD, starting and counting up from ATD 1.

ATD 1 – Pilot

ATD 1 was Hybrid II 50th percentile seated in the pilot seat, which was unmodified. The seat was positioned in the furthest forward location and the hands were taped to the yoke and feet were taped to the pedals. The ATD was restrained with a 5-point harness which was tightened using the two finger method and the armrests were moved out of the way as to not interfere with the ATD motion. Unfortunately, there were no onboard cameras present to capture the motion during the event. Figure 30 shows the pilot ATD.

Figure 30. ATD 1

Figure 31 shows the accelerations in the horizontal (left) and vertical (right) directions, measured in the head, chest, and pelvic regions of the ATD. During the impact event, three distinct kinematic response periods were measured. Over the first 0.1 s, the ATD exhibited similar acceleration magnitude to the seat along the horizontal (X) direction. The vertical (Z) acceleration of the ATD was magnified compared to the seat base, peak acceleration in the pelvis almost doubled the average peak seat acceleration. During this period of the impact, the ATD's motion along the horizontal direction was driven by the 5-point belt which provided a relatively stiff connection between the seat motion and ATD. In the vertical direction, ATD motion was driven by the relatively soft seat foam. This soft connection between input acceleration and ATD motion likely drove the magnified acceleration within the ATD vertical response.

Between 0.1 and 0.2 s, acceleration in the chest and head reversed direction. This indicated the ATD slipped through the torso restraints, which was verified post-test, and rotated forward over the lap restraint. There was also a spiking response in the head acceleration which indicated potential contact with the aircraft. After 0.2 s, little motion was measured in the chest and pelvis of the ATD, while there is another spike in head acceleration response which indicated another head strike. Although there is no video to confirm the timing of ATD contact with the aircraft, the ATD was found under the control console post-impact indicating significant contact did occur.

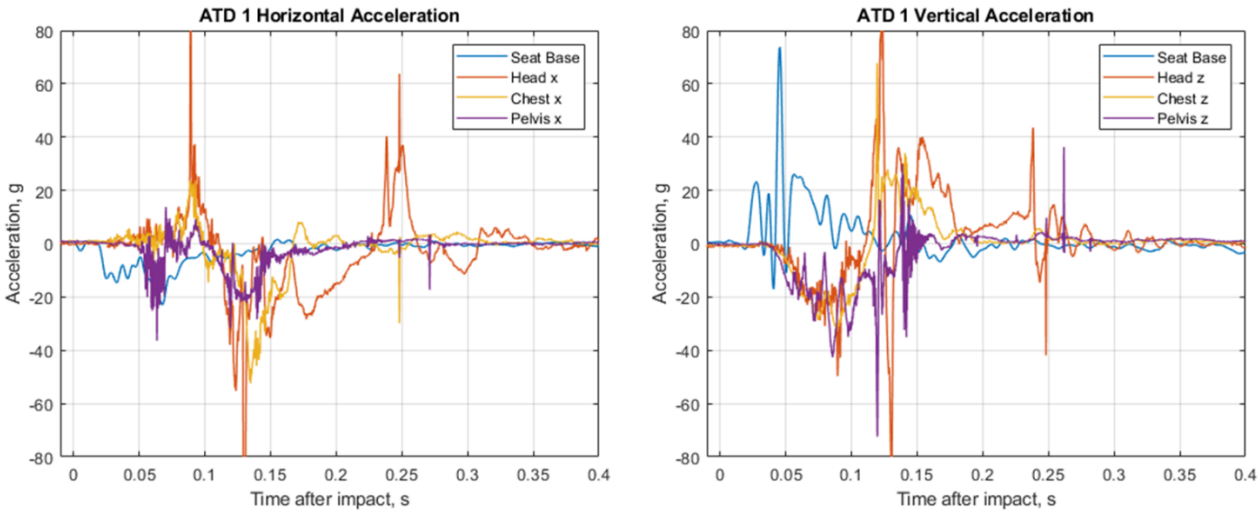

Figure 31. ATD 1 Accelerations

The lumbar load response of ATD 1, which is shown in figure 32, followed the kinematic response previously discussed. Over the first 0.1 s, the lumbar spine was loaded primarily along with vertical direction (Z) as the pelvis was accelerated by the seat. Lumbar compressive load values exceeded the 1500 lb injury limit during this time period, reaching a maximum value of 1,657 lb. After 0.1 s, forward torso rotation was indicated by the increase in lumbar moment (My), which reached a maximum value of 3,021 in-lb at 0.142 s after impact. The rotation also caused an increase in the lumbar shear load (X).

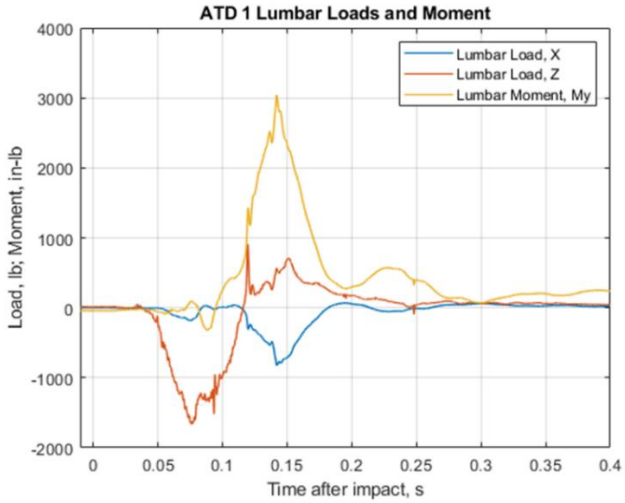

Figure 32. ATD 1 Lumbar loads and moment

ATD 3 – Seat 6A

ATD 3 was a Hybrid II 50th percentile seated in Seat 6A. An onboard high-speed camera was used to record the ATD kinematics during the crash event, which is shown in figure 33. Within this figure, ATD 3 is in the background, nearest to the window. The high-speed camera captured the ATD rotating forward about the lap restraint and impacting into the forward seat back at 0.160 s after impact. At 0.590 s after impact, the ATD rebounded close to its original pre-impact position, and then began to rotate forward again due to the second impact of the aircraft. The final image in the lower right shows the ATD in its position after all motion has stopped.

Figure 33. ATD 3 Image sequence

The ATD 3 acceleration data are shown in figure 34. The horizontal pelvis acceleration of ATD 3 generally followed the seat base acceleration magnitude, however with a slight lag due to the stiff connection between pelvis and seat through the lap belt. Chest and head horizontal acceleration followed the pelvis as the deformable lumbar spine component of the ATD allowed the torso to rotate forward while the pelvis was accelerated with the seat. The head acceleration showed a noticeable spike at 0.15 s after impact which was due to the ATD's head impacting the seat back of the seat in front.

Vertical acceleration can only be partially compared to the seat vertical acceleration channel for approximately the first 0.1 s after impact. After this time, the seat cable severed, and the data was unusable. However, the accelerations in all parts of the ATD were nearly uniform and tracked the seat base acceleration. The maximum negative acceleration was measured in the ATD pelvis, which reached a maximum negative value of 38.2 g approximately 0.07 s after impact. After this time, the measurements trended toward the positive region and reached a positive maximum at the same approximate time as the head strike occurred. Maximum values in the head were somewhat skewed by the large oscillations in the head due to the contact, but the maximum value in the pelvis was approximately 20.4 g at this time.

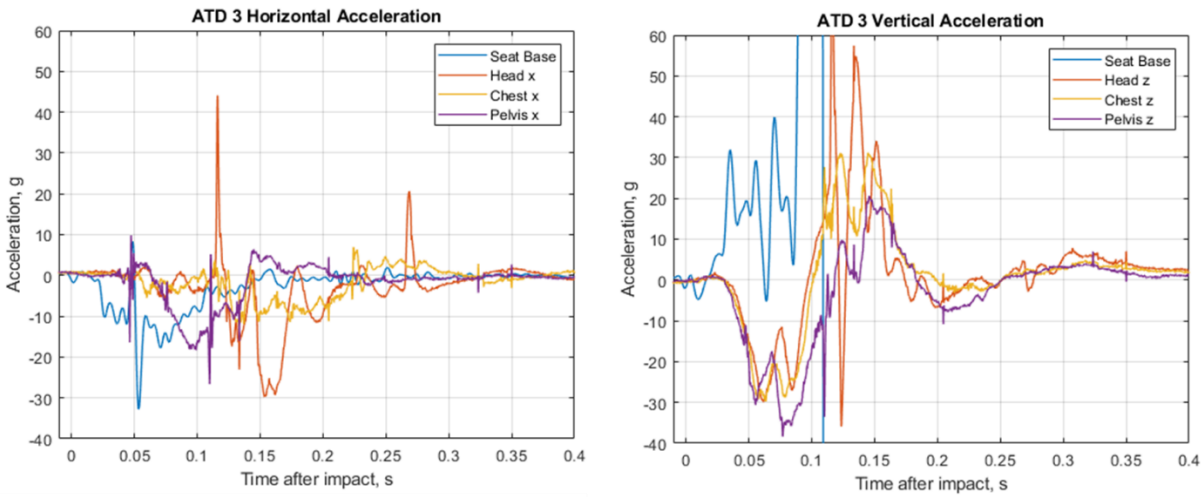

Figure 34. ATD 3 Accelerations

The lumbar load response of ATD 3, shown in figure 35, followed the kinematic response of the ATD pelvis. Compressive lumbar load increased over the first 0.1 s as the pelvis was accelerated into the seat foam, resulting in a peak compression value of 1,675 lb, which was greater than the 1,500 lb injury limit. After 0.1 s, the forward rotation of the torso around the lap belt resulted in an increase in lumber spine moment until a maximum of 2,031 in-lb. was reached approximately 0.14 s after impact. Lumbar tension was also measured after 0.1 s; this was likely caused by the ATD pelvis rebounding upward from the seat foam into the lap belt. As the body accelerated upward, the pelvis became restrained by the lap belt and the lumbar spine was loaded in tension due to the inertial force of the torso pulling upward on the lumbar load cell.

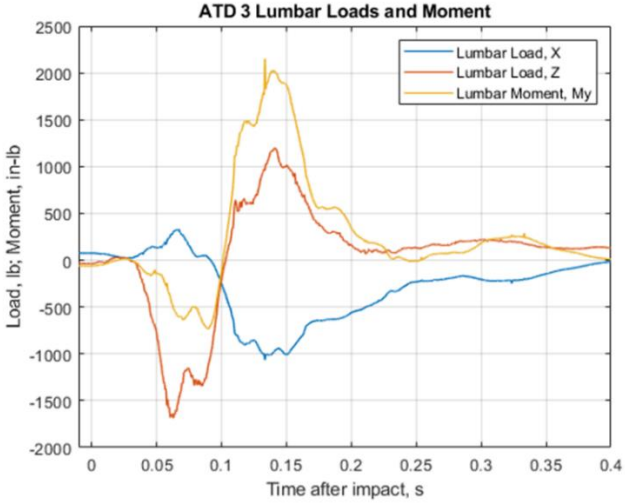

Figure 35. ATD 3 Lumbar load and moments

ATD 4 – Plinth Seat 1B

ATD 4 was a Hybrid II 50th percentile seated in Seat 1B. Though this ATD was instrumented, the measurements recorded in this ATD were grossly out of phase from the other ATDs measured within this study. The source of these differences is thought to be related to instrumentation issues and thus were not included within this report. ATD 8 was of matching ATD configuration seated next to ATD 4 in Seat 1A and is used to evaluate the plinth seat within the test data.

ATD 5 – Seat 12A

ATD 5 was an FAA Hybrid III 50th percentile seated at the rear of the aircraft in Seat 12A. An onboard high-speed camera was used to record the ATD kinematics during the crash event, which is shown in figure 36. ATD 5 was seated next to a WIAMan in seat 12B and is seated farthest from the camera in the window seat. The high-speed camera captured both ATDs rotating forward about the lap restraint and impacting into the forward seat back during the crash event at approximately 0.15 s. The head strike was verified at this time within the head acceleration response measured in ATD 5. Increased torso and neck flexibility is observed in the WIAMan compared to the FAA Hybrid III during the impact event, particularly the neck extension and torso compression observed under vertical acceleration which occurred over the first 0.05 s of impact. The WIAMan results are not included within the scope of this study.

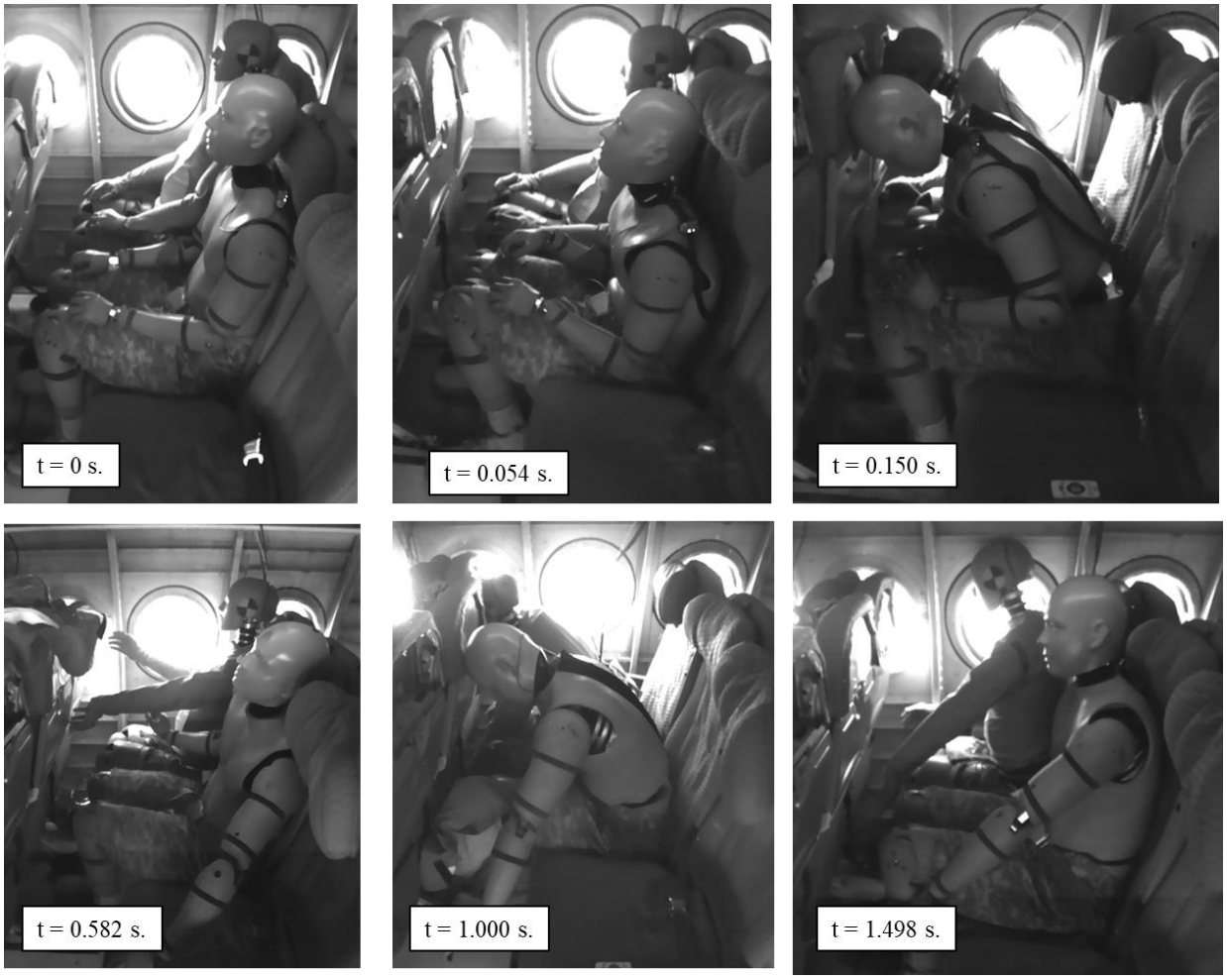

Figure 36. ATD 5 Image sequence

Figure 37 shows the accelerations in the horizontal and vertical directions. Over the first 0.1 s, pelvis peak horizontal acceleration was magnified compared to seat base, reaching a maximum of 27.1 g. Head and chest accelerations were in phase with the pelvis though they were lower in magnitude. Vertical acceleration was similar throughout the ATD over the first 0.1 s. This result indicated the pelvis, with a peak value of 41.4 g, was vertically aligned with torso and head during this phase of the impact. At approximately 0.14 s, there was a large spike in head horizontal acceleration, indicating head strike which confirmed what was

observed in the high-speed video. Head vertical acceleration was not shown to increase during this time period indicating the strike was perpendicular to the face of the ATD head.

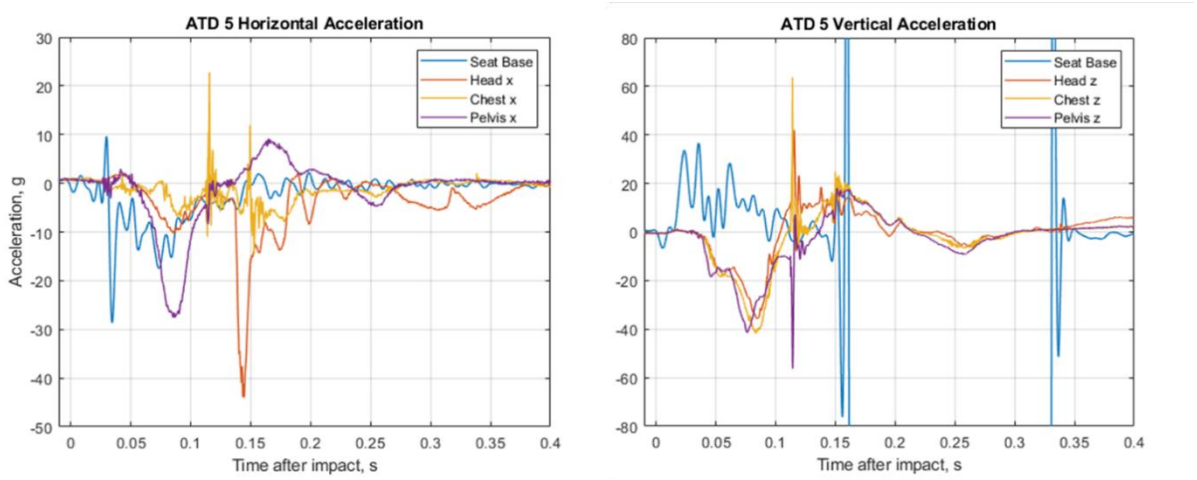

Figure 37. ATD 5 Accelerations

Figure 38 shows the lumbar loads and moment measured in ATD 5. Peak compressive lumbar load was 2,955 lb, approximately double the injury metric limit. This was the largest vertical lumbar load measured in the 50th percentile ATDs. This large compressive load did not correlate with a significant increase in pelvis vertical acceleration compared to the other ATDs. One potential source of this large lumbar load may be identified by the low horizontal lumbar load component. Although pelvis horizontal acceleration was relatively high, the horizontal lumbar load was low. These factors indicated the lumbar spine of ATD 5 may have been more vertically aligned with the upper body mass than the other ATDs resulting in the larger compressive load measured and reduced shear force acting on the spine.

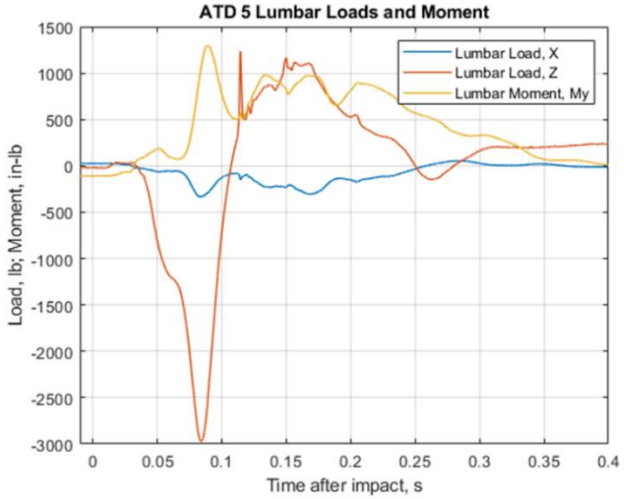

Figure 38. ATD 5 Lumbar loads and moment

ATD 6 – Seat 10C

ATD 6 was an FAA Hybrid III 50th percentile seated in Seat 10C. ATD 6 was the only ATD tested in an overhung seat. The kinematics of ATD 6 are generally similar to the other ATD responses. Figure 39 shows the accelerations in the horizontal and vertical directions. Head horizontal acceleration closely follows seat base acceleration over first 0.150 s; however, it lags in its timing. Chest horizontal acceleration was

minimal, and pelvis acceleration was not recorded in this ATD. Head and chest vertical acceleration closely tracked vertical seat base acceleration. Magnification of ATD vertical acceleration compared to seat base was not prevalent in this seat configuration. The effect of the seat foam to magnify the impact acceleration within the ATD was likely offset by energy absorbed by the overhung seat as it deformed under the impact load. Head strike was indicated with the forward seatback at approximately 0.2 s by a spike in head horizontal and vertical acceleration.

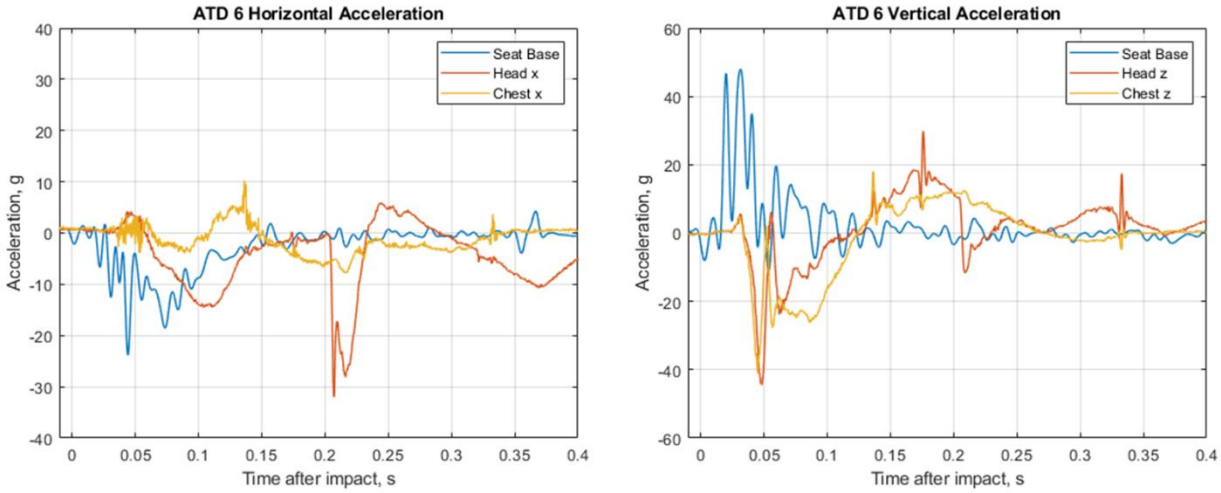

Figure 39. ATD 6 Accelerations

Figure 40 shows the head rotation rates in ATD 6. The head rotation response of ATD 6 primarily occurred in the sagittal plane (*y*-rotation). The head initially rotated in extension as the torso accelerated upward. As the torso began to rotate forward, the head rotation reversed direction into flexion. Head strike was indicated by an abrupt change in head extension rotation at approximately 0.2 s. Some degree of out-of-plane motion is exhibited by *x*-axis rotation which increased to 2/3 of the magnitude of peak *y*-rotation prior to head strike. This out-of-plane motion was likely driven by the bending in the overhung seat, which caused the ATD to rotate sideways during the impact event.

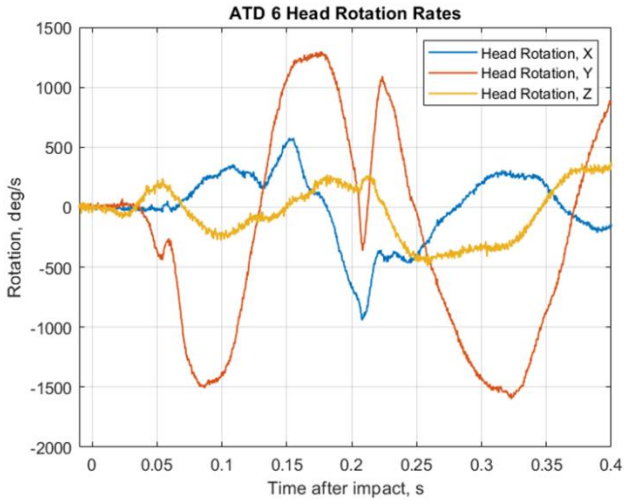

Figure 40. ATD 6 Head rotation rates

Figure 41 shows the upper neck forces and moments of ATD 6. The upper neck forces and moment primarily tracked with the head response of the ATD. Compressive neck force peaked at 0.05 s at

approximately 443 lb. The shape of this response matched head vertical acceleration. Neck shear force peaked at 0.1 s at approximately 125 lb and matched the shape of head horizontal acceleration. Upper neck moment matched the shape of head rotation, peak moment occurred in extension at 0.22 s at approximately 331 in-lb. This occurred after head strike.

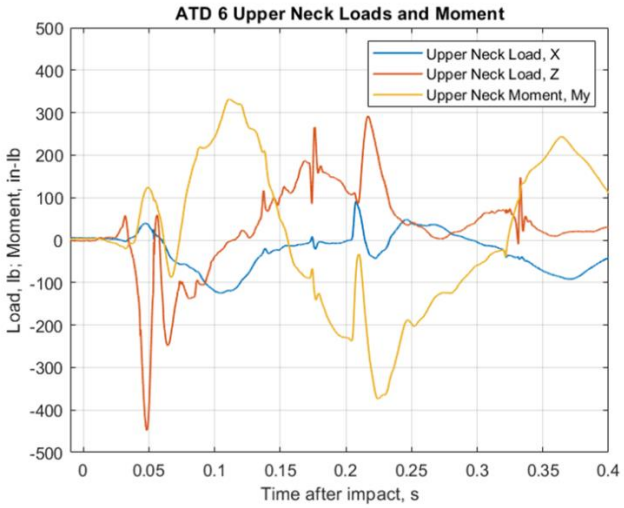

Figure 41. ATD 6 Upper neck loads and moment

Compared to the other 50th percentile ATDs tested in this region of the aircraft, the compressive lumbar load in ATD 6, shown in figure 42, was relatively low, but briefly above the injury metric limit. This indicated that the overhung seat did absorb some of the impact energy within this test, verifying the trends observed in the fuselage component tests. Shear force was also low in this ATD compared to others tested. The lumbar moment closely tracked the shape of the lumbar force response throughout the impact event.

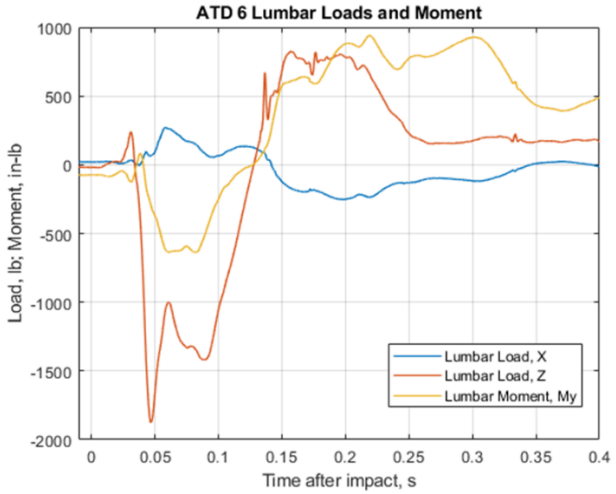

Figure 42. ATD 6 Lumbar loads and moment

Although ATD 6 did not have an instrumented pelvis, lap belt load was measured for this ATD, and is shown in figure 43. A maximum value of 666 lb was measured in the lap belt. The lap belt began taking load at approximately 0.05 s, which tracked with the onset of chest and head horizontal acceleration measured in the ATD.

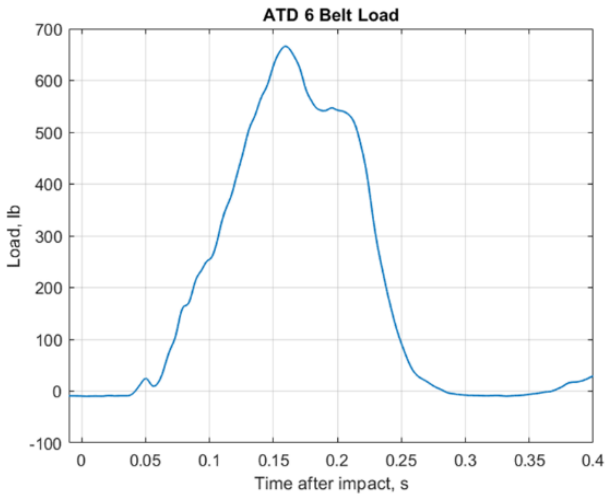

Figure 43. ATD 6 Belt load

ATD 8 – Plinth Seat 1A

ATD 8 was a Hybrid II 50th percentile seated in Seat 1A which was one of the ATDs seated in the plinth seat. The horizontal kinematics of ATD 8 differed from the majority of ATDs of similar type in this test, likely because of the seat mounted onto the plinth configuration. Due to the plinth plate being offset from the actual cabin floor because of the added distance of the load cells, rotational velocities induced in the seat due to floor deformation would be amplified, which could lead to oscillations measured on the ATDs. These oscillations manifested in the ATD kinematics along the horizontal direction. Figure 44 shows the acceleration in the horizontal and vertical directions. Pelvis horizontal acceleration reversed direction, opposite of the seat acceleration at the beginning of impact. After approximately 0.02 s, the acceleration direction reversed and the pelvis acceleration tracked the seat acceleration for the remainder of the impact. Chest horizontal acceleration tracked pelvis acceleration while head acceleration lagged pelvis acceleration by approaximately 0.025 s. Head acceleration was in the opposite direction of the pelvis at the time of peak pelvis and seat acceleration. Vertical acceleration tracked similarly between head, chest, and pelvis with peak ATD acceleration closely following the peak seat acceleration. Significant vertical acceleration was observed with the head vertical acceleration ranging from –40 to +40 g during the impact. There was no forward seatback in this seat configuration and no obvious indication of head strike from the ATD kinematic response. This likely allowed the head acceleration to grow to this magnitude as the ATD rebounded upward in the seat.

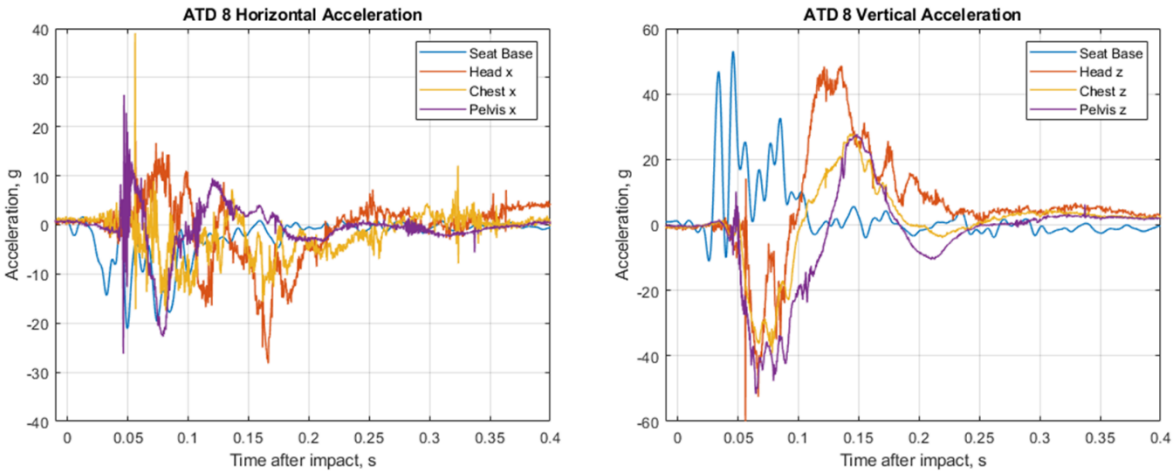

Figure 44. ATD 8 Accelerations

The lumbar load response of ATD 8 followed the kinematic response of the ATD pelvis and is shown in figure 45. Compressive lumbar load built up over the first 0.05 s as the pelvis was accelerated into the seat foam, resulting in a peak value of approximately 2,462 lb. After 0.1 s, the forward rotation of the torso around the lap belt resulted in an increase in lumber spine flexion moment, which reached a maximum value of 2,720 in-lb 0.157 s after impact. Lumbar tension was also measured after 0.1 s, with peak tension load corresponding with peak lumbar flexion.

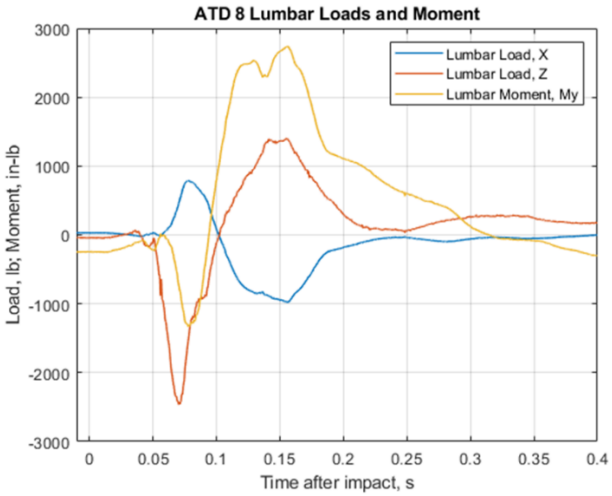

Figure 45. ATD 8 Lumbar loads and moment

The lap belt load measurement on ATD 8 suffered from significant noise in the signal. Unlike other lap belt load results plotted in this report, the belt load response shown in figure 46 is unfiltered in order to examine the underlying pulse shape. Much of the short duration spikes that occurred at instances such as 0.097 s, 0.134 s, 0.178 s, 0.3 s along with the longer duration spike that began at 0.068 s all showed characteristics of a saturated signal in the sensor and should be ignored when investigating overall magnitude of loading. Because the entire measurement time history was not saturated, the most likely explanation indicated a loose connection in the sensor connector. Care must be taken when examining this signal in attempting to differentiate between actual measurement and sensor saturation. From the trace shown in Figure 46, there is a noticeable parabolic shape which results in a maximum value of 820 lb, which occurred 0.148 s after impact. There is a second smaller parabola that began at 0.25 s and reached another localized maximum of approximately 155 lb which occurred 0.317 s after impact.

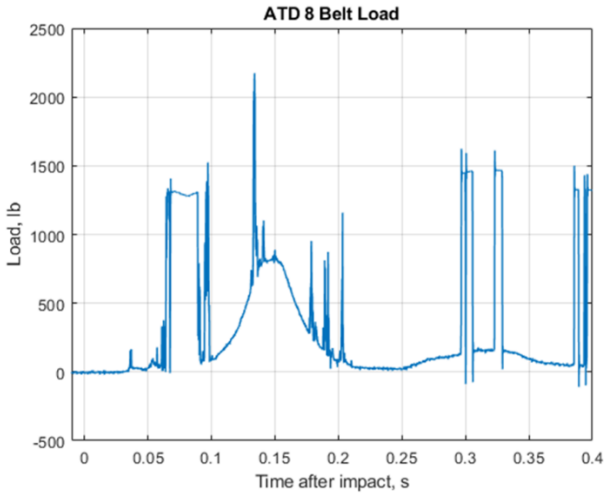

Figure 46. ATD 8 Belt load

ATD 13 – Seat 6D

ATD 13 was an FAA Hybrid III 50th percentile seated in Seat 6D. The motion sequence in figure 47 depicts six distinct events of this ATD during the impact event. The first in the upper left image is the ATD position at the time of impact. The upper middle image depicts the ATD at its maximum vertical deflection, which occurred 0.058 s after impact. The image in the upper right depicts the ATD as it experienced the head strike event. The lower left image depicts the ATD at its maximum forward position which occurred 0.152 s after impact. The maximum rebound of the ATD is shown in the bottom middle image, and finally the post-impact position of the ATD is shown in the lower right. Note that the lower right image depicts a time well after the motion stop of the aircraft.

Figure 47. ATD 13 Image sequence

Chest horizontal acceleration tracked the seat base acceleration, though motion was delayed by approximately 0.05 s which is shown in figure 48. Head horizontal acceleration was even further delayed with minimal horizontal motion measured until after 0.1 s. A spike in head horizontal acceleration occurred at 0.125 s, which was indicative of a head strike condition. Vertical acceleration tracked through the chest and head with peak acceleration closely matching that measured in the seat.

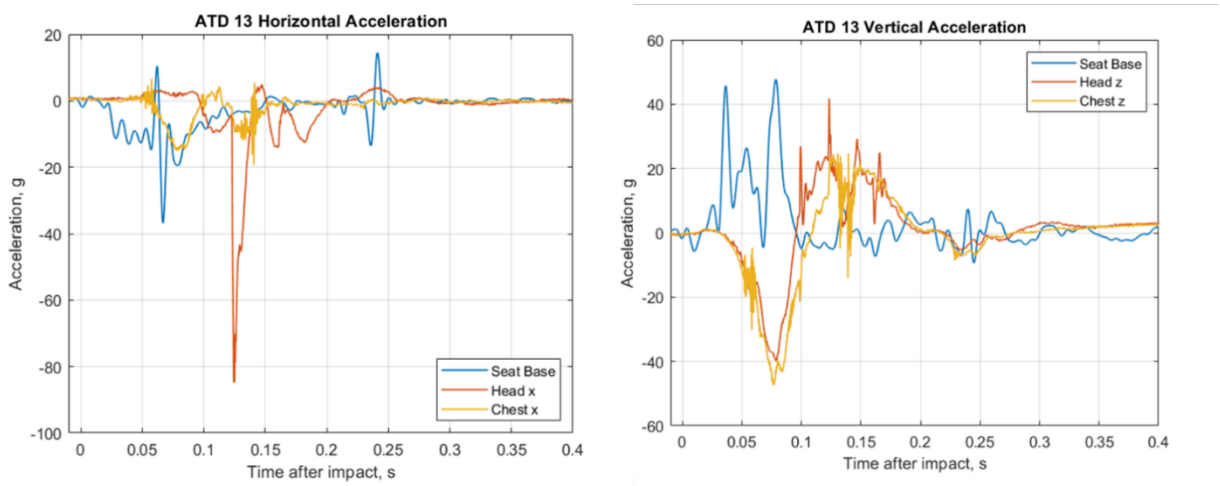

Figure 48. ATD 13 Accelerations

The head rotation rate measured in ATD 13 is shown in figure 49. The majority of head rotation measured occured in the impact plane, about the *y*-axis, prior to the head strike event. The rotation reached a peak value of 1,839 deg/s just prior to the head strike, which occurred at 0.118 s after impact. After head strike,

z-axis rotation became the dominant motion in the ATD head. This result indicated the ATD's head struck the forward seat with some non-zero out-of-plane tilt, inducing this off-axis head rotation.

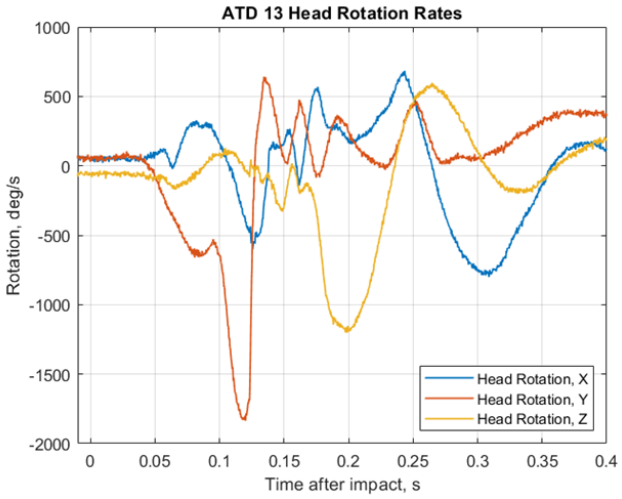

Figure 49. ATD 13 Head rotations

Upper neck loads and moments were next examined and are shown in figure 50. An examination of the data showed that there was minimal upper neck shear force measured in ATD 13. Over the first 0.125 s, neck compression tracked the vertical acceleration of the chest and head. Peak neck compression occurred during the head strike event when the head was accelerated into the neck and forward moving torso mass. Moment generally followed head rotation, though its potential effect on neck injury risk would have been relatively low compared to neck compression in this condition. Neck shear force was minimal throughout the impact event.

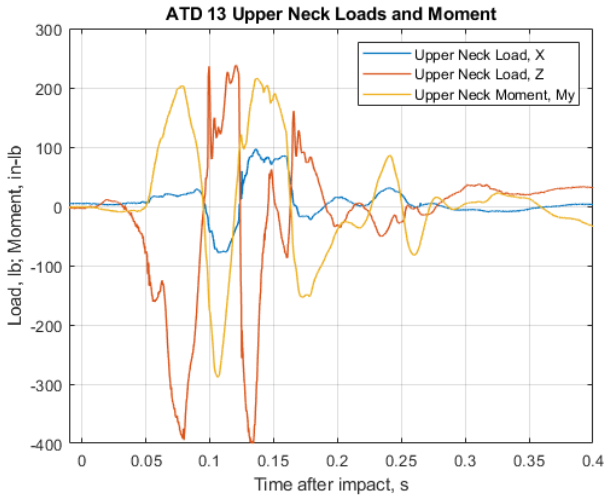

Figure 50. ATD 13 Upper neck loads and moment

Measured lumbar load response of ATD 13 is shown in figure 51. Compressive lumbar load tracked the pelvis acceleration throughout the test and tracked upper neck compressive force prior to head strike. Peak lumbar load was 2,695 lb, which was well above the injury metric limit. There was minimal lumbar moment until the lumbar spine went into flexion at which point it tracked the lumbar tension force. Lumbar shear force was also minimal throughout the impact event.

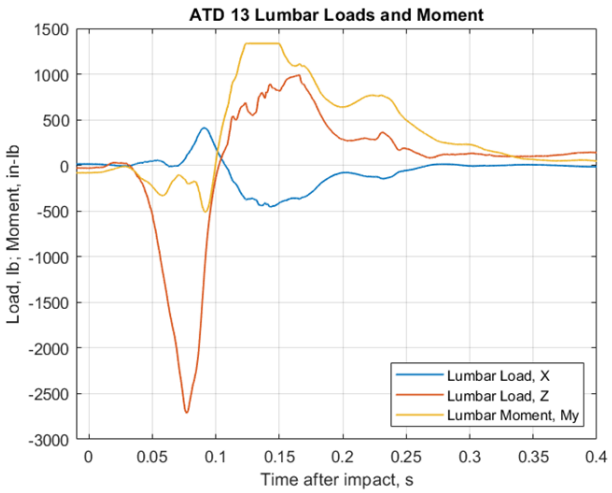

Figure 51. ATD 13 Lumbar loads and moment

A continuous lap belt load was measured on ATD 13 which is shown figure 52. The belt was not significantly loaded until after 0.1 s, which was primarily due to the ATD compression into the seat, which generated some slack between the belt and ATD. There was a minor hump in the response which occurred at 0.082 s after impact and at the approximate time of maximum lumbar compression. After the maximum compression, the ATD began to rotate forward in the seat, leading to a rise in the tension in the lap belt. The maximum belt load was 1,002 lb and occurred 0.153 s after impact. This was the time of maximum forward motion of the ATD.

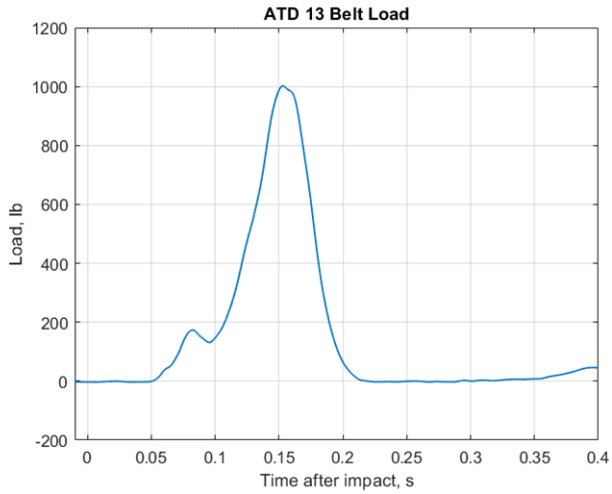

Figure 52. ATD 13 Belt load

ATD 14 – Seat 3D

ATD 14 was a Hybrid II 50th percentile seated in Seat 3D. High-speed video was taken of this seat row and is shown in figure 53 with ATD 14 in the foreground, closest to the aisle. Over the first 0.06 s, ATD 14 was vertically loaded into the seat, and its upright posture was maintained as it sunk downward into the seat foam. After this point it began forward rotation about the lap belt and can be seen impacting the forward seatback at 0.126 s. The impact of ATD 14 into the forward seatback caused the seat adjustment mechanisms to fail and the forward seatback collapsed forward. This limited the rebound of ATD 14, which ultimately ended up in a forward folded position at the end of the impact event.

Figure 53. ATD 14 Image sequence

Accelerations in the horizontal and vertical directions are shown in figure 54. Pelvis horizontal acceleration initially occurred in the opposite direction of seat acceleration until approximately 0.075 s. After this time, it reversed direction and tracked the end portion of the seat acceleration pulse. Chest horizontal acceleration tracked this second portion of pelvis acceleration. Head acceleration tracked the initial portion of pelvis acceleration, in both direction and magnitude, though it is delayed by approximately 0.015 s. Head strike was indicated at approximately 0.125 s by a large spike in head acceleration of 68.5 g. Pelvis, chest, and head acceleration all closely tracked seat acceleration along the vertical direction, indicating upright ATD posture with a direct transfer of energy through the seat on impact. The maximum value of the pelvic acceleration in the vertical direction was 58.1 g at 0.084 s after impact.

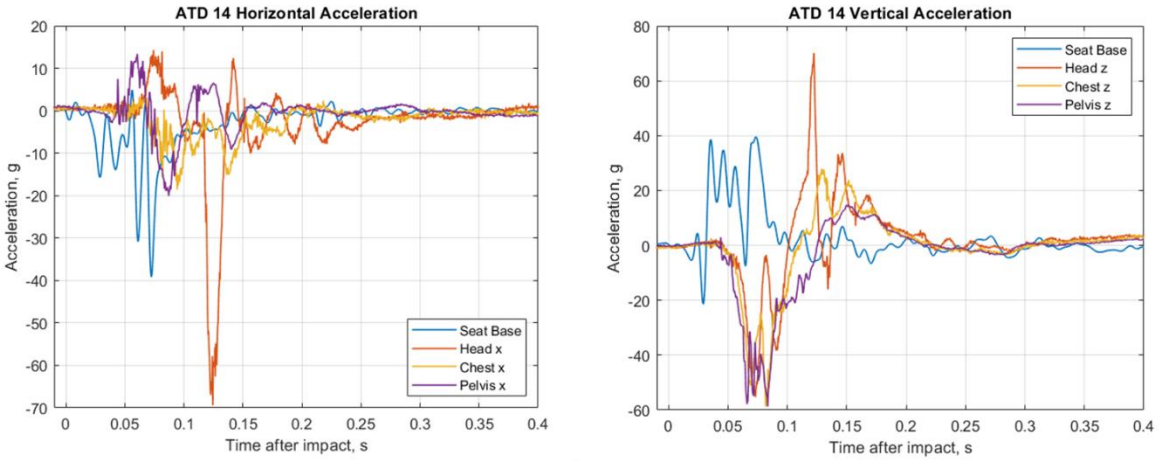

Figure 54. ATD 14 Accelerations

The lumbar loads and moment are next presented in figure 55. The compressive lumbar load measured in ATD 14 reached a peak value of approximately 2,560 lb, which was well above the injury metric requirement. Force and moment were in phase throughout the impact event indicating a continuous transition from torso extension, as the ATD was initially loaded into the seat vertically, into flexion, as it rebounded upward at approximately 0.1 s. The shape and magnitude of both the ATD kinematics and lumbar load responses were similar to ATD 8, a Hybrid II 50th also tested in the front section of the aircraft though on a plinth seat base configuration.

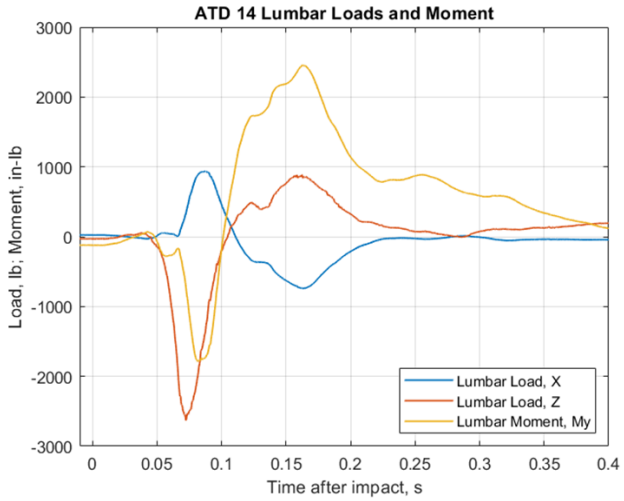

Figure 55. ATD 14 Lumbar loads and moment

The lap belt load measured on ATD 14 is shown in figure 56. The lap belt load was similar to those measured on other ATDs in the test. The compression into the seat did not create any significant tension in the belt; however, once the ATD began to rotate forward after the initial compression, the belt tension began to increase. The belt tension increased to a maximum value that was at the same approximate time as the head strike event which was typically at the maximum of torso rotation and maximum horizontal motion in the pelvis.

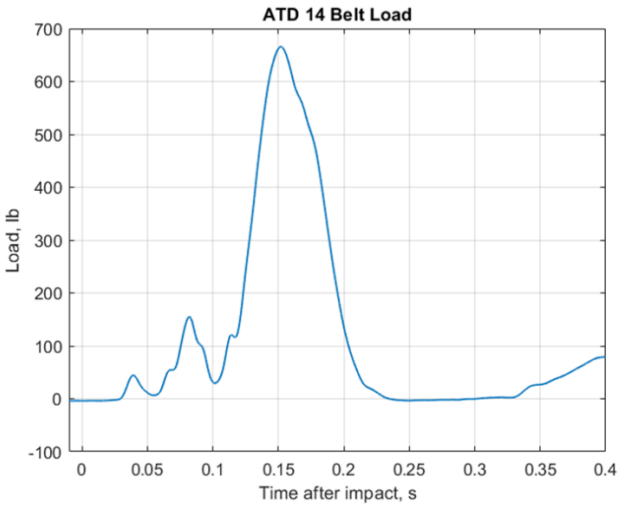

Figure 56. ATD 14 Belt loads

ATD 18 – Seat 9D

ATD 18 was a Hybrid II 50th seated in Seat 9D which was a representative exit seat configuration. An image sequence from the high-speed video is first shown in figure 57. The upper left image shows the ATD's position at impact. The upper middle image shows the ATD at its maximum vertical compression into the seat, which occurred 0.032 s after impact. The upper right image shows the maximum torso flail which occurred 0.142 s after impact. The bottom three images show maximum rebound (lower left), second forward flail due to the second nose impact (lower middle), and the ATD in its post-test position (lower right).

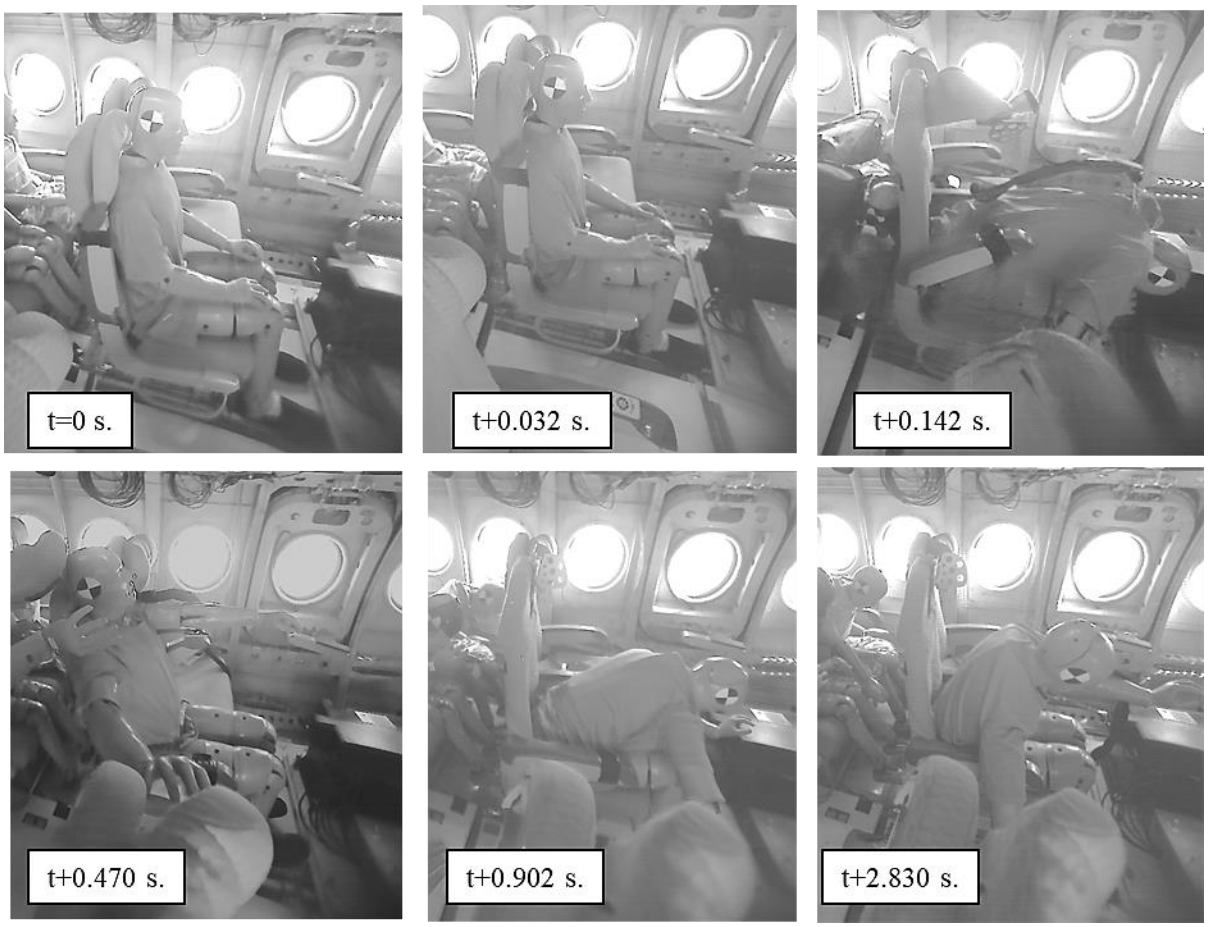

Figure 57. ATD 18 Image sequence

Accelerations in the horizontal and vertical directions are shown in figure 58. Pelvis horizontal acceleration began in the opposite direction of the seat base, then reversed direction after 0.05 s and ultimately increased to approximately 10 g higher than the peak seat base acceleration. The initial reversal and lag in pelvis acceleration was likely due to slack between the lap belt and ATD pelvis. There was a spike in pelvis vertical and horizontal acceleration at 0.11 s, but the source of this spike is not clear. Chest and head horizontal acceleration lagged seat base acceleration by approximately 0.1 s. Head horizontal acceleration spiked at approximately 0.18 s which indicated head strike with the upper leg, as there was no forward seatback. Head, chest, and pelvis vertical acceleration were in phase with the seat base though peak acceleration was magnified in the ATD to approximately double what was measured in the seat.

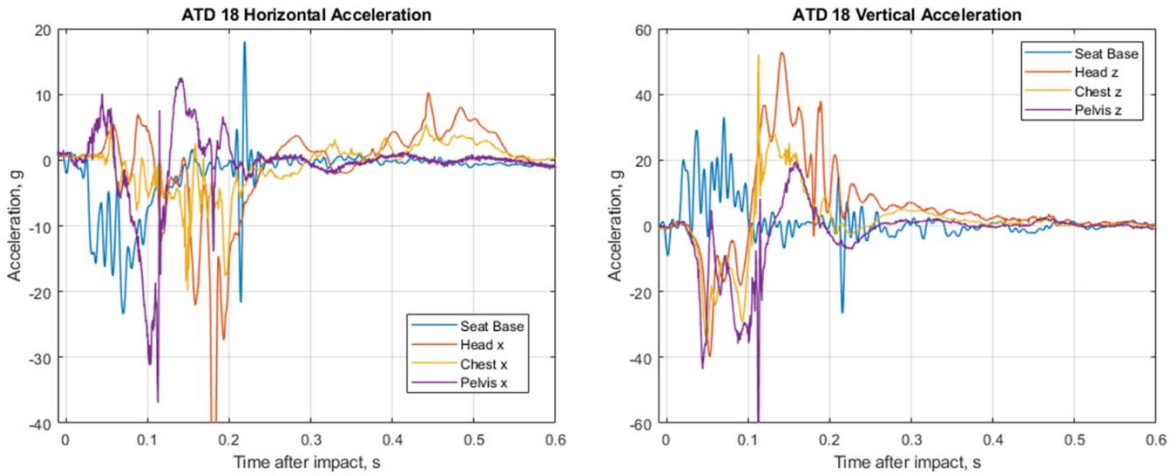

Figure 58. ATD 18 Accelerations

Next, the lumbar loads and moments are shown in figure 59. The maximum compressive lumbar force was 1,855 lb and, as with the other certification ATDs, was above the injury metric limit. The lumbar moment was in phase with the lumbar load and measured a peak flexion moment of just over 3,250 in-lb at approximately 0.14 s. Lumbar tension and shear force both also measured maximum values at this time, with the shear force measuring 1,224 lb. The lack of forward seatback to arrest the torso rotation was likely responsible for the large lumbar moment and shear force measured within this ATD.

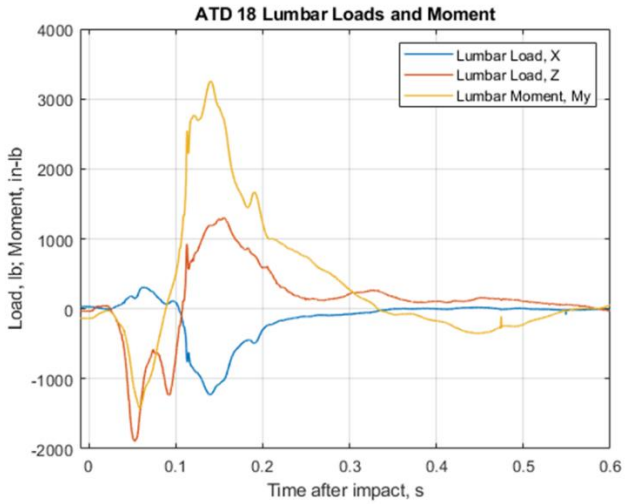

Figure 59. ATD 18 Lumbar loads and moment

ATD 20 – Seat 6B

ATD 20 was a Hybrid II 50th seated in Seat 6B and placed in a braced posture configuration. An image sequence from the captured high-speed video is shown in figure 60 with ATD 20 in the foreground. The impact position of the ATD is shown in the upper left image of figure 60. Head strike, which occurred approximately 0.04 sec after initial impact, is shown in the upper middle image. The upper right image shows the time around the maximum forward motion of the ATD. The lower three images show the ATD rebound (lower left), the second head strike event due to the secondary aircraft impact (lower middle), and a post-test position (lower right).

Figure 60. ATD 20 Image sequence

Accelerations in the horizontal and vertical directions are shown in figure 61. Horizontal acceleration in the pelvis was delayed from initial seat acceleration measured in the seat by approximately 0.04 s. Additionally, the pelvis acceleration was significantly less than both the head and chest accelerations, which saw localized peak values of 45.2 g and 50.2 g, respectively. The increased head and chest acceleration are likely due to the orientation of the ATD at impact. As the ATD torso was rotated forward with the head near the seat back, head strike occurred earlier in the impact event than the other ATDs tested. The braced position appeared to trade an earlier and longer duration head acceleration increase for the larger short duration head strike acceleration measured on the upright ATDs. Along the vertical direction, initial peak vertical occurred at 0.059 s, which was slightly delayed from the initial head strike. The peak pelvis vertical acceleration closely tracked the seat acceleration, though the vertical acceleration data in the seat was corrupted at approximately 0.1 s.

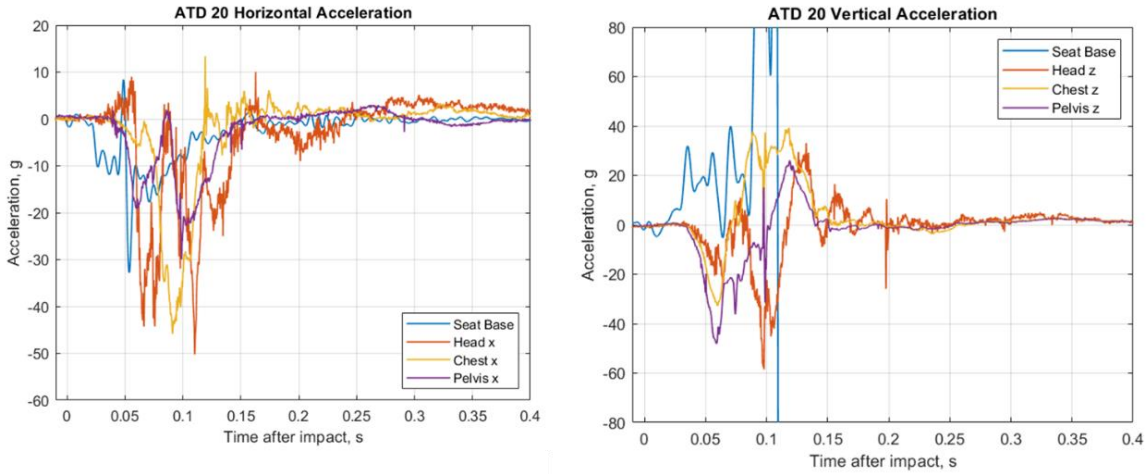

Figure 61. ATD 20 Accelerations

Figure 62 shows the lumbar loads and moments from ATD 20. When examining spinal compression, ATD 20 was the only 50th percentile ATD to measure below the 1,500 lb injury metric limit, with a peak compressive lumbar load of approximately 1,383 lb. The braced posture of this ATD likely accounted for this lower value as the vertical acceleration vector from the impact was not directly aligned with the lumbar spine load cell in this condition. Although compressive lumbar load was limited in this posture, the lumbar moment during rebound remained significant reaching a peak value of 2,817 in-lb.

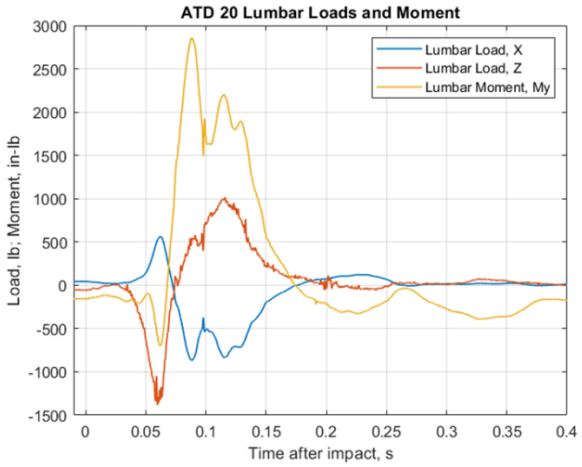

Figure 62. ATD 20 Lumbar loads and moment

Lap belt load is next shown in figure 63. A continuous belt load was measured on ATD 20, with significant belt force measured during peak horizontal motion of the ATD out of the seat. A peak belt force of 1,622 lb was measured, well above that measured on other ATDs of this size. This large belt force did correspond with the large lumbar moment measured at approximately the same time in the ATD. The large belt force may be somewhat associated with the ATD being positioned more forward in the seat due to the braced postures, and thus in more direct contact with the belt throughout the impact event.

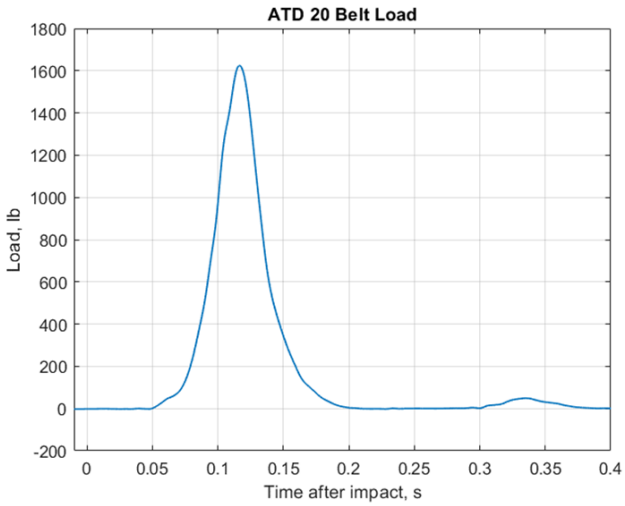

Figure 63. ATD 20 Belt load

ATD 23 – Seat 3A

ATD 23 was an FAA Hybrid III 50th seated in Seat 3A. Accelerations in the horizontal and vertical directions are shown in figure 64. Unfortunately, the horizontal seat base and ATD chest acceleration data channels were lost during the test, so only partial examination of the data could be completed. Pelvis horizontal acceleration peaked at 16.1 g, which was similar to the other ATDs of this size measured within the test. Head strike was indicated at approximately 0.115 s with a large spike in head horizontal acceleration. Pelvis, chest, and head acceleration closely tracked seat base acceleration in the vertical direction and the pelvis measured the highest vertical accelerations of the three ATD locations. The maximum value of the pelvis acceleration was 47.7 g, which occurred approximately 0.06 s after impact.

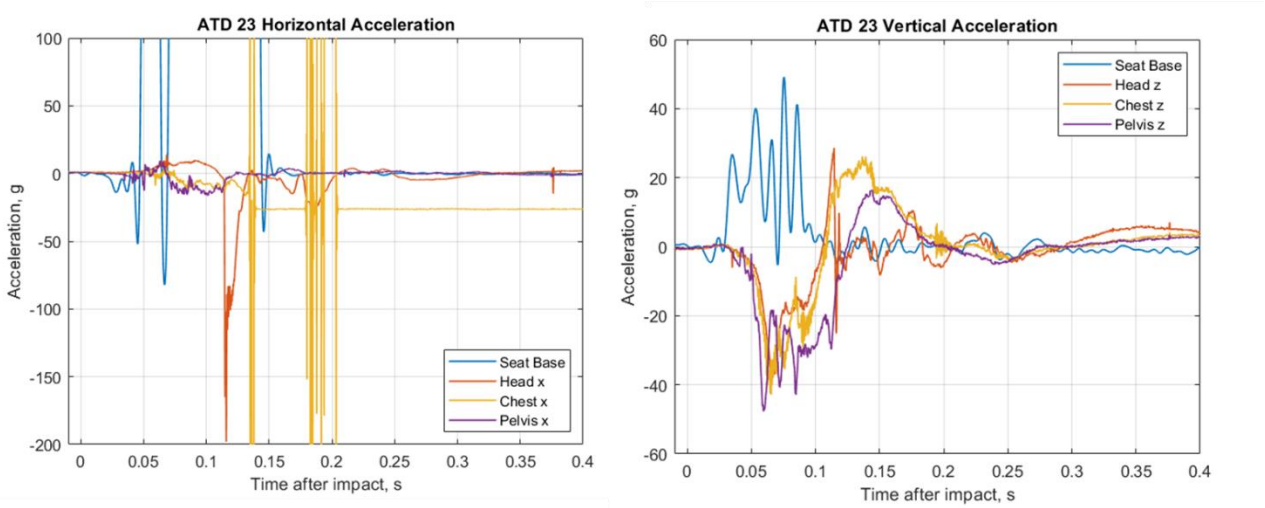

Figure 64. ATD 23 Accelerations

Head rotation is shown in figure 65. Rotation was measured about the *y*-axis, which was along the plane of the primary impact vector. The peak rotational velocity prior to head strike was 1,495 deg/s which occcurred just prior to the head strike at 0.114 s after impact. Peak rotational velocity during head strike was 4,870 deg/s. The abrupt change in the rotational rate, along with a large spike in the data indicated the head strike occurred at this time.

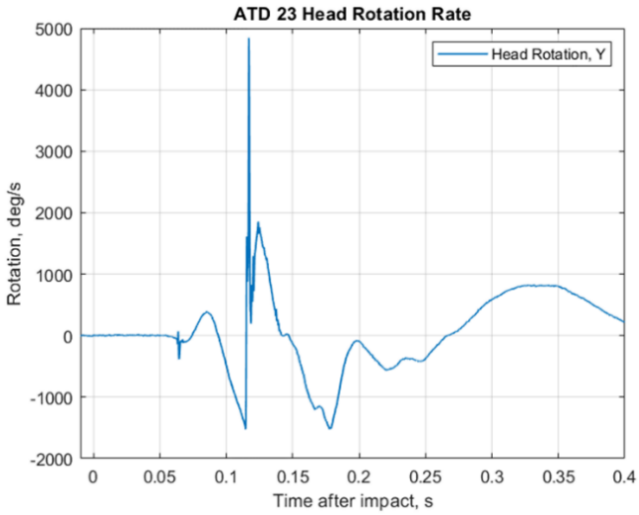

Figure 65. ATD 23 Head rotations

Figure 66 shows the upper neck load and moment measurements. The upper neck forces generally tracked the torso kinematics, with the upper neck vertical force tracking the shape of torso vertical response and upper neck horizontal force tracking the head horizontal acceleration response shape. The upper neck moment was in extension for the majority of impact, head strike did off-load this moment temporarily, but a second peak soon followed with a maximum moment of 488 in-lb.

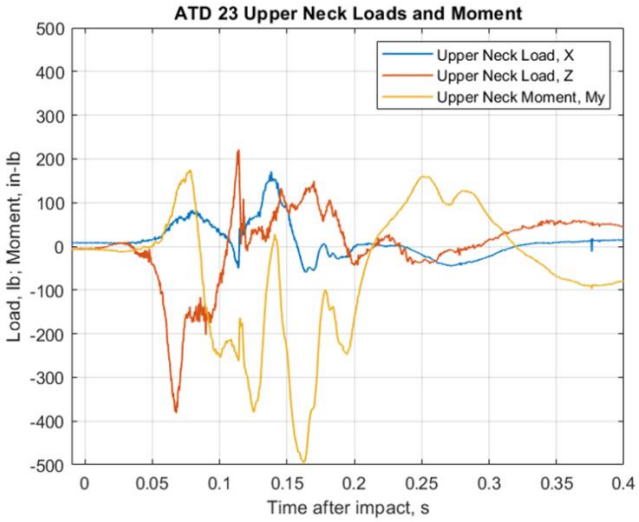

Figure 66. ATD 23 Upper neck loads and moment

Lumbar loads and moment are shown next in figure 67. The lumbar compressive load reached a maximum value of 2,105 lb which occurred at 0.074 s after impact. Following the trend of the other 50th percentile ATDs, this value was above the 1,500 lb limit. During rebound of the ATD within the seat a maximum tension force of 913 lb and a maximum flexion moment of 1,177 in-lb was measured, both of which occurred at approximately 0.15 s.

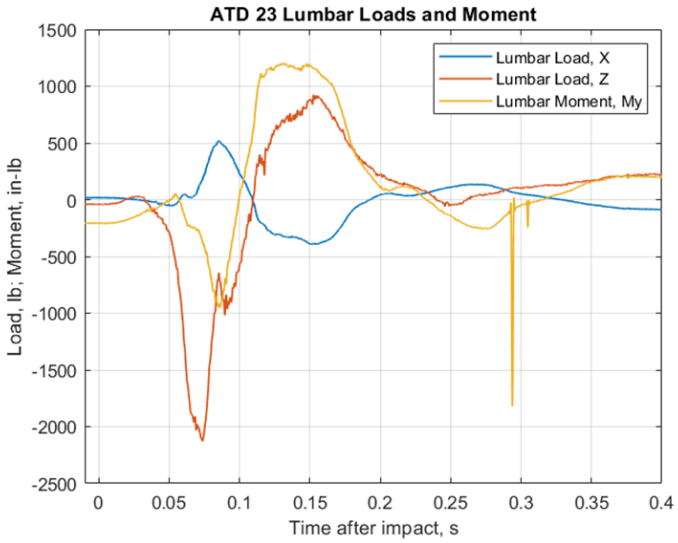

Figure 67. ATD 23 Lumbar loads and moment

ATD Results – Other Adult ATDs

The non-standard sized and type ATDs were next examined, and results are presented in this section of the report. There were three non-standard-sized ATDs and three non-standard types. These ATDs were seated in the front, middle, and rear of the cabin in order to determine the effects (if any) of seated location on response. Figure 68 shows the locations of the non-standard size or type ATDs, and table 5 provides the ATD details.

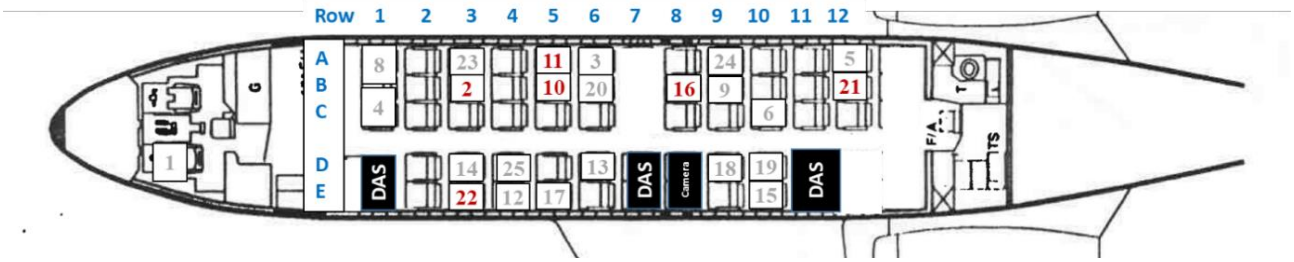

Figure 68. Non-standard sized and type ATD locations

Table 5. Non-standard sized and type ATDs

ID #	ATD Type	Size	Seat	Owner	Notes
2	WIAMan	50	3B	ARL	
10	Hybrid III	5	5B	NASA	
11	Hybrid III	95	5A	NASA	
16	THOR	“Obese”	8B	Humanetics	
21	WIAMan	50	12B	ARL	
22	THOR	50	3E	NHTSA	

The ATDs that will be covered in this section are the Hybrid and THOR ATDs only. The WIAMan ATDs will be a subject of a separate report.

ATD 10 – Seat 5B

ATD 10 was a Hybrid III 5th percentile female seated in Seat 5B which was next to a Hybrid III 95th percentile male. An image sequence captured from the high-speed video is shown in figure 69, with ATD 10 in the foreground of the images. The upper left image shows the ATD at impact. Over the first 0.054 s ATD 10 was loaded vertically into the seat, with the torso remaining primarily upright, which is shown in the upper middle image. After this point, the torso began forward rotation ultimately impacting the forward seatback at approximately 0.0128 s after impact. Due to the shorter torso length of the 5th percentile female ATD, the torso underwent greater rotation than the larger ATD sizes before the head impacted the seat back, resulting in the contact being with the top of the head rather than the ATD face. After the primary impact occurred the ATD rebounded into its seat at 0.552 s which is shown in the lower left image, and then rotated forward again during the second aircraft impact, which is shown in the lower middle image. Finally, as the lower right image shows, the ATD came to rest turned laterally out of the seat after the impact event. During the impact, the lap belt came unbuckled which allowed the ATD to wind up out of its seat in this position; however, the precise timing of when the belt became unbuckled could not be determined. The belt was observed to be connected during the rebound of the first impact, and first image that the unbuckled belt can be observed occurred 0.682 s after impact, so it is presumed that the beginning of the secondary impact, which is shown in the lower left image in figure 69 is the approximate time the unbuckling event occurred.

Figure 69. ATD 10 Image sequence

Accelerations in the horizontal and vertical directions are next shown in figure 70. The pelvis horizontal acceleration measured in ATD 10 did not align with the seat base acceleration as measured in the other ATDs within this test. Acceleration occurred in the opposite direction from the seat base for the majority of the initial impact with a short duration change in direction at 0.075 s. Chest horizontal acceleration did track the seat base while head horizontal acceleration peaked approximately 0.05 s after chest and was magnified by approximately 10 g. Head strike was indicated at 0.015 s by a large spike in head horizontal acceleration. This spike appeared in head vertical acceleration, of similar magnitude likely due to the fact that the top of the head impacted the seatback rather than the face as in the majority of the other adult ATDs tested. Chest and pelvis acceleration in the vertical direction were magnified to double the seat base vertical acceleration. Head vertical acceleration showed sharp reversal in direction at 0.075 s; however, the source of this reversal is unclear.

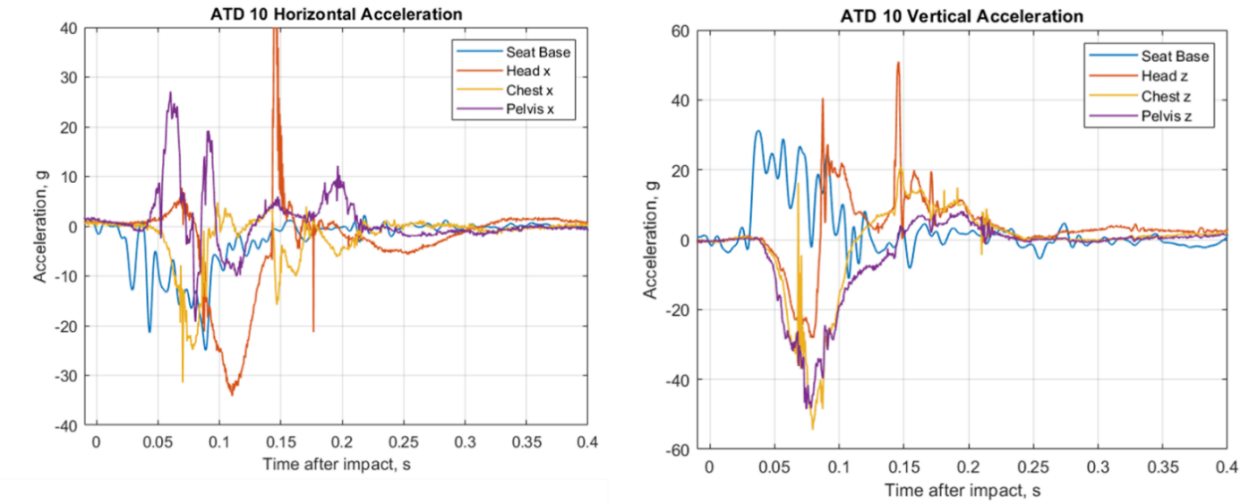

Figure 70. ATD 10 Accelerations

Head rotation rate is shown in figure 71. Head rotation was measured about the *y*-axis along the primary plane of impact. Peak rotation was measured approximately 0.093 s after impact at 3,093 deg/s. Head strike was indicated by the abrupt change in the signal at 0.144 s. Note that unlike the larger ATDs, the head of ATD 10 was allowed to fully rotate through its range of motion, which was indicated by the parabolic shape of the rotation rate in the negative direction, then trending back to the positive direction before the head strike event occurred.

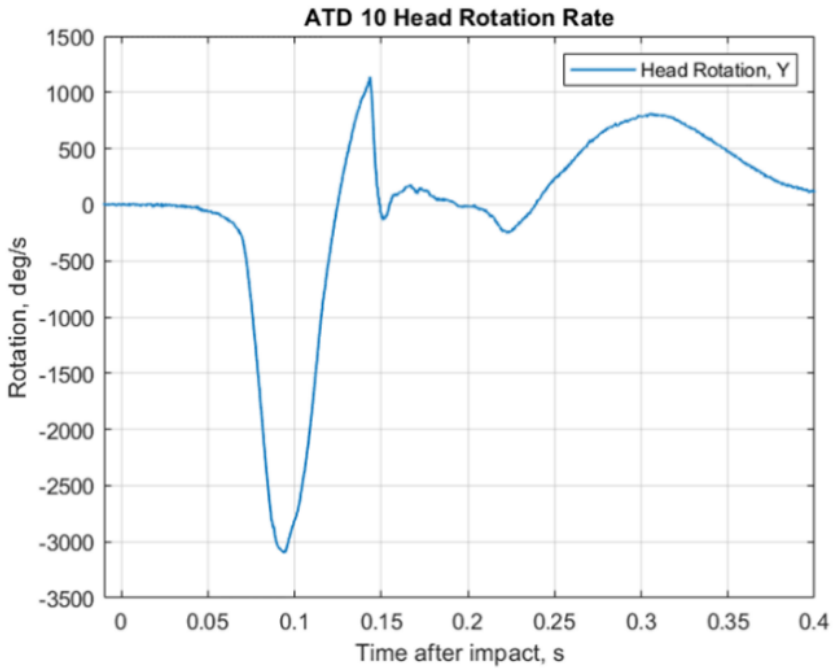

Figure 71. ATD 10 Head rotation rate

Upper neck forces and moment are next shown in figure 72. Upper neck forces measured in ATD 10 tracked the inertial response of the ATD head, with the force response shapes matching the acceleration response along each direction during the inertial phase of the impact. Upper neck horizontal force did not indicate any changes due to head strike, indicating the load cell was aligned perpendicularly to the contact force.

Upper neck vertical force recorded its highest peak during head strike with a compressive force of 314 lb. Neck moment exhibited a peak value in flexion prior to head strike of 296 in-lb.

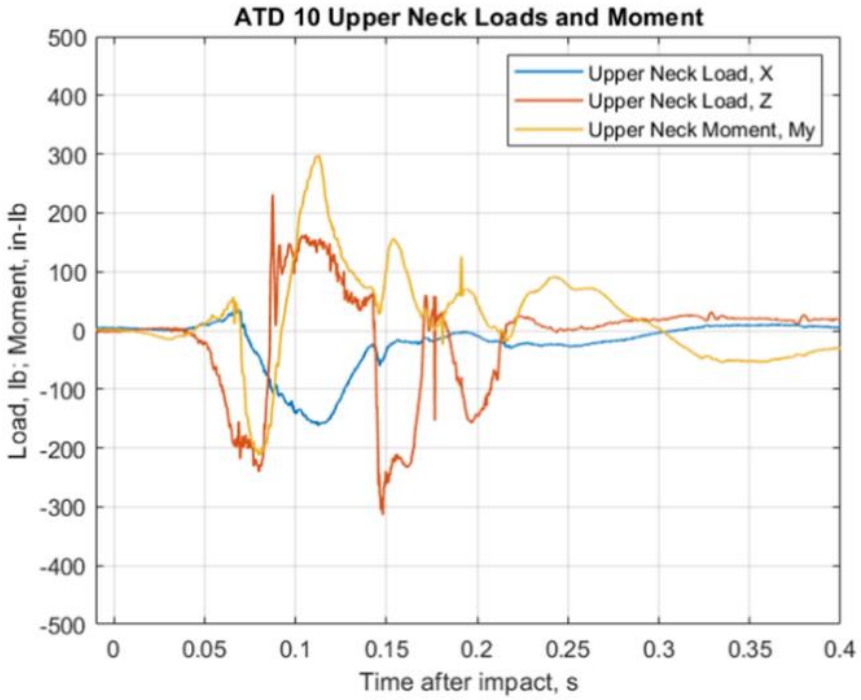

Figure 72. ATD 10 Upper neck loads and moment

Figure 73 next shows the lumbar forces and moments recorded for ATD 10. The maximum lumbar spine compressive force recorded was approximately 706 lb. This value was below the 933 lb limit used for the Hybrid III 5th female ATD, which has been scaled down from the 1,500 lb limit of the 50th percentile male ATD [23]. The lumbar spine moment, similar to the pelvis horizontal acceleration, was much different in this ATD than the other adult ATDs tested. The moment plot indicated flexion from the start and remained in that direction throughout the impact, reaching a maximum value at the same approximate time as the lumbar compression maximum. The other ATD configurations generally began in extension, transitioning to flexion in the upward rebound. It is difficult to discern precisely what drove the differences between the Hybrid III 5th and other ATD sizes, though it is possible that its smaller size and weight caused differences in seat compression and horizontal motion from the larger ATDs.

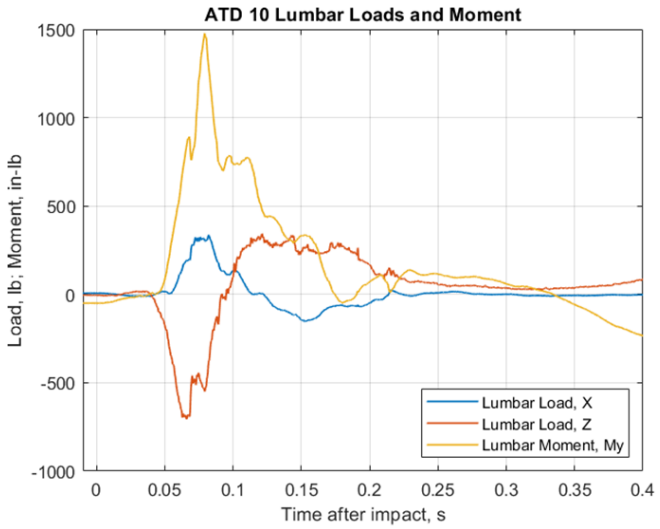

Figure 73. ATD 10 Lumbar loads and moment

The lap belt load measurements are next shown in figure 74. The belt loads, though lower than the rest of the ATDs measured, did not indicate a behavior during the primary impact which could be attributed to the differences observed in the response of this ATD. The belt loading curve had a similar curve shape to the other lap belts measured and indicated that the belt was attached for at least the initial impact event. The maximum value of the lap belt load measured was 261 lb, which occurred 0.13 s after impact, and was at the same approximate time that the ATD underwent maximum forward motion.

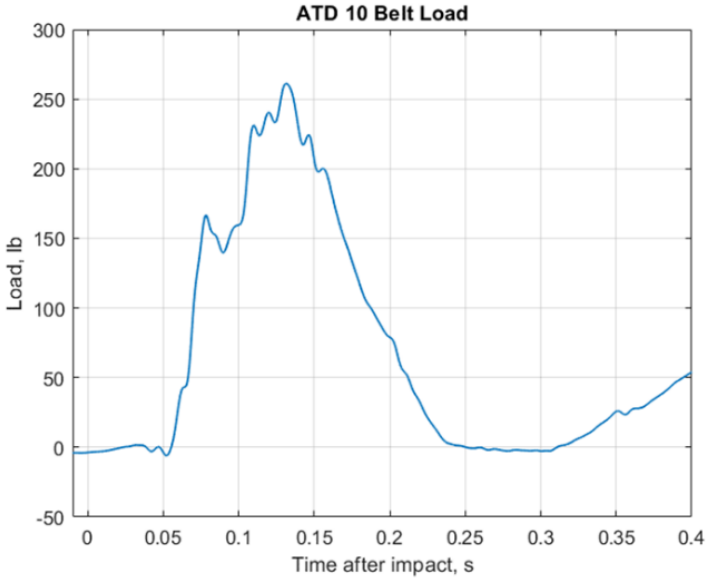

Figure 74. ATD 10 Belt load

ATD 11 – Seat 5A

ATD 11 was a Hybrid III 95th male seated in Seat 5A. An image sequence from the high-speed camera is shown in figure 75, with ATD 11 in the background. The upper left image shows the ATD at impact. At approximately 0.054 s after impact, the ATD experienced its maximum vertical deflection into the seat, which is shown in the upper middle image. After the maximum vertical deflection, the ATD began to rotate

forward, eventually striking the seat back 0.094 s after impact, which is shown in the upper right image. Head strike with the forward seatback occurred earlier in this ATD compared to other ATD sizes due to its longer torso. After the initial head strike the ATD rebounded into the seat at 0.552 s, which is shown in the lower left image, and then re-struck the forward seatback at 1.0 s. In its post-test configuration, the ATD settled close to its original position within the seat, which is shown in the lower right image.

Figure 75. ATD 11 Image sequence

Accelerations in the horizontal and vertical directions are next shown in figure 76. The horizontal pelvis acceleration tracked the seat base acceleration closely, which indicated a tight connection to the seat through the lap belt on this ATD. Chest horizontal acceleration lagged the pelvis, while head lagged the chest. A large spike in head horizontal acceleration was observed at approximately 0.113 s, which indicated a head strike event occurred. There are a few smaller spikes in the acceleration response in the head, occurring at 0.163 s and 0.337 s, indicating the size of this ATD generated measurable secondary and tertiary head strike events. In the vertical direction, head, chest, and pelvis closely tracked each other, with maximum values of 34.6 g, 34.5 g, and 23.6 g occurring in the pelvis, chest, and head, respectively.

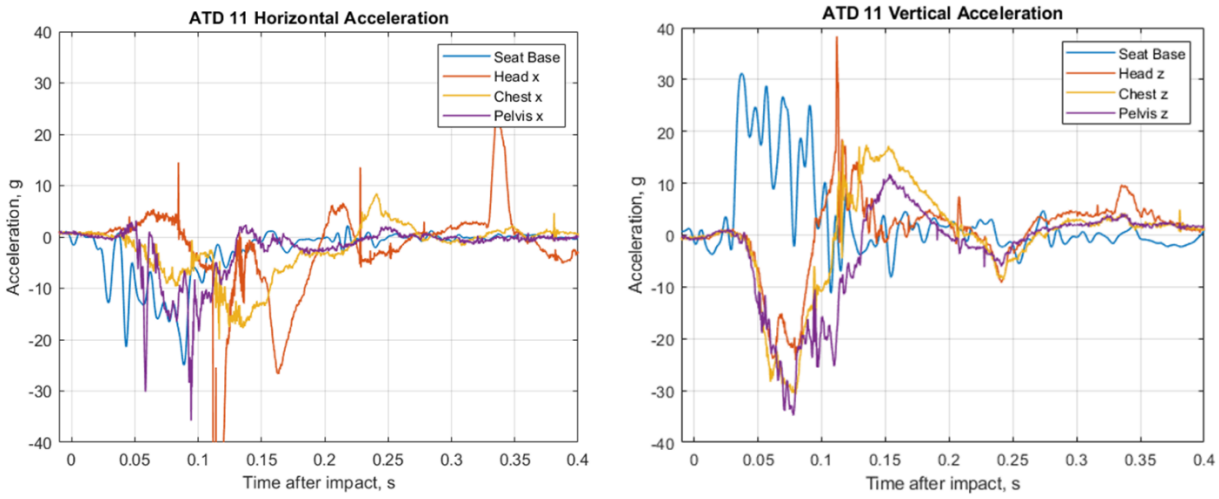

Figure 76. ATD 11 Accelerations

Figure 77 shows the head rotations rate along the axis of motion. The head strike event is further verified in the head rotation rate time history noting that an abrupt change in the direction of the rotation occurred 0.113 s after impact. This matches the head horizontal acceleration data spike at this time. Prior to the head strike event, the maximum rotational rate the head experienced was 1,192 deg/s.

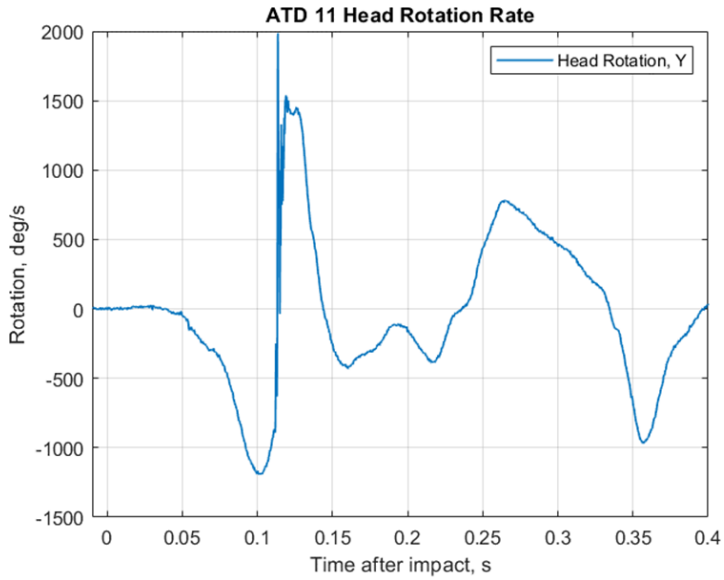

Figure 77. ATD 11 Head rotation

Figure 78 shows the measured forces and moment from the upper neck load cell in ATD 11. Upper neck forces and moments measured in ATD 11 were similar to other ATDs measured within the test article. The largest neck force was measured during head strike in which neck compression reached 550 lb. Neck moment was highest later in the impact event with peak moment of 397 in-lb, at approximately 0.164 s after impact.

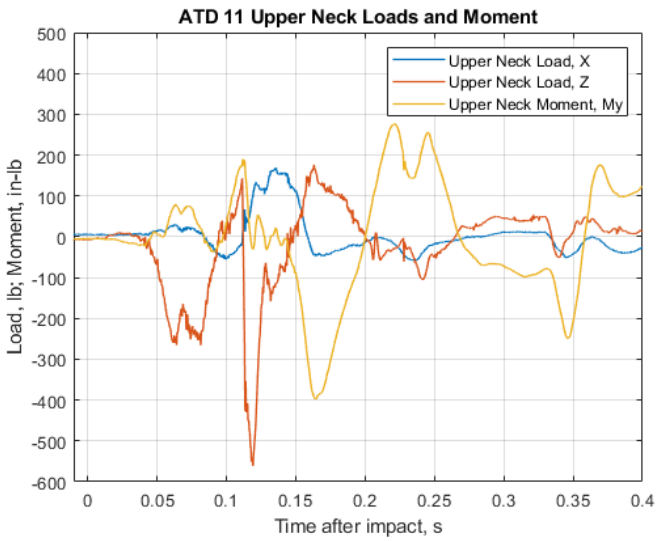

Figure 78. ATD 11 Upper neck loads and moments

Figure 79 shows the lumbar load and moment measurements obtained from ATD 11. The maximum compressive lumbar load in ATD 11 was approximately 1,781 lb, which occurred 0.067 s after impact. Although ATD 5 has a larger torso mass than the certification ATDs, the measured compressive lumbar load was relatively low in comparison. This result can be attributed to the configuration of the Hybrid III 95th, which has a curved lumbar spine, as opposed to the straight spines present in the Hybrid II and FAA IIII 50th certification ATDs. The curved shape of the lumbar spine would be expected to result in a greater portion of the vertical acceleration translating into bending rather then compression compared to the straight spine. This behavior corresponds with the outputs measured in this ATD. Lumbar spine extension moment peaked at the same time as compressive force and then transitioned into flexion as the lumbar spine went into tension. A large lumbar flexion force was recorded during this rebound phase with a maximum value of 3,404 in-lb.

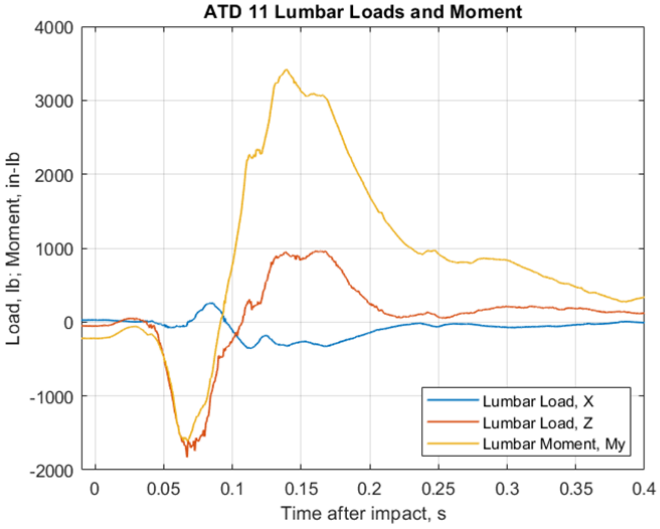

Figure 79. ATD 11 Lumbar loads and moments

The lap belt load measurements are next shown in figure 80. A continuous belt force was measured on the lap belt load cell of ATD 11, indicating the belt did not fail during the test event. Belt force began increasing

at 0.05 s which matched the time at which pelvis horizontal acceleration began increasing in the ATD. Peak belt force measured just 872 lb, which was also within the range of belt forces measured on the 50th percentile ATDs and well above the belt force measured on the Hybrid III 5th seated next to ATD 11.

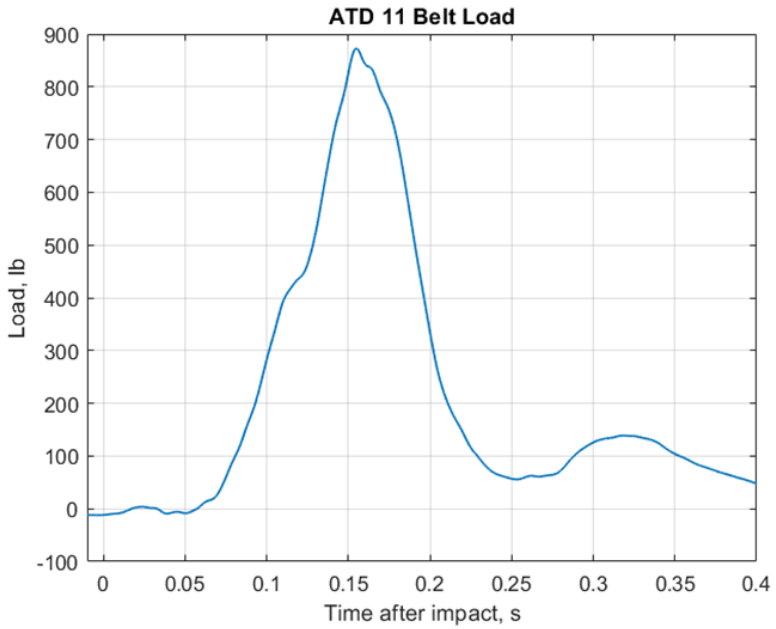

Figure 80. ATD 11 Belt load

ATD 16 – Seat 8B

ATD 16 was an Obese THOR ATD seated in Seat 8B. The Obese ATD did not include any internal load cells so the only measurements that were collected were from the internal accelerometers only. The Obese ATD had a similar kinematic instrumentation set as the hybrid and THOR ATDs, with sensors in the head, chest, and pelvis. In addition, the ATD had two load cells measuring lap belt loads attached to either side of the ATD. The Obese ATD was secured using the standard lap belt which included a seat belt extender, and the two load cells were used because it was deemed necessary to measure loads on either side of the extender. Accelerations in the horizontal and vertical directions are shown in figure 81.

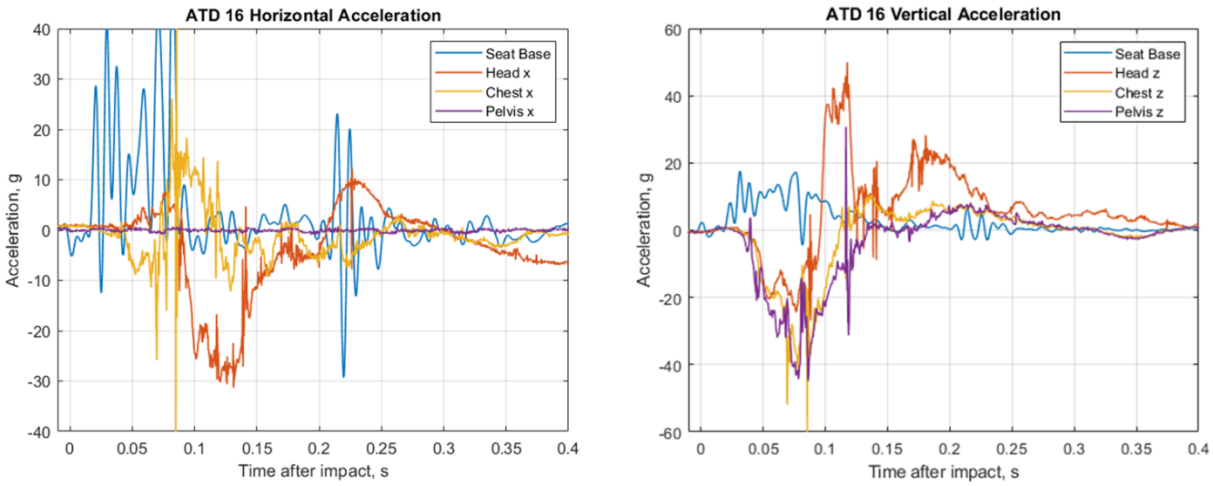

Figure 81. ATD 16 Accelerations

In the horizontal direction, acceleration in the head and chest lag behind the seat base accelerations. Head horizontal acceleration was similar in magnitude to the peak average seat base acceleration, while chest acceleration was approximately 10 g lower than head acceleration. The pelvis horizontal accelerometer did not appear to measure any significant acceleration. In the vertical direction, pelvis and chest vertical acceleration had a magnitude of more than double that measured in the seat base. These results indicated that the magnification in ATD vertical acceleration through the seat foam increased with the larger occupant mass. Head vertical acceleration was not magnified and closely tracked the seat base acceleration. The difference in head vertical acceleration was likely due to flexibility in the upper torso and neck within the THOR ATD which reduced vertical alignment between the chest and head throughout the vertical loading phase compared to the Hybrid II and III ATDs.

The lap belt load measurements are next shown in figure 82. The two load cells instrumented on either side of the lap belt of ATD 16 did not measure equal force within the belt. The right belt measured 633 lb and the left belt measured 416 lb. However, the peak forces did occur in either side of the belt simultaneously at approximately 0.21 s after impact. A variety of factors could be responsible for this discrepancy in loads. The ATD mass may have not been centered between the load cells, causing one side to take more force. Additionally part of the belt may have been caught between the torso and pelvis as it rotated forward causing it to pull the belt unequally as the pelvis moved forward. Lastly, significant damage was observed to the ATD pelvis post test, the damage to the ATD structure may have altered the symmetry of its motion and caused this unequal loading of the belts.

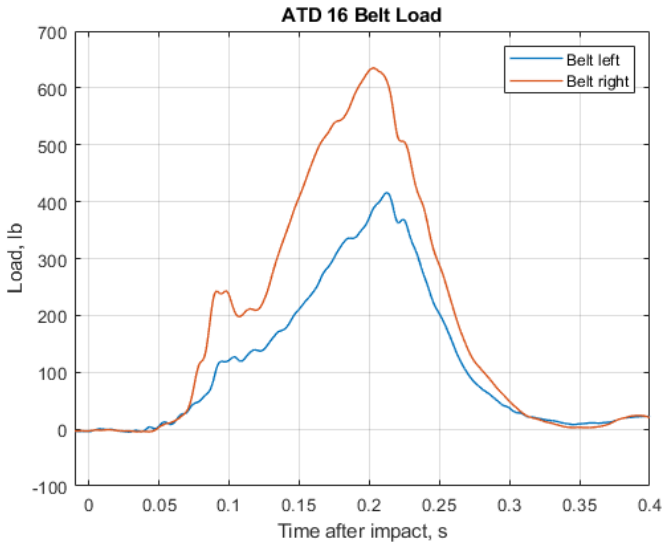

Figure 82. ATD 16 Belt loads

The post-test condition of ATD 16 is shown in figure 83. The ATD pelvis was damaged during the impact event. This resulted in the torso being flexed forward between the knees and the right femur joint of the ATD separating from the pelvis. The THOR Obese ATD configuration tested was a concept prototype still in the developmental stages, these results will be used to improve its durability under dynamic loading environments in the future.

Figure 83. ATD 16 Post-test position (left), and pelvic to femur joint separation (right)

ATD 22 – Seat 3E

ATD 22 was a THOR 50th percentile located in Seat 3E. An image series obtained from the high-speed video is shown in Figure 84, with ATD 22 shown closest to the window in the background. ATD 22 was loaded vertically over the first 0.06 s after which point it began to rotate forward. Unlike the Hybrid II seated next to it, the torso of ATD 22 did not move forward significantly; rather it rotated downward upon itself. The head of ATD 22 rotated about the lower neck causing the ATD's chin to fold into its chest. After ATD 22 folded downward, it began to translate horizontally, with the head ultimately becoming wedged underneath the forward seatback. The ATD remained in this position, wedged under the forward seatback, throughout the remainder of the impact and was found this way during post-test inspections.

Figure 84. ATD 22 Image sequence

Accelerations in the horizontal and vertical directions are shown in figure 85. Pelvis horizontal acceleration began in the opposite direction of the seat base at 0.05 s after impact, then reversed direction at 0.025 s after which point it tracked the seat base acceleration. These results indicated a significant delay in horizontal force being transferred from the seat into the pelvis, potentially due to a gap between the pelvis and the belt or slippage of the belt. Due to failure of the belt load cell, the source can not be verified. Both chest and head horizontal acceleration were larger in magnitude than the pelvis acceleration with head acceleration showing the largest horizontal acceleration though it peaked much later in the impact. A long duration head contact was indicated in both acceleration directions and head rotation rate, which is shown in figure 86 at just before 0.1 s. At this point head horizontal acceleration increased, vertical acceleration reversed direction, and rotation rate increased significantly. Based on the high-speed video data, it appeared this event occurred when the ATD chin struck its upper torso. Head strike with the forward seatback occurred at approximately 0.15 s, indicated by a reversal in horizontal acceleration direction and a hump in both vertical acceleration and rotation rate. The effect of the head strike with forward seatback was minimal in this ATD as its relative forward velocity was low at the time of contact. Pelvis and chest vertical acceleration closely tracked the seat base throughout the impact event.

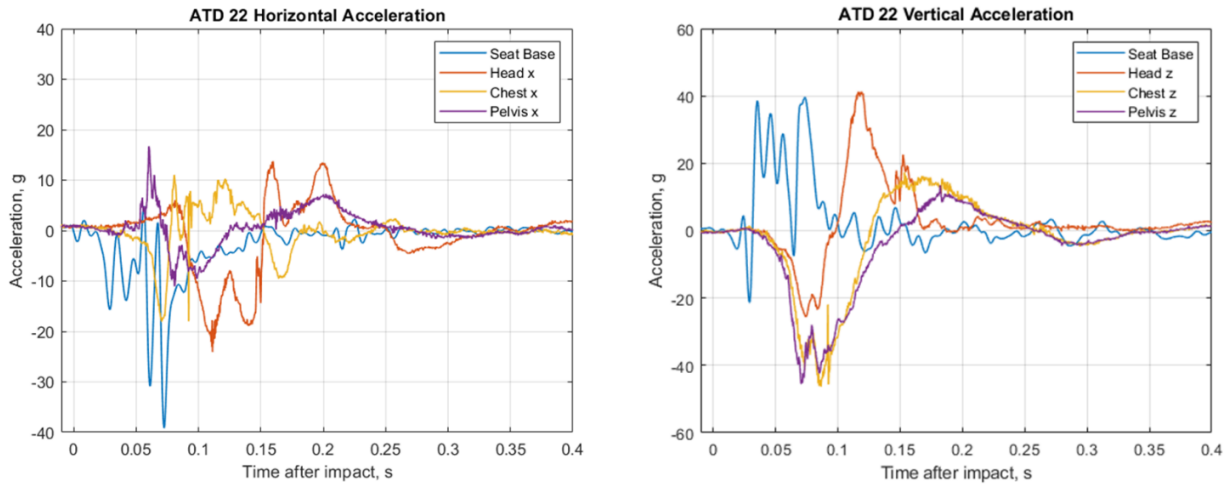

Figure 85. ATD 22 Accelerations

The rotation rate of the head is shown in figure 86. The rotation rate reached a minimum value of 3,897 deg/s which occurred 0.114 s after impact. It was at this approximate time that the head folded into the chest. The ATD's head tucking under the seatback can be observed at approximately 0.15 s where there was a slight hump in head rotation rate. The minimal change in head rotation at this time further indicated the head tucking under the seat was a low-energy impact event.

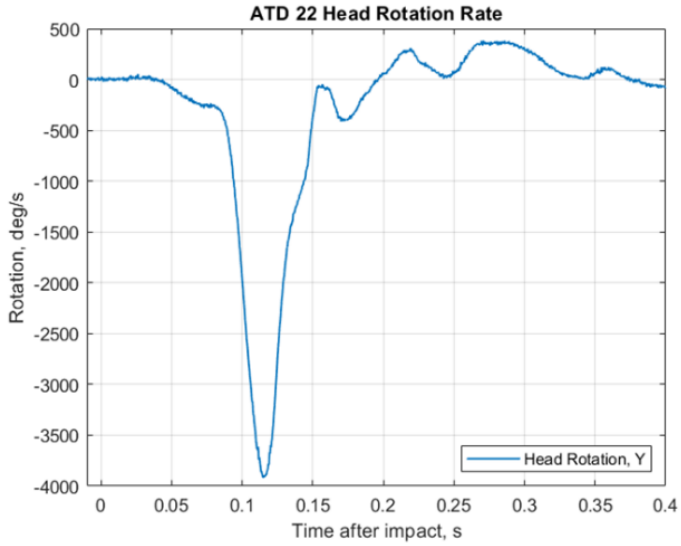

Figure 86. ATD 22 Head rotation rate

Figure 87 shows the loads and moments from both the upper and lower neck load cells. ATD 22 exhibited upper neck compression and flexion until the head contacted the chest at which point the upper neck experienced tension and extension. Shear force in the neck increased until approximately 0.15 s when the head appeared to tuck under the forward seatback. A very large lower neck flexion moment was measured in ATD 22, which corresponded with the kinematics observed in the high-speed video. The post-test position of the head tucked under the forward seatback sustained a flexion moment in the ATD throughout the impact event. Lower neck shear force was similar in magnitude to that measured in the upper neck, and lastly it appeared that the lower neck vertical force channel was lost during the test.

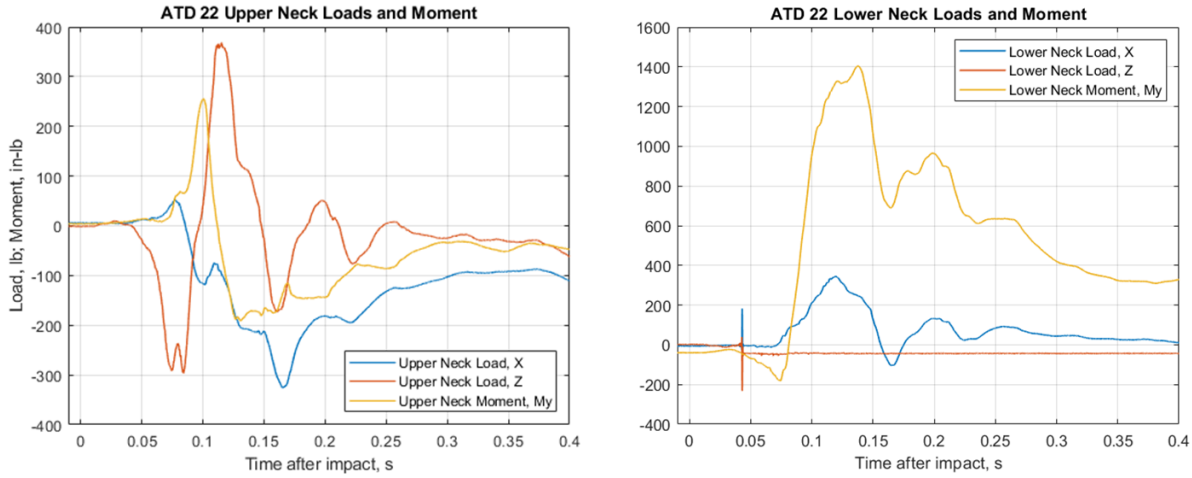

Figure 87. ATD 22 Neck loads and moments

Figure 88 shows the lumbar loads and moment from ATD 22. In the vertical direction, the ATD measured a maximum of 1,551 lb of compressive lumbar load which occurred 0.085 s after impact. It was at this approximate time that the ATD also experienced the maximum lumbar extension moment of 2,560 in-lb. The compressive load was lower than the other 50th percentile ATDs tested while the extension moment was higher. These differences are explored in more detail in the "ATD Results – Comparative Analyses" section. ATD 22 also did not exhibit any significant rebound within the seat after the primary impact event, with very little spinal tension and no flexion moment. Lumbar shear force was minimal within this ATD.

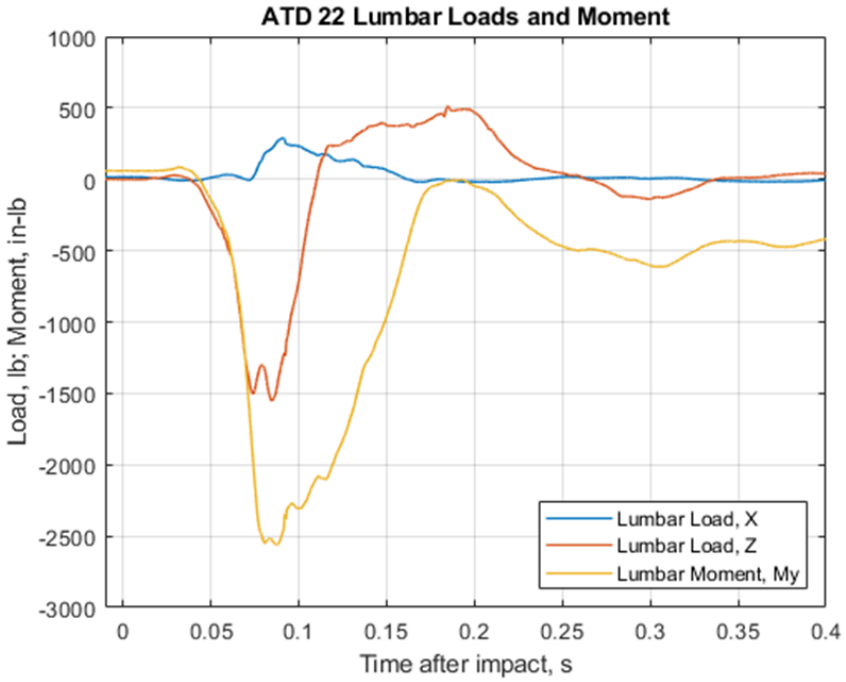

Figure 88. ATD 22 Lumbar loads and moment

The lap belt load cell on the lap belt of ATD 22 measured an anomalous signal, which was likely due to the cable severing during the impact, and therefore is not plotted in this section.

ATD Results – Child ATDs

The child ATDs were located in the highlighted rows in figure 89 and identified in table 6. There were six different types of ATDs seated in configurations recommended by the FAA, with the smallest being a Q1 child, and the largest being 10 YO sized. Note that most did not include lumbar load cells to measure spinal compression, so most comparisons utilized the head accelerations and belt loads to gain an understanding of how the child responded during the test.

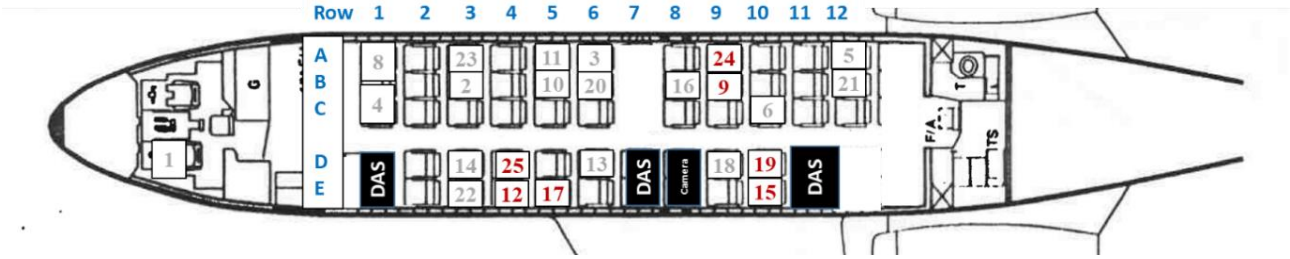

Figure 89. Child ATD locations

Table 6. Child ATD locations

ID #	ATD Type	Size	Seat	Owner	Notes
9	Hybrid III	3 YO	9B	NASA	
12	Hybrid III	6 YO	4E	NASA	
15	Hybrid III	10 YO	10E	NASA	
17	Q1	Q1	5E	FAA	CARES restraint
19	LODC	10 YO	10D	NHTSA	
24	Hybrid III	3 YO	9A	FAA	CARES restraint
25	CRABI	18mth	4D	FAA	

ATD 9 – Seat 9B

ATD 9 was a Hybrid III 3 YO sized child seated in Seat 9B. This ATD was placed in this seat to be used for comparisons with the ATD seated in Seat 9A, which included the CARES device. It only contained instrumentation in the head, along with a load cell on the lap belt. The accelerations in the head are shown in figure 90. In the horizontal direction, the head acceleration lagged the seat base acceleration by approximately 0.1 s. There were two distinct events in the horizontal acceleration, with the first occurring at approximately 0.1 s after impact and the second occurring at approximately 0.183 s after impact. The shape of the pulses was roughly triangular; however, the data was noisy so peak value numbers were hard to identify. In the vertical direction, there are two distinct events that occurred. The first, which began 0.022 s after impact, reached a minimum value of 50.8 g approximately 0.048 s after impact. It was during this time that the ATD was experiencing downward motion into the seat foam. After the downward motion, the ATD experienced a rebound, signified by positive vertical acceleration, which reached a maximum value of 30.1 g, approximately 0.124 s after impact.

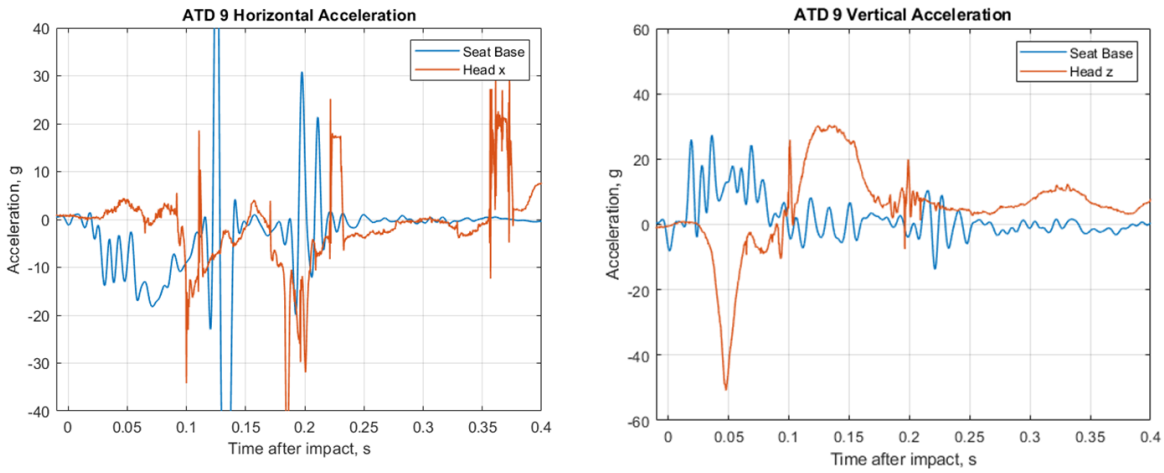

Figure 90. ATD 9 Accelerations

Figure 91 shows the lap belt load in the ATD. There are two distinct peak values that occurred in the data. The first, which measured a value of 488 lb, occurred 0.081 s after impact, while the second value reached 439 lb, and occurred 0.15 s after impact. These two peaks occur just prior to the two peaks measured in head horizontal acceleration. This response indicates the ATD experienced a bouncing motion within the seat in which it pushed forward into the lap belt during the intial impact, rebounded into its seatback, and then bounced again into the lap belt as it rebounded upward in the seat from the vertical load.

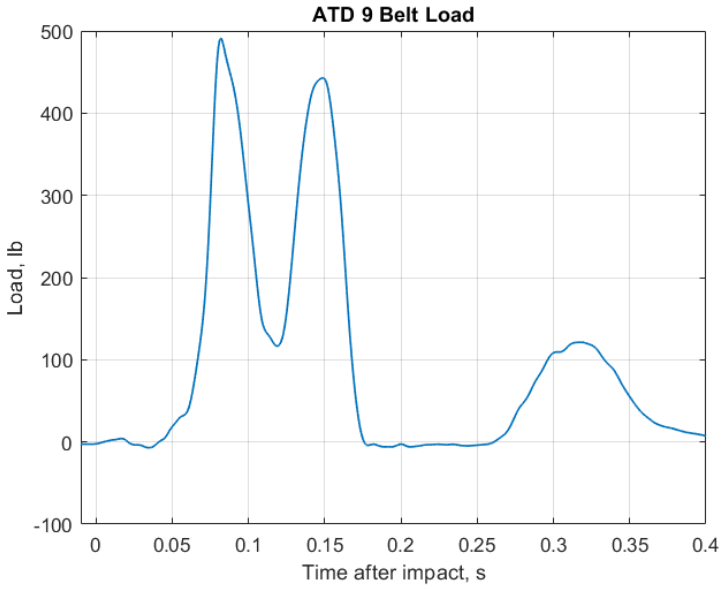

Figure 91. ATD 9 Belt loads

ATD 12 – Seat 4E

ATD 12 was a HIII 6 YO ATD, which was uninstrumented during the test. Therefore, there are no results to report.

ATD 15 – Seat 10E

ATD 15 was a Hybrid III 10 YO ATD seated in Seat 10E. It was placed in this seat such that it could be compared to the LODC 10 YO. It contained instrumentation in the head, neck, pelvis and lumbar regions, recording accelerations, forces and moments. Figure 92 first shows the horizontal and vertical accelerations for the head and pelvis. In the horizontal direction, the pelvis acceleration tracked that of the seat base. The acceleration reached a local peak of 20.2 g, which occurred 0.049 s after impact. The acceleration then turned positive, indicating the beginning of the ATD forward rotation. In the head, the acceleration lagged seat base and pelvic response, reaching 13.7 g approximately 0.094 s after impact. In the vertical direction, both head and pelvis exhibited similar responses until approximately 0.54 s after impact. The pelvis acceleration reached a minimum value of 31.4 g while the head reached a minimum value of 24.5 g before returning positive.

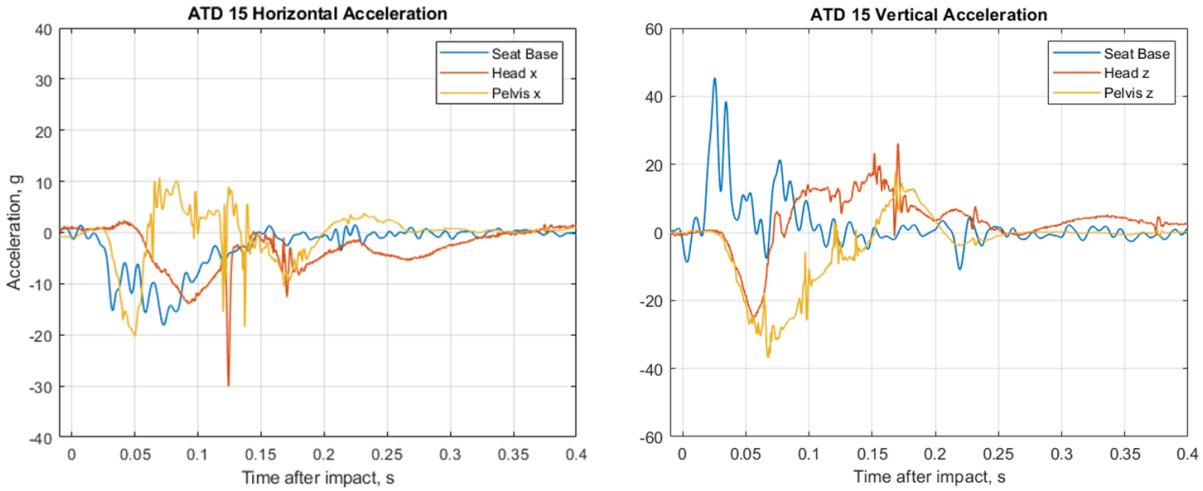

Figure 92. ATD 15 Accelerations

Neck loads and moment were next examined and shown in figure 93. The upper neck measured a compressive vertical load of 196 lb approximately 0.057 s after impact. After this point, minimal response was indicated until neck moment peaked in extension at 0.173 s after impact. It was difficult to determine the magnitude of this event due to noise in the moment signal, but the magnitude was in the range of 200 in-lb.

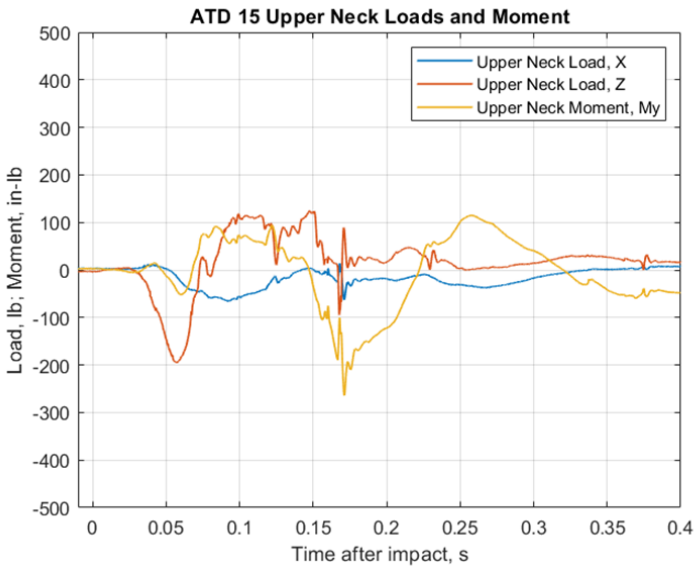

Figure 93. ATD 15 Upper neck load and moment

Figure 94 next shows the lumbar load and moment in ATD 15. Both the lumbar vertical load and the lumbar moment registered peak values at the same approximate time of 0.058 s after impact. The maximum lumbar compressive load was 928 lb, while the maximum lumbar flexion moment was 1,209 in-lb. The moment then went into extension and reached a maximum value of 933 in-lb, which occurred 0.145 s after impact. The timing of the shear load peaks closely tracked the other measurements. The maximum shear load was 405 lb, which occurred 0.058 s after impact, and the minimum was 210 lb, which occurred 0.144 s after impact.

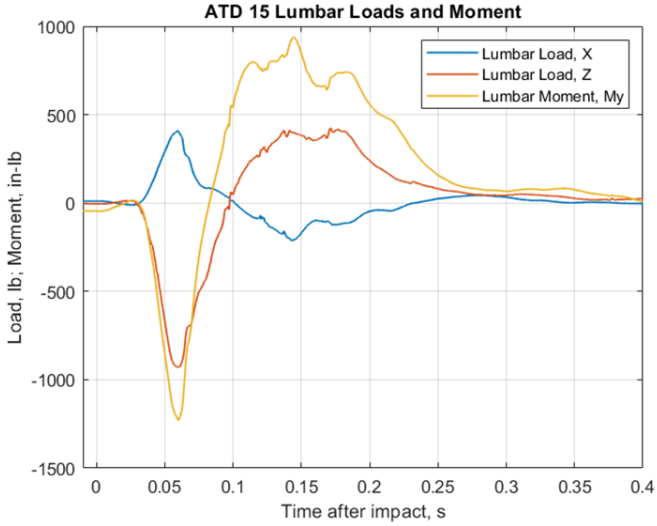

Figure 94. ATD 15 Lumbar load and moment

ATD 17 – Seat 5E

ATD 17 was a Q1 child seated upright in Seat 5E restrained via the lap belt and the CARES device. The Q1 child only had sensors in the head and neck, along with a lap belt load cell. The accelerations measured

in the head are first shown in figure 95. In the horizontal direction, the head acceleration slightly lagged the seat base acceleration. The head acceleration reached a minimum value of 30.8 g at approximately 0.085 s after impact. After this event, there was a second event that occurred at 0.211 s after impact. This event was the head strike of the ATD head against its seat back. In the vertical direction, the acceleration reached a minimum value of 28.5 g, which occurred 0.065 s after impact. The ATD then began to rebound and ultimately reached a minimum acceleration of 38.1 g which occurred 0.119 s after impact.

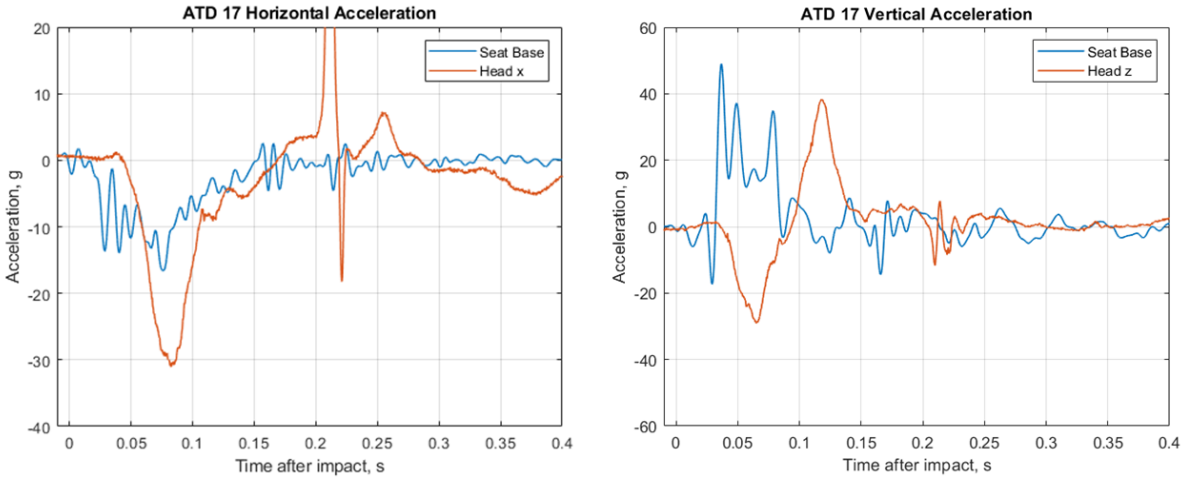

Figure 95. ATD 17 Accelerations

Upper neck moments and loads are next shown in figure 96. The neck loads and moments, while smaller for the child ATD, resembled the trends of the loads and moments obtained from the adult-sized ATDs. The maximum compression load in the neck was 74.6 lb, which occurred 0.055 s after impact. After initial neck compression, forward rotation occurred and both neck tension force and flexion moment soon followed at 0.08 s and 0.11 s, respectively. Neck shear force peaked at approximately the same time as neck tension with a force of 50 lb. After this loading period, the only significant neck measurement was a spike in neck tension measured during head strike.

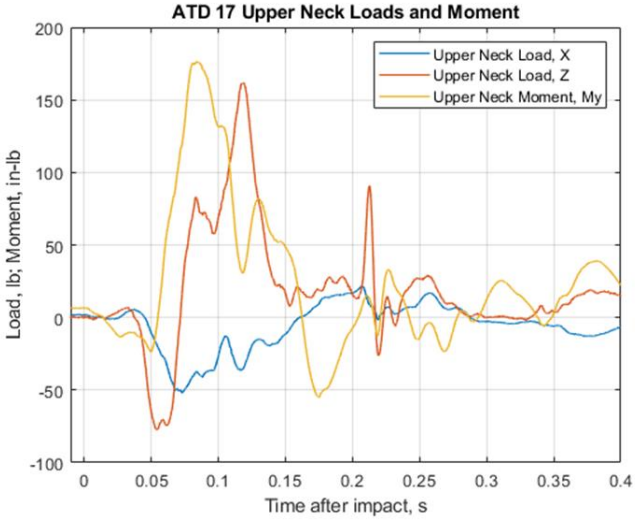

Figure 96. ATD 17 Upper neck loads and moments

Figure 97 shows the lap belt load in ATD 17. The maximum tension in the belt was 212.6 lb, which occurred 0.12 s after impact. It was during this time that the maximum tensile force was measured in the neck and the maximum vertical acceleration was measured in the head. This maximum value represented the lap belt restraining the ATD from rebounding out of the seat.

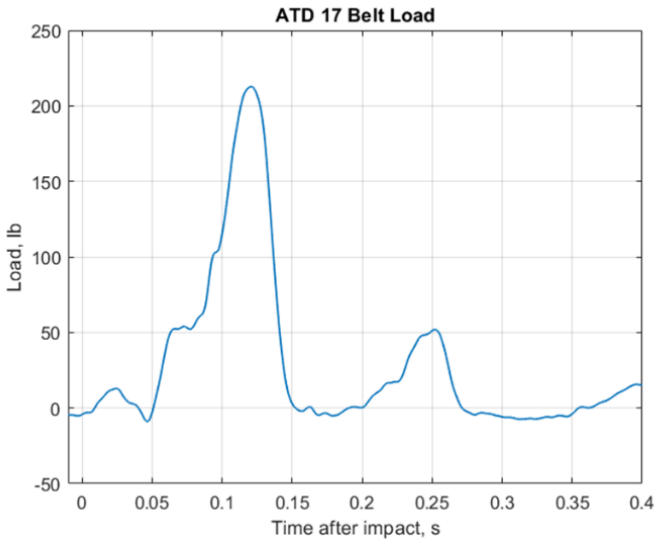

Figure 97. ATD 17 belt loads

ATD 19 – Seat 10D

The 10 YO LODC ATD was seated in Seat 10D. Along with sensors in the head and pelvis, LODC ATD had additional instrumentation that most other ATDs did not. Additional instrumentation included a lower neck load cell, pelvis rotation sensor and abdomen pressure sensors. These channels will be included in the report for completeness; however, most of these data were not analyzed in depth, and since other ATDs did not include these sensors, the data was not used in comparative analyses. The head acceleration and pelvis are first shown in figure 98. In the horizontal direction, the pelvis acceleration was in phase with the seat base acceleration, indicating tight restraint of the pelvis into the seat. The peak acceleration in the pelvis was approximately 10 g higher than that measured in the seat base. After the first initial peak, pelvis horizontal acceleration quickly reveresd direction, indicating potential slippage of the lap belt as the ATD pelvis was accelerated down into the seat. Pelvis horizontal acceleration direction begins reversing again at approximately 0.1 seconds indicating the belt began to reengage with the pelvis. This oscillation in pelvis horizontal acceleration continued throughout the first 0.25 s of impact. Head horizontal acceleration was low for the majority of impact but spiked at approximately 0.21 s to 38.0 g indicating head strike. Head and pelvis vertical accelerations were similar in shape and with the pelvis having a larger magnitude during the primary loading phase. Both peaked at 0.045 s with a maximum of 26.5 g and 34.7 g, respectively. The pelvis vertical accleration closely tracked the seatbase acceleration, with an initial peak of approximately 40 g followed by a second reduced peak of approximately 20 g.

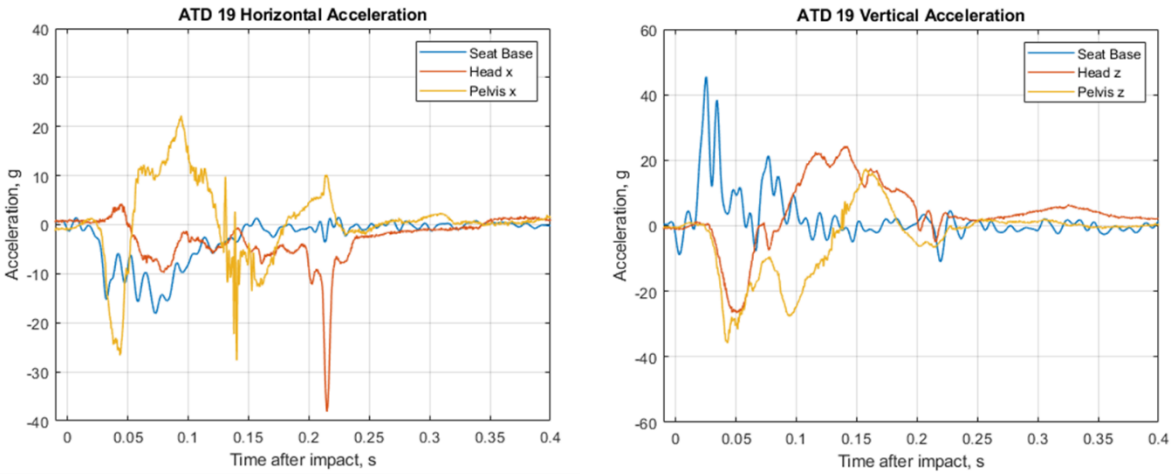

Figure 98. ATD 19 Accelerations

Upper and lower neck moment and loads are next shown in figure 99. The upper and lower neck responses were similar in shape within ATD 19, though the lower neck had a larger moment than the upper neck. This difference was expected due to the larger moment arm from the head mass reacting by the lower neck. The neck response first peaked in tension and flexion with the moment delayed from the tension force by approximately 0.02 s. The neck then rotated into compression and extension at approximately 0.15 s, and the lower neck did not measure significant extension during this time indicating the upper neck moment was primarily driven by head rotation. After this period, the lower neck rebounded into flexion, peaking at 0.21 s the time of head strike. Neck shear force was minimal throughout the impact.

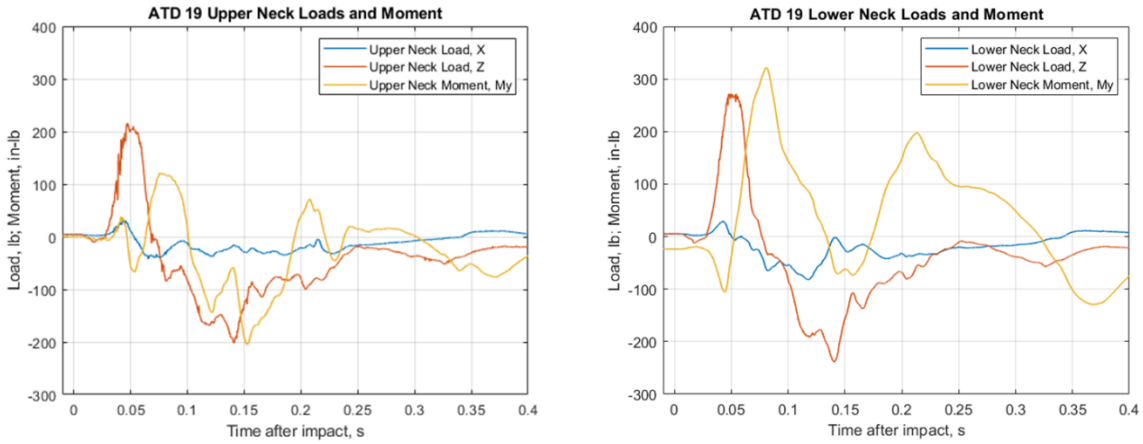

Figure 99. ATD 19 Neck loads and moments

Head and pelvis rotation rates are shown in figure 100. Rotation rates were offset between the head and pelvis with the pelvis trailing the head by approximately 0.1 s. Magnitudes were similar; however, the head exhibited two distinct peak values, the first of approximately 2,000 deg/s at 0.07 s after impact and the second 1,500 deg/s approximately 0.2 s after impact. This response matched that measured in the upper neck moment.

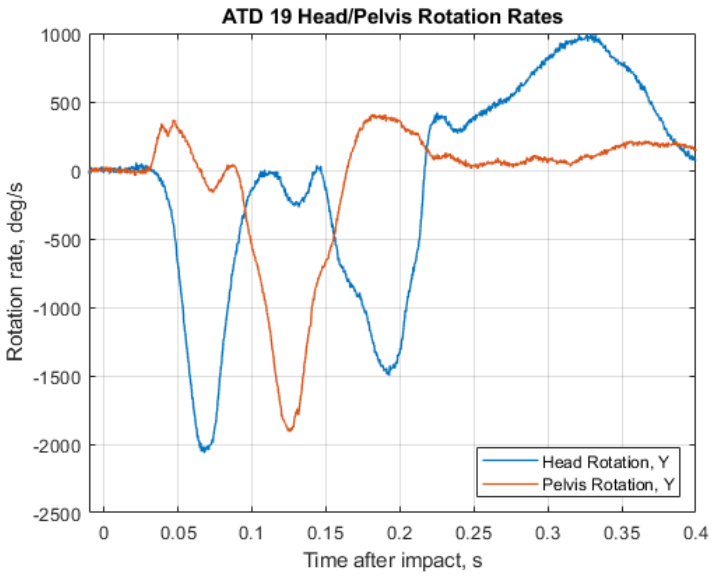

Figure 100. ATD 19 Rotations

Finally, the pressures from the abdomen are shown in figure 101. The pressure transducer on the left side of the abdomen did not record during the test so its data was not analyzed further. The sensor on the right side, however, recorded a maximum pressure of 17.9 psi approximately 0.106 s after impact. This occurred near the time of maximum forward torso rotation, which can be gathered from the time where the maximum value of pelvic rotation occurred. The measured abdomen pressures are driven by loading of the lap belt into the ATD. Belt slipping indicated in the pelvis horizontal acceleration wass verified by the hump in abdomen pressure which showed the load into the abdomen from the belt dropped off and then reengaged as the torso rotated forward. The LODC ATD did not include a lap belt load cell so lap belt force was not measured.

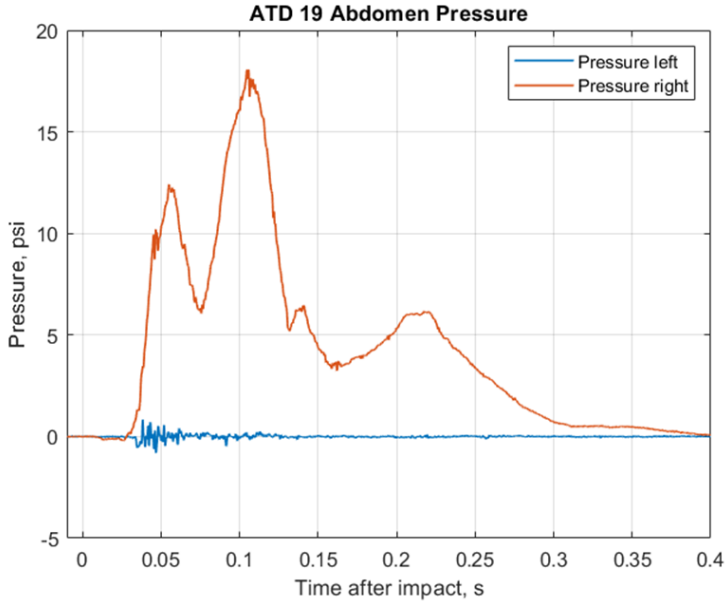

Figure 101. ATD 19 Pressures

ATD 24 – Seat 9A

ATD 24 was a Hybrid III 3 YO sized child ATD seated in a CARES device within seat 9A. This ATD was seated next to a Hybrid III 3 YO in the standard aircraft seat in 9B for comparison into the effect of the CARES device on occupant response. ATD 24 contained instrumentation in the head, chest, upper neck, and lap belt. Figure 102 shows the horizontal and vertical accelerations in the head and chest. In the vertical direction, the ATD experienced maximum horizontal acceleration in the head of 19.6 g at 0.09 s after impact. This was followed by peak chest acceleration of 25.8 g at 0.12 s after impact. Both of these peaks lagged the seat base horizontal acceleration which peaked at 0.07 s and was similar in magnitude to the head acceleration at 19.0 g. Minimal horizontal acceleration was measured within the ATD after these initial peaks until approximately 0.25 s after impact in which both head and chest acceleration measured a short 10.1 g spike likely induced by the ATD rebounding into the seat back. Head and chest vertical acceleration both exhibited an initial downward peak at 0.05 s similar to timing of the seat base acceleration. The peak measured in the ATD was magnified compared to the seat with a peak acceleration of 36.0 g in the ATD and approximately 20 g in the seat base. A significant head vertical acceleration was measured during rebound within the seat with peak upward acceleration measuring 41.5 g in the head. The chest rebound acceleration only reached 17 g indicating a large portion of the head acceleration was due to motion of the ATD neck.

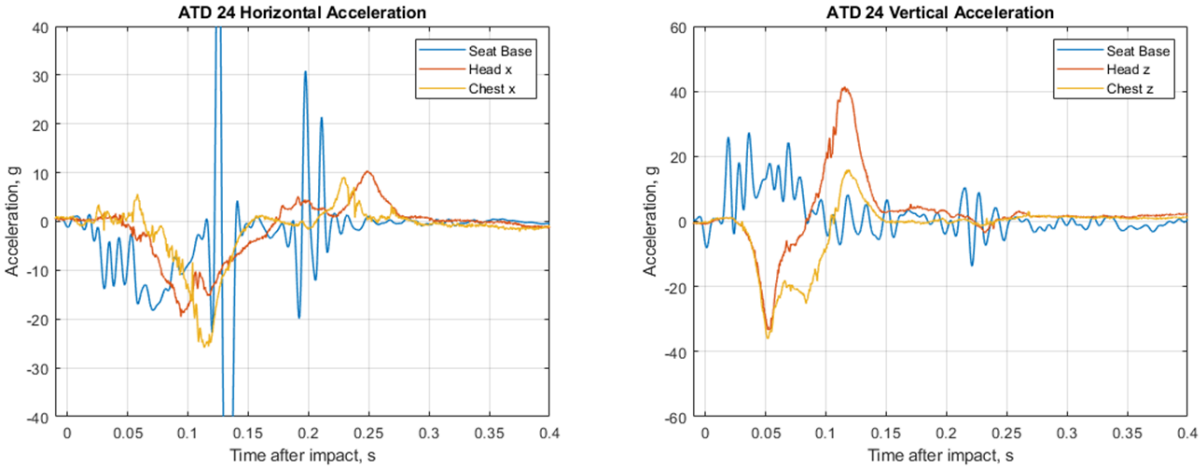

Figure 102. ATD 24 Accelerations

Upper neck forces and moments measured on ATD 24 are shown in figure 103. The upper neck vertical force tracked the shape of the head vertical acceleration response in ATD 24. Peak compressive force of 200 lb occurred at 0.05 s while peak tension force of 245 lb occurred at 0.16 s. Upper neck moment was minimal with a peak of approximately 30 in-lb in both flexion and extension throughout the impact. Shear force peaked at 90 lb at 0.1 s.

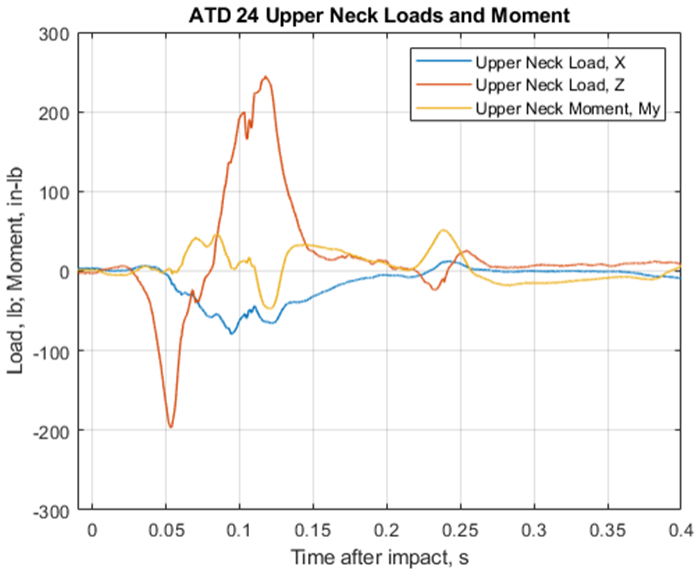

Figure 103. ATD 24 Upper neck loads and moment

Lap belt load measured on the lap restraint of ATD 24 is next shown in figure 104. Maximum lap belt load was approximately 300 lb in the lap belt restraining the ATD. The maximum belt load occurred where the ATD experienced the highest amount of positive vertical acceleration, indicating that the ATD was traveling upward out of the seat. The belt load curve exhibited a continuous rise and fall throughout the primary impact event indicating a tight contact between ATD pelvis and restraint with no belt slippage.

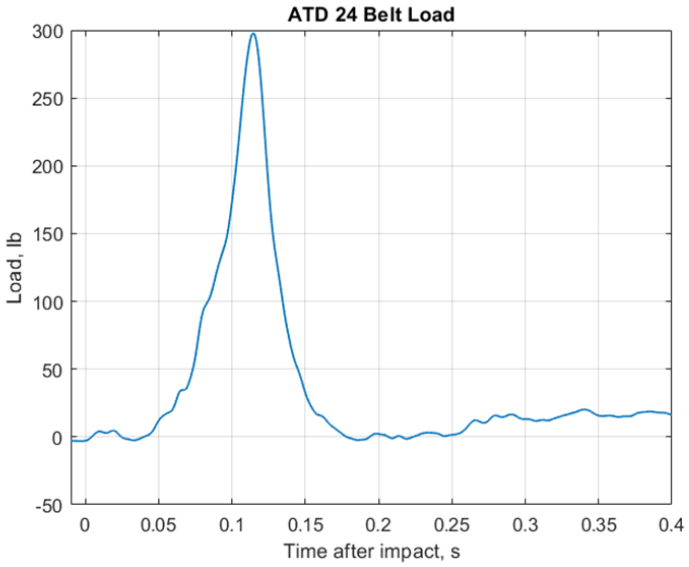

Figure 104. ATD 24 Belt load

ATD 25 – Seat 4D

ATD 25 was a CRABI 18 month old ATD seated in a rear-facing car seat within seat 4D. The car seat was attached to the aircraft seat through the lap belt. The CRABI ATD was uninstrumented, but the belt tension

within the lap belt was recorded. The belt load measured on ATD 25 is shown in figure 105. The belt load measured on ATD 25 was not smooth indicating movement between the lap restraint and the rear-facing seat the ATD was seated in. The lap belt provided a single line of restraint into the rear facing child seat, which would have allowed the seat to undergo rotation about that line during the impact event. The oscillations seen in the belt force indicate that this likely occurred with the seat bouncing against the restraint. The sensor wiring severed at approximately 0.092 s after impact, which can be observed within the unfiltered data. All data beyond this time are unusable; however, data that are shown averages to 441 lb before this point. At the time the sensor wire severed no belt slippage was indicated as the belt remained attached through the rear facing seat in its original configuration. Belt configuration at the time of data loss is shown in figure 106.

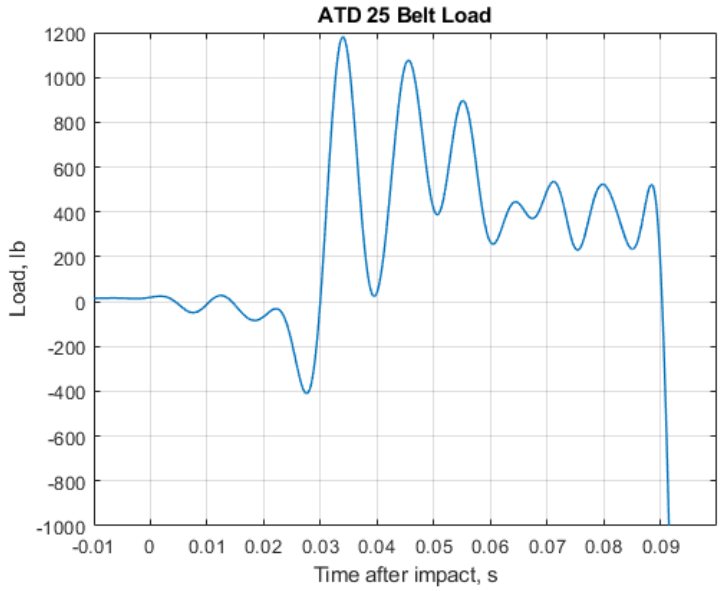

Figure 105. ATD 25 belt load

Figure 106. ATD 25 configuration at load cell loss of signal

ATD Results – Comparative Analyses

The ATDs were placed in the cabin of the aircraft in such a way that many comparisons between the ATDs can be examined. The first of these comparisons will primarily focus on injury metrics as a function of cabin location and seat position. Comparisons are then made between the various types of ATDs used, specifically examining the differences in response between some of the advanced ATDs and the Hybrid II and III ATDs. These comparisons will cover both the adult and child ATDs. An additional comparison will examine the effect of the braced position on the ATD response. The final comparisons will examine methods of securing the child ATDs via the various restraints used and differences between child ATD types. The first comparison will examine the effect of cabin location on the lumbar load response. Examination of ATD position within the aircraft post-test is also provided at the conclusion of this section.

Lumbar Load Response vs. Cabin Location

The first major ATD comparison made was to examine the lumbar load values for all of the upright Hybrid II and FAA Hybrid III ATDs, which are used for certification. This comparison examines whether the placement of the ATD in the cabin had an affect on the lumbar load value. Figure 107 shows the measured lumbar load values throughout the aircraft cabin as a function of seat row. The lumbar loads measured in the Cargo Hold section of the cabin were similar between ATD configurations and measured an average peak value of approximately 2,500 lb. Although differences were observed between Hybrid II and FAA Hybrid III ATD configuration seated in the same rows, 3 and 6, the differences were not consistent in a manner to conclude an effect of ATD configuration on lumbar load. The Wingbox section had the lowest lumbar load compared to the average lumbar load measured in the Cargo Hold and Aft Fuselage sections. Subcomponent tests of Fokker F28 fuselages sections exhibited an opposite trend with the Wingbox section having larger lumbar load values than the Cargo Hold [3]. The cause of this discrepancy was hypothesized to be due to the pitch rotation of the aircraft about the Wingbox section at impact resulting in higher vertical impact velocities at the front of the vehicle [10]. The highest lumbar load is measured in the very rear of the aircraft in Row 12. The high lumbar load measured in this region of the aircraft corresponded with significant cabin intrusion observed in this portion of the aircraft during the test. The fuselage structure

lifted 8.4 inches up through the aft cabin floor at the Row 11 and 12 locations [10]. This intrusion signified minimal energy absorption by the aft structure under the floor, resulting in larger vertical loading of the ATDs seated in Row 12.

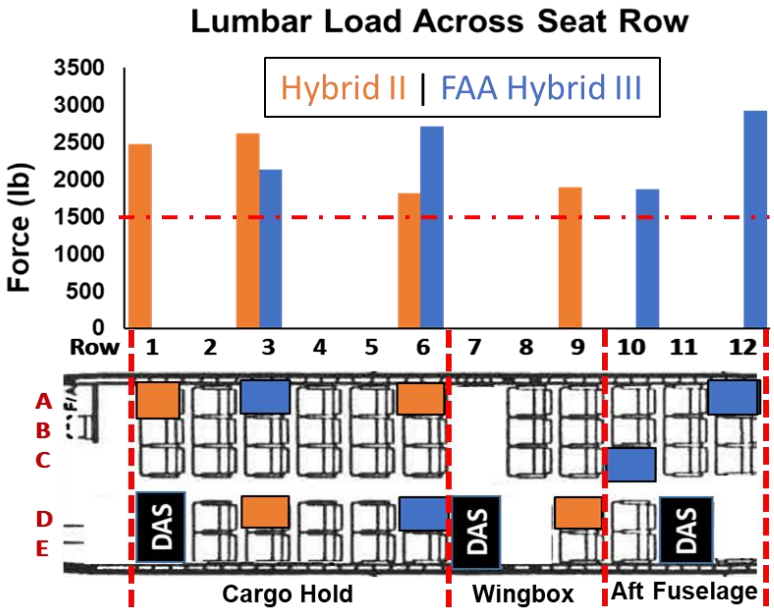

Figure 107. Lumbar load as a function of row position

Lumbar Load Response vs. Seat Location

Hybrid II and FAA Hybrid III ATDs were placed within three seat locations throughout the aircraft: A, C, and D. Figure 108 shows the compressive loads averaged over each seat location for both ATD configurations. When averaged over seat location, the FAA Hybrid III had slightly higher lumbar loads within the same seat compared the Hybrid II, though this does not factor in differences due to row location. Seat C was shown to have the lowest lumbar load value across those tested, which matched trends observed in the subsection tests of this aircraft. In both of those tests, lower lumbar load values measured in seat C were attributed to greater energy absorption by this seat due to deformation on impact [3].

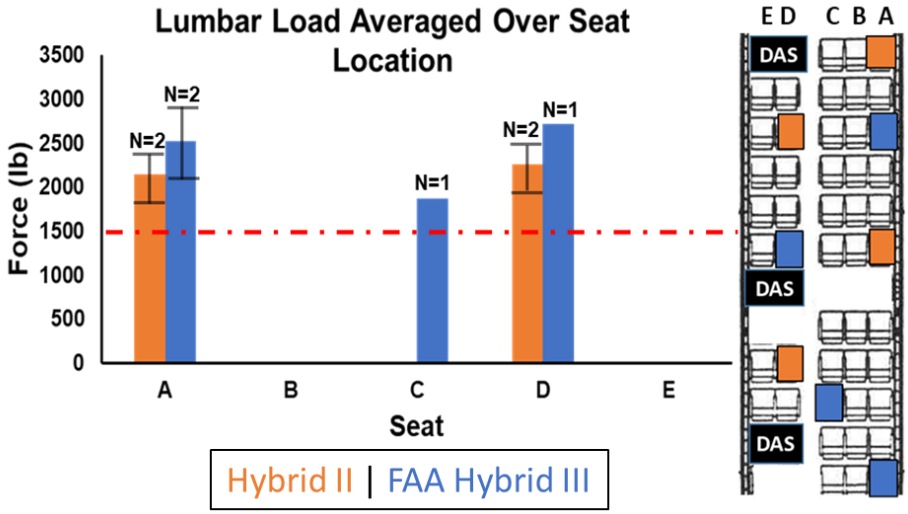

Figure 108. Lumbar load as a function of seat location

Head Injury Criteria (HIC) Response vs. Cabin Location

In addition to lumbar load values, Head Injury Criteria [22] over a 36 millisecond (ms) duration (HIC 36), was calculated for all of the certification ATDs to quantify head injury risk due to head strike. HIC 36 values calculated for each seat row are shown in figure 109. Although head strike of some sort occurred in all ATDs except ATD 8, all values were below the certification injury limit of 1,000. The Hybrid II ATDs were shown to exhibit larger HIC 36 values than the FAA Hybrid III ATDs. This result can be attributed to the Hybrid II having a stiffer, less biofidelic neck component, resulting in a more forceful contact with the forward seatback. The aft section had the lowest HIC values, with the head strike occurring later within the impact event compared to the other sections resulting in reduced head strike energy. The Wingbox Section ATD, a Hybrid II in Seat 9D, did not have a seat in front, and instead the HIC 36 value was driven by head strike with its knees.

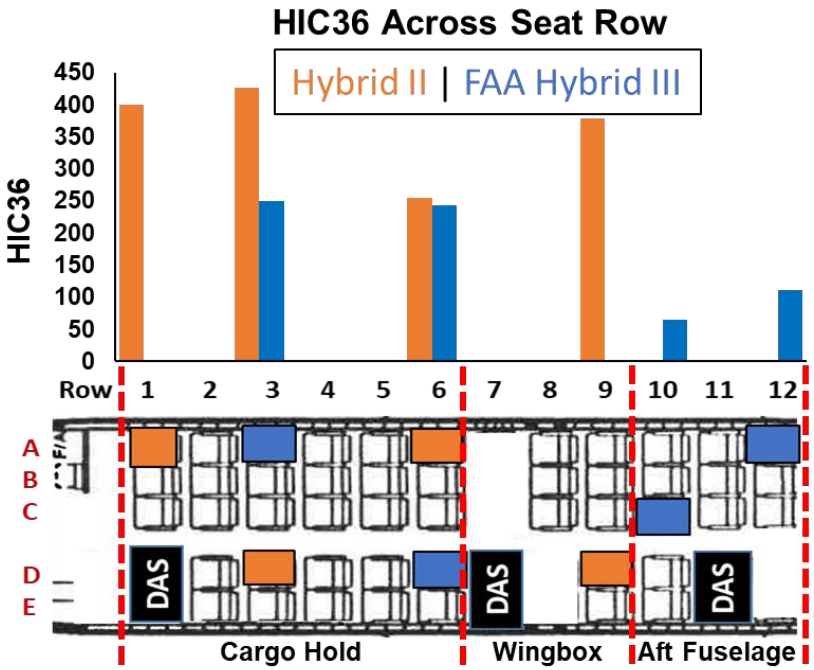

Figure 109. HIC36 as a function of row position

Lap Belt Load vs. Cabin Location

Lap belt loads for the Hybrid II and FAA Hybrid III ATDs instrumented with lap belt load cells are provided in figure 110. The largest belt load, 1,329 lb, was measured in a Hybrid II in Seat 1A. There were no clear trends observed between ATD type or position on belt load in this test. All of the belts on the these ATDs remained intact throughout the impact event, meeting certification requirements.

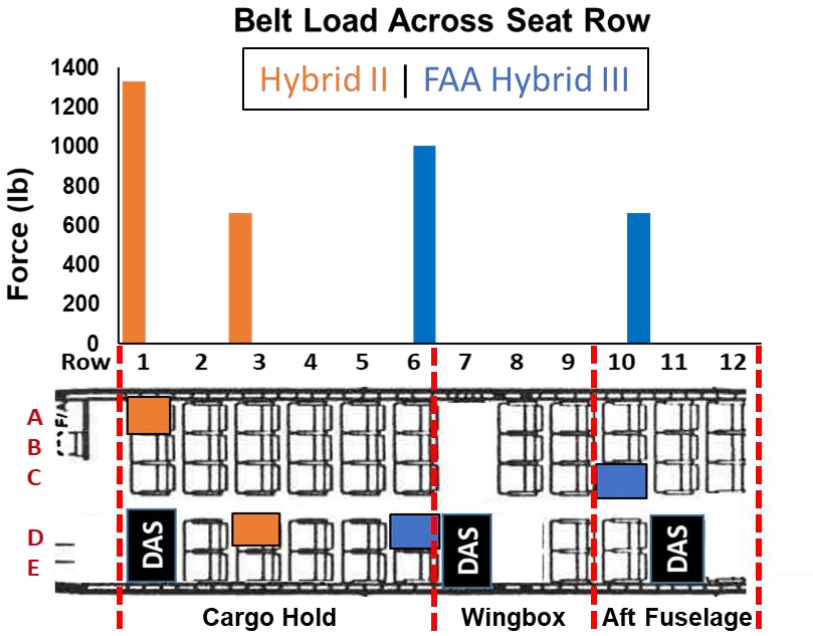

Figure 110. Belt load as a function of row position

Braced Position vs. Non-Braced Position

The effect of positioning on occupant response during the crash can be evaluated by comparing ATD 3 and ATD 20, which were an upright and braced Hybrid II ATD, respectively, seated side by side in the starboard side of Row 6. ATD 20 was placed with its torso rotated forward and head on forward seatback to approximate one of the braced positions recommended for passengers to assume in a crash event by the FAA. This braced position caused ATD 20 to experience head horizontal acceleration earlier in the crash event than the upright ATD 3, as its head quickly struck the forward seatback, which is shown in the upper left plot in figure 111. Though initial head acceleration was increased in the braced ATD 20, the upright ATD 3 experienced the larger ultimate peak acceleration of 101.1 g in vertical acceleration when head strike occurred at 0.10 s post impact. Head injury risk calculated using HIC 36 shows slightly higher risk in the braced ATD as the high head acceleration experienced by the braced ATD was much longer in duration.

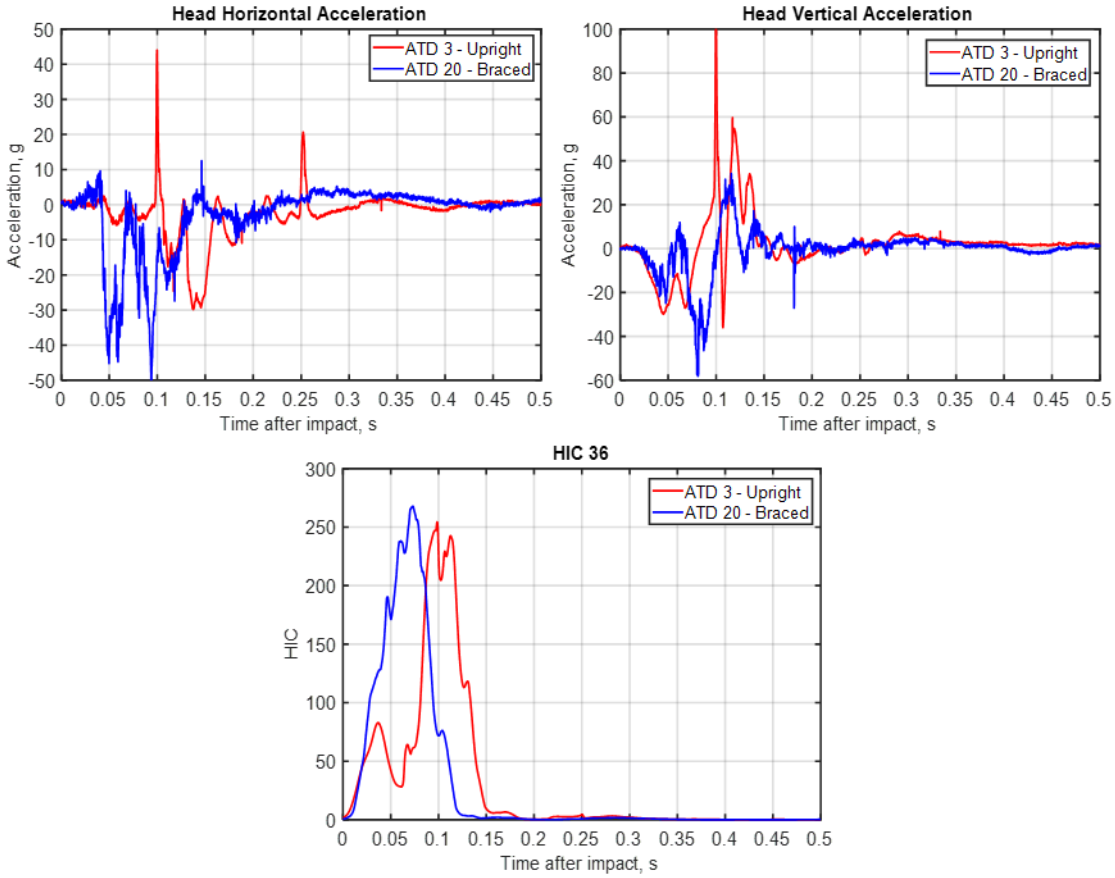

Figure 111. Head kinematic response – Upright vs. Braced position

The compressive lumbar load and lumbar moment are plotted in figure 112. The braced position was shown to reduce the compressive lumbar load compared to the upright ATD. The forward rotation of the torso reduced the transfer of body weight into compressive force under the vertical acceleration induced by the crash impact. The braced position resulted in ATD 20 being the only certification ATD to pass the 1,500 lb injury metric limit within this test. Although the braced position resulted in reduced compressive load, it traded that load for increased moment induced on the lumbar spine. In the upright ATD 3, lumbar moment began to increase as the ATD rotated forward about its lap belt, which occurred after the initial compression into the seat. As the braced ATD 20 was already rotated forward, lumbar moment was induced during the primary vertical load, resulting in a larger moment. Lumbar moment is not included in current certification

requirements, though it does represent a potential spinal injury mechanisms, and this tradeoff between compressive force and moment should not be ignored.

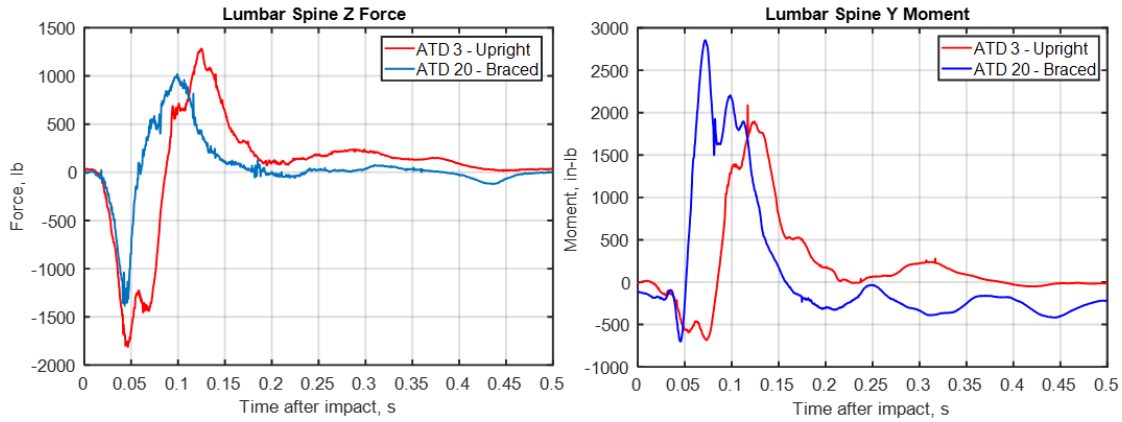

Figure 112. Lumbar response – Upright vs. Braced position

Hybrid III 5th vs. Hybrid III 95th

Row 5 on the starboard side contained a Hybrid III 5th Female (ATD 10) and a Hybrid III 95th Male (ATD 11). These ATDs are compared to understand the effect of occupant size on response within an aircraft crash event. Accelerations in the horizontal and vertical direction are shown in figure 113. In the horizontal direction, the larger 95th ATD was shown to experience much larger head acceleration than the 5th ATD. The longer torso of the 95th can be thought of as a larger moment arm around the rotation point of the lap belt, which resulted in a more forceful swing of the head into the forward seatback. In the vertical direction, after the initial compression into the seat at 0.05 s, the rebound of the 5th ATD showed higher sustained acceleration values.

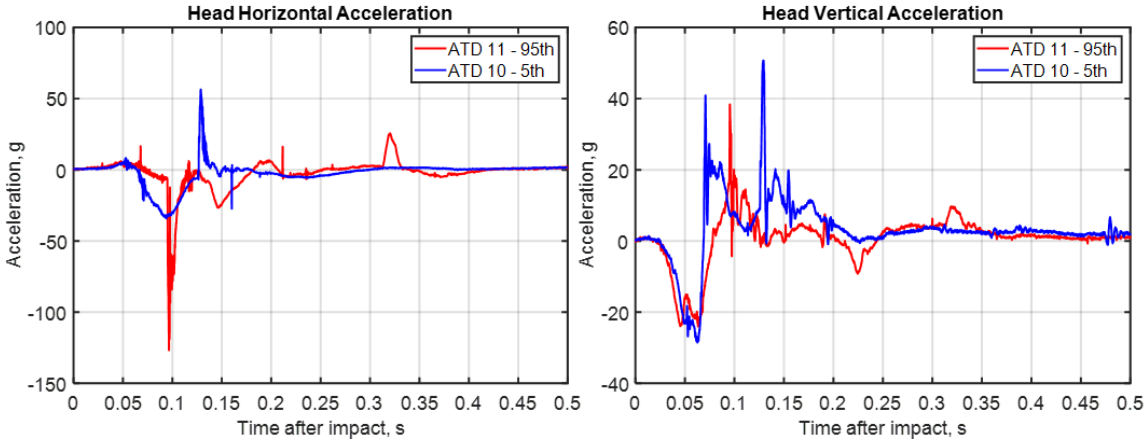

Figure 113. Head kinematic response – 95th vs. 5th

The neck forces and moments are next examined. The neck injury metric Nij is also compared between these ATD. Nij calculates injury risk to the cervical spine through summing forces and moments computed at the occipital joint location on the ATD and normalized by injury limit thresholds designated for each direction of neck motion [22]. Neck forces, moments, and computed Nij response for ATDs 10 and 11 are shown in figure 114. The upper neck compressive force and moment were similar between the two ATD sizes prior to head strike in the 95th ATD. This result is interesting because of the larger head mass of the 95th ATD which would be expected to increase both neck force and moment. In addition, the injury limit

thresholds for the 5th ATD are lower due to reduced neck muscle and bone size with the smaller anthropometry. This resulted in higher neck injury risk within the smaller representative occupant as calculated by Nij for the duration of the crash impact. Although higher neck injury risk is exhibited in the 5th ATD, it remains below the injury metric of limit of 1 defined for Nij.

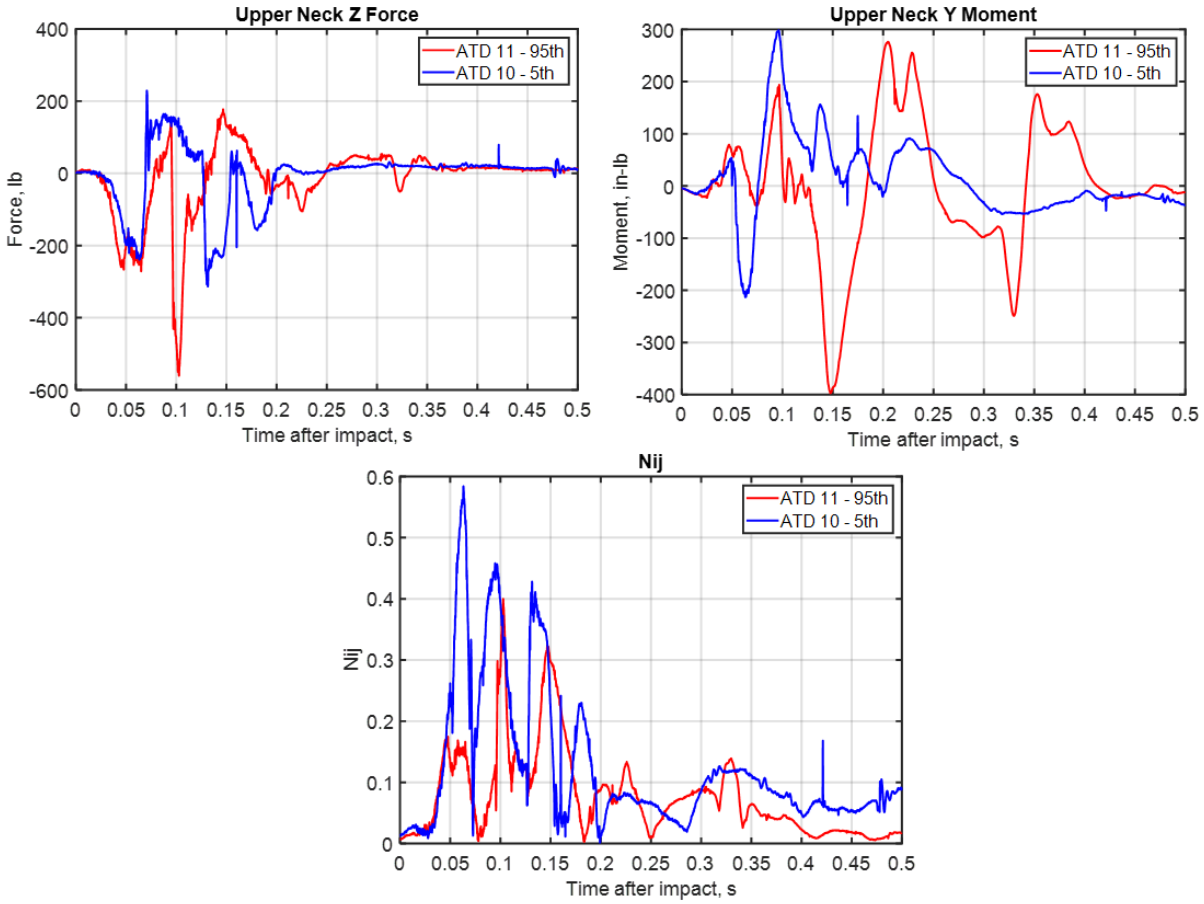

Figure 114. Upper neck response – 95th vs. 5th

Unlike head and neck response, lumbar spine output diverged significantly between the 5th and 95th ATDs. Lumbar spine force and moment for ATD 10 and 11 are shown in Figure 115. The 5th ATD had a peak compressive load of approximately 705 lb compared to 1,832 lb in the 95th ATD. Differences in torso mass over the lumbar spine are the main cause for the differences in these results. Additionally, the divergence in lumbar moment indicated that differences in torso kinematics may have also played a part in the lower lumbar moment in the 5th ATD. The early onset of lumbar flexion moment with no extension indicated the torso of the 5th began forward rotation much earlier than the 95th. This would have offloaded the compressive force applied into the spine by the torso further reducing it compared to the larger ATD.

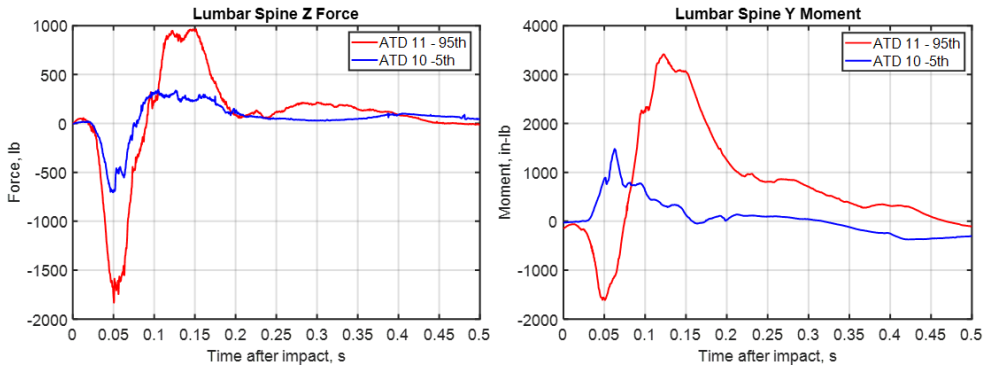

Figure 115. Lumbar response – 95th vs. 5th

THOR vs. Hybrid II

The THOR 50th (ATD 22) was compared to the Hybrid II 50th (ATD 14) which were both seated in Port Row 3. A comparison of head acceleration between the two showed head strike occurred in the Hybrid III at approximately 0.11 s while no significant head strike was indicated in the THOR over the 0.5 s post impact, as shown in figure 116. Looking beyond the difference in head strike, the THOR measured a higher horizontal acceleration than the Hybrid II but a lower vertical acceleration. During the test, the neck of the THOR underwent greater flexion around the lower neck attachment than the Hybrid II. This result is shown in the high-speed video frames provided in figure 84, where the THOR head is shown to flex downward until it contacted the torso. This flexibility in the neck drove the differences in head acceleration as the vertical impact acceleration was converted into bending moment and horizontal acceleration within the THOR head as the neck rotated forward.

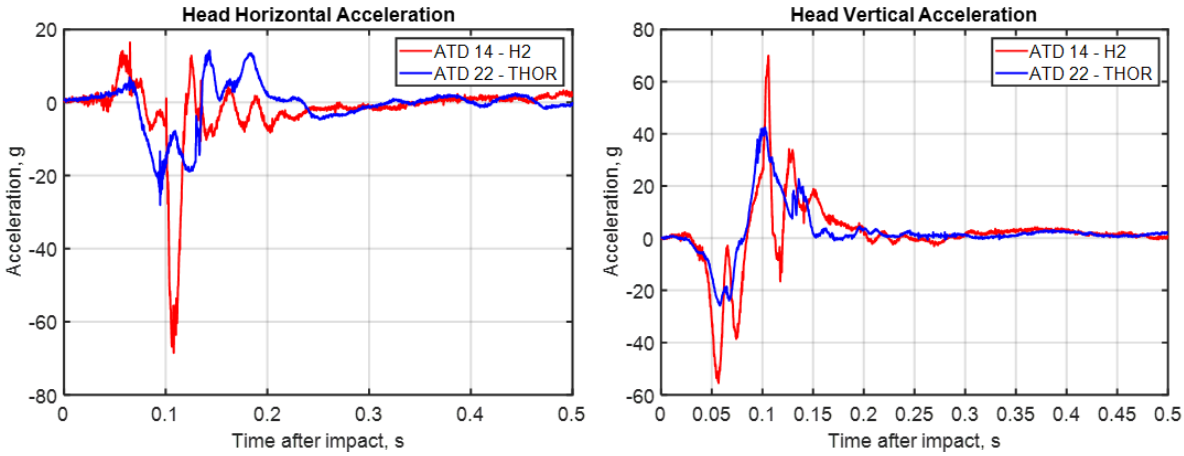

Figure 116. Head kinematic response – Hybrid II vs. THOR

Next, the chest accelerations were examined and are shown in figure 117. The THOR and Hybrid II ATDs showed similar vertical acceleration in the chest throughout the impact event. Chest horizontal acceleration was similar at the onset of impact but quickly reversed direction within THOR. The torsos of all adult Hybrid ATDs tested were shown to rotate about the lap belt like a lever arm during the crash event. This is due to the thoracic spine region of the ATD being practically rigid and attached to the pelvis through a single rubber component representative of the lumbar spine. THOR on the other hand did not rotate forward around the lap belt; rather its torso rolled downward during the impact. The THOR ATD has two rotation points within the thoracic spine region: an upper and lower thoracic flex joint. This allows more biofidelic rotation of the thoracic spine and may attribute to the difference in kinematics observed between the two

ATD configurations. The THOR ATD also has more significant foam abdomen inserts than the Hybrid ATD which may further attribute to the reduced flexion of the thorax around the pelvis belt.

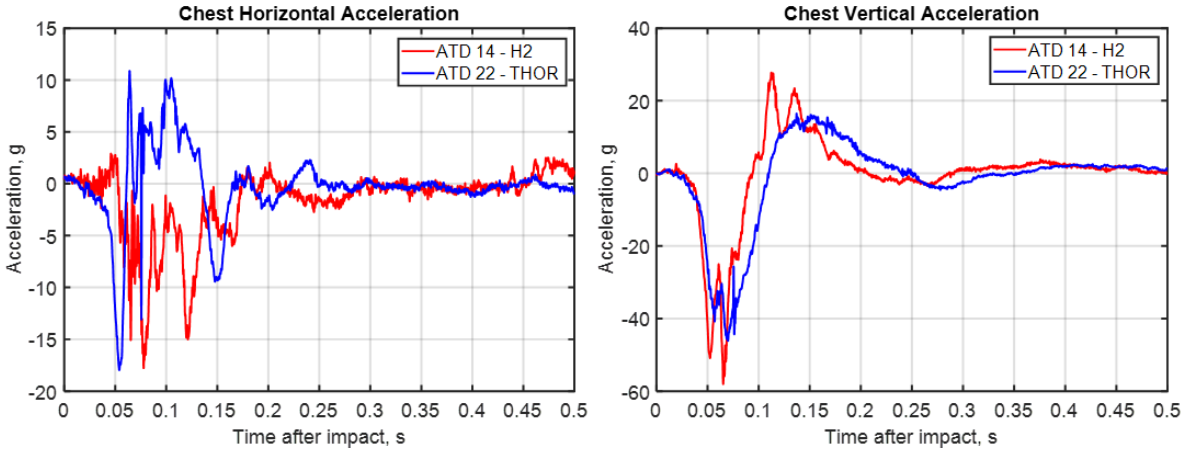

Figure 117. Chest kinematic response – Hybrid II vs. THOR

Finally, lumbar forces and moments were examined and are shown in figure 118. The Hybrid II measured a much higher lumbar spine shear force then the THOR, with peak value of approximately 936 lb in the Hybrid II compared to 289 lb in THOR, both occurring at 0.075 s. Lumbar compression force was also much higher in the Hybrid II, 2,630 lb vs. 1,552 lb, though the shape of the response was similar. THOR exhibited a higher extension moment than the Hybrid II, though THOR did not exhibit any lumbar spine flexion which was the larger moment in the Hybrid II ATD. These differences are in line with the kinematic differences observed in the torso motion of the two ATDs. The THOR did not undergo torso flexion around the pelvis/lumbar spine like the Hybrid II; rather it folded about the flex joints within its torso. This upper torso flexion was responsible for the lack of lumbar spine flexion and likely contributed to the reduction in lumbar compression as the upper torso mass shifted out of alignment with the lumbar spine. Another major difference between the two ATDs is the location of the lumbar spine load cell: in the Hybrid II, the load cell is below the flexible lumbar spine component at the L6-S1 anatomical location. The lumbar load cell within THOR is above the flexible lumbar spine component, placed at the T12-L1 location. As a result, the THOR has a flex point both below and above the load cell, while there is a rigid load path to the pelvis flesh below the load cell and a single flex point above in the Hybrid II. The difference in location as well as flexibility through the load path both likely contributed to differences in measured lumbar response between these ATDs.

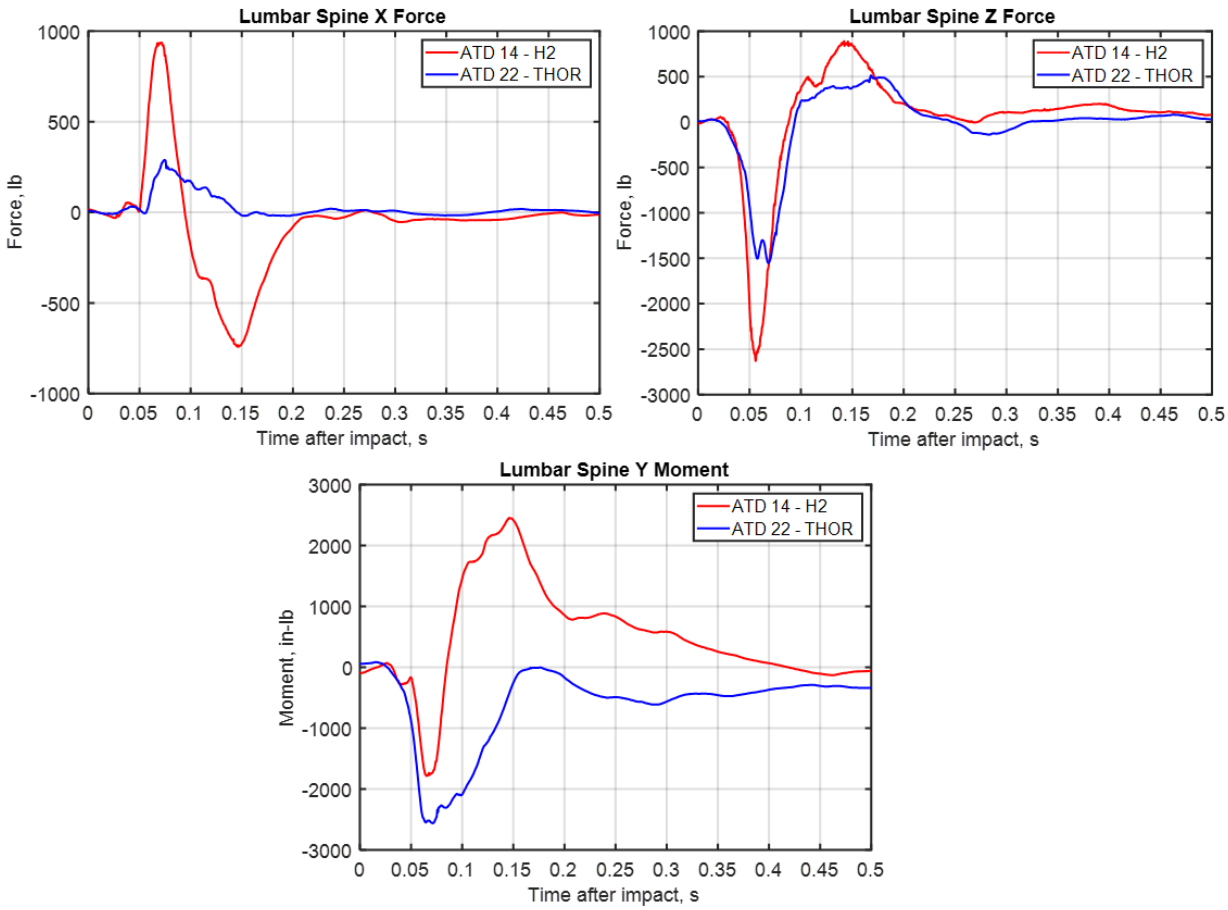

Figure 118. Lumbar response – Hybrid II vs. THOR

CARES Restraint vs. Standard Lap belt

The effect of the CARES restraint on child occupant response was quantified by comparing ATD 9 and ATD 24 seated in Seat 9B and Seat 9A, respectively, with ATD 24 in a CARES restraint. The head acceleration of each ATD and measured lap belt forces were compared as these were the only common instrumentation recorded between these two ATDs. The head horizontal acceleration comparison is shown in figure 119. The head horizontal acceleration measured in ATDs 9 and 24 was similar during the initial impact phase. Peak acceleration occurred at approximately 0.10 s in both ATDs and other than the short duration spike in ATD 9 was of similar magnitude. The onset of head horizontal acceleration did occur earlier in ATD 24, likely due to the tighter connection between ATD torso and seat with the CARES device. Divergence between these two ATD responses also occurred at approximately 0.15 s post impact when a secondary peak in head horizontal acceleration occurs in ATD 9 while acceleration in ATD 24 continued to remain low. The second head acceleration spike was a result of subsequent contacts between the ATD head with the seat back because the ATD exhibited little forward flail.

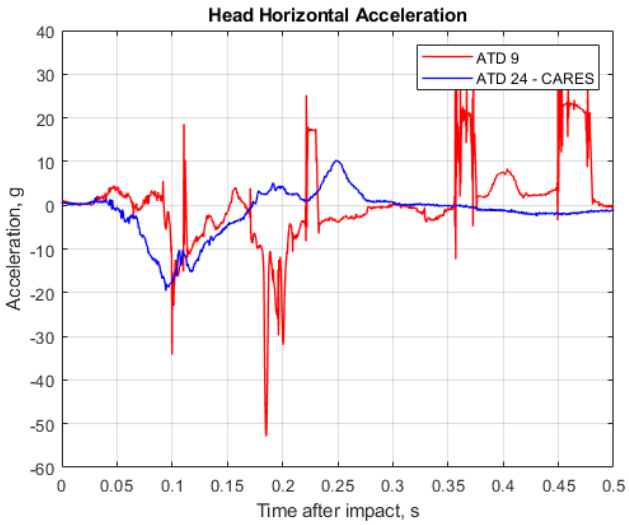

Figure 119. ATD 9 to 24 Head horizontal acceleration comparison

Head vertical acceleration is next compared in figure 120. Head vertical acceleration was similar between the standard and CARES-restrained ATDs throughout the impact. This is to be expected as the CARES restraint restricts forward torso motion and was not expected to have significant effect along the vertical direction. Though shape of response was similar between the two, peak downward vertical acceleration was higher in the standard restraint system. This may be due to slight positioning differences between the ATDs with the belt implementation. The CARES restraint had a higher peak upward vertical acceleration on rebound, this is likely due to the ATD being more upright throughout the impact within the CARES system.

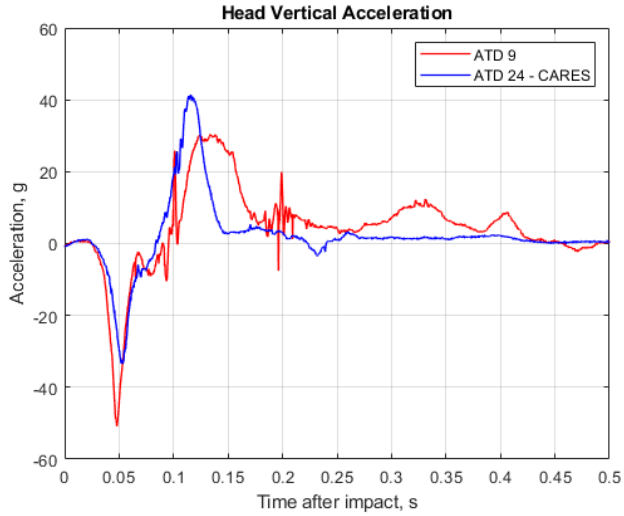

Figure 120. ATD 9 to 24 Head Vertical Acceleration Comparison

The measured belt load on the two ATDs is shown in figure 121. The lap belt on ATD 9 measured much higher belt loads than the lap belt of ATD 24 which had the CARES restraint. This result was expected as the lap belt on ATD 9 restrained the full mass of the ATD, while the torso mass of ATD 24 was restrained by the shoulder restraints of the CARES system. This would have offloaded the force in the lap belt of ATD 24 which is shown in the measured data.

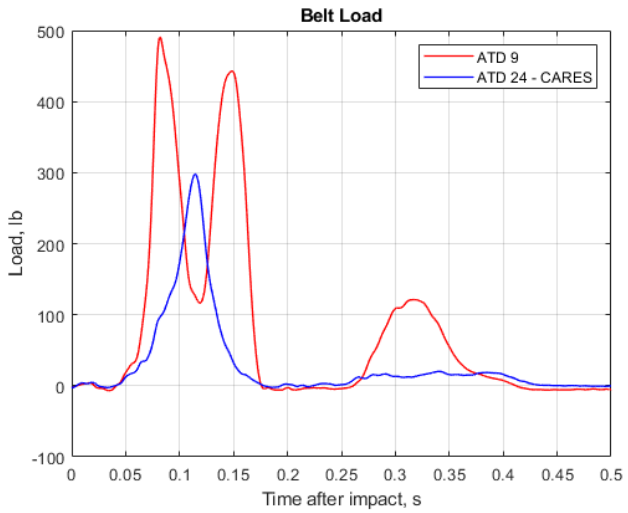

Figure 121. ATD 9 to ATD 24 Lap belt load comparisons

Hybrid III 10 YO vs. LODC 10 YO

The final ATD comparison made was between ATD 19 and ATD 15 seated in Seats 10D and 10E, respectively. ATD 19 was the LODC 10 YO, while ATD 15 was the standard Hybrid III 10 YO. The Hybrid III 10 YO is scaled from the Hybrid III 50th ATD to approximate the size of a 10 year old. The LODC, on the other hand, was developed to be anthropometrically accurate to a 10-year-old occupant, with primary differences between the Hybrid III and LODC being a flexible thoracic spine and age relevant pelvis geometry in the LODC ATD. The LODC ATD was developed to be more biofidelic than the Hybrid III for the automotive industry, and comparison of these ATDs within this crash test allows a better understanding of the effect of these differences within the aerospace loading environment.

Kinematic comparison captured in high-speed video is shown in figure 122.The kinematics between the Hybrid III and the LODC ATD show similar responses throughout the impact sequence. At time of impact, both ATDs are seated with the same approximate posture, then experience maximum sink into the seat at 0.044 s after impact. At 0.080 s after impact, the head rotation reached a maximum for both, and then both experienced forward rotation of their upper torso until a minimum point was reached at 0.136 s after impact. Rebound occurred at 0.548 s after impact, and they fell into their post-impact posture afterward. The main difference observed between the two in the high-speed video is that the Hybrid III developed a slightly higher slouch post-test.

Figure 122. ATD 19 and ATD 15 Image sequence

Head kinematic response measured in ATDs 15 and 19 is compared in figure 123. Head horizontal acceleration exhibited similarities between the Hybrid III and LODC ATDs over the first 0.05 s post-impact. After this point, the Hybrid III horizontal acceleration continued to increase while the LODC dropped off. At approximately 0.11 s, head strike with the forward seatback occurred in the Hybrid III, while head strike was not indicated in the LODC until approximately 0.2 s. This difference is similar to what was seen between the Hybrid III 50th and THOR in which the Hybrid III impacted the forward seat back much earlier within the impact event. Both the LODC and THOR had increased flexibility in the thoracic spine which reduced the forward moment arm effect around the pelvis. The downward rotation of the torso in the LODC did match that of the THOR, and thus the LODC still impacted the forward seatback with significant force though later in the impact then the Hybrid III. The vertical acceleration measured in the head of the Hybrid III and LODC were very similar throughout the impact event indicating the changes made between the two ATDs did not significantly effect loading in the vertical direction.

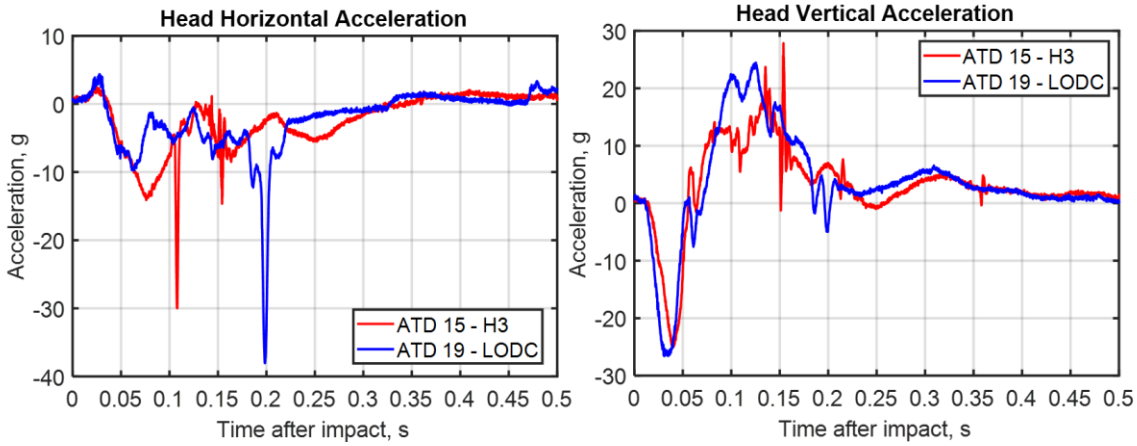

Figure 123. Head kinematic response – Hybrid III 10 YO vs. LODC 10 YO

Pelvis kinematic comparisons between the two ATDs are next shown in figure 124. Pelvis kinematic response was similar between the Hybrid III and LODC ATDs. Both horizontal accelerations began similarly; the Hybrid III peaked slightly lower at 20.2 g while the LODC peaked at 27.3 g. The shape of both responses were very similar with the acceleration droping after the initial peak, going positive, and then rebounding to a second negative peak. Pelvis vertical acceleration was closely matched in shape and magnitude between the two ATDs. Initial negative peak vertical acceleration was 36.7 and 35.6 in the Hybrid III and LODC, respectively. The rebound positive peak vertical acceleration was 17.5 and 17.3 in the Hybrid III and LODC, respectively. Although the pelvis geometry of the LODC is altered compared to the Hybrid III, this difference was not observed to have a significant effect on kinematic response within the tested impact environment.

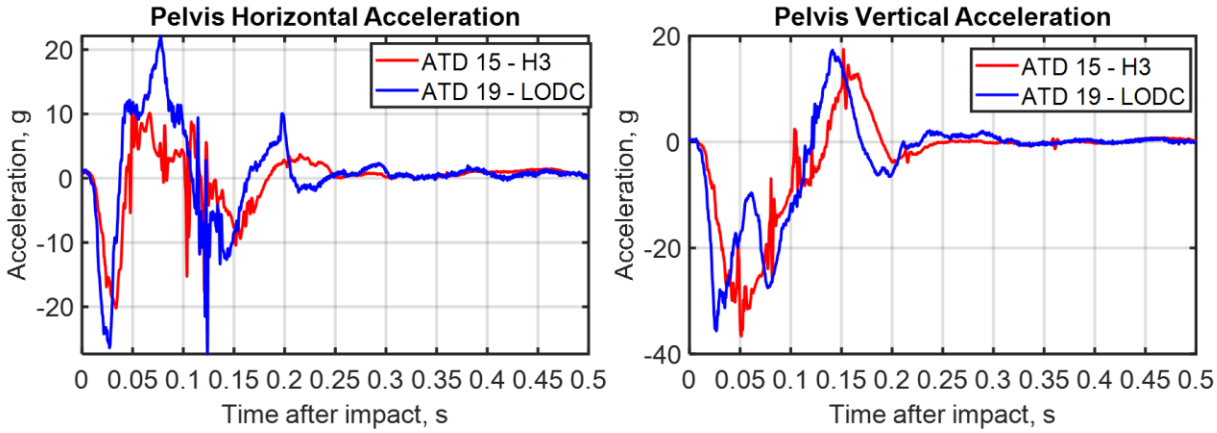

Figure 124. Pelvis kinematic response – Hybrid III 10YO vs. LODC 10 YO

Upper neck forces compared between these two ATDs are shown in figure 125. The design of the upper neck is also different between these two ATDs. The LODC has an updated neck rubber geometry as well as a twist mechanism at C2 which is designed to increase lateral rotation biofidelity of the neck. In comparing the upper neck loads measured between the LODC and Hybrid III, these differences were not shown to have a significant effect within the loading environment tested. Upper neck vertical force was similar between the two ATDs throughout the impact event, with the LODC peak compression measured to be 216 lb at 0.03 s, while Hybrid III peak compression was mesured to be 195 lb at 0.04 s. During rebound, neck tension in the LODC was approximately 100 lb higher than the Hybrid III, though the response shape was very similar. The shape of neck moment response was similar for both ATDs throughout the impact event, beginning in flexion which reached a peak value at 0.06 s in both, followed

by a larger extension moment peaking at approximately 0.15 s, and a final extension moment in which the peak occurred approximately 0.05 s later in the Hybrid III than the LODC. The changes in the LODC upper neck likely did not significantly influence differences between these ATDs within this impact environment because the loading was primarily front-back, and the changes in the LODC were made to improve lateral response.

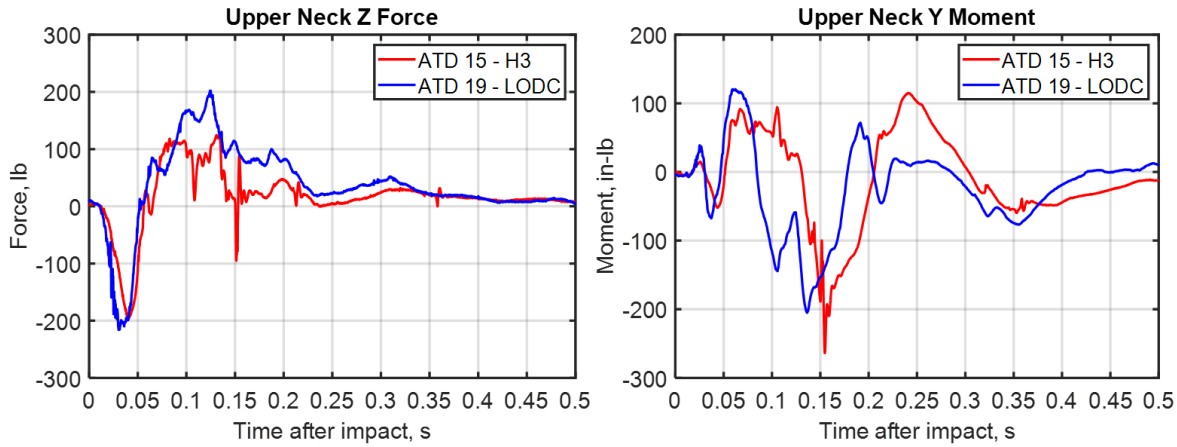

Figure 125. Upper neck response – Hybrid III 10YO vs. LODC 10 YO

Post-Test ATD Position

Post-test ATD laser scans were taken of both the exterior and interior aircraft in order to document airframe deformation and the post-test occupant state. Similar to the pre-test scans, the NTSB conducted and provided all of the laser scan measurements and data. The interior post-test scan showing the starboard-side cabin section is shown in figure 126.

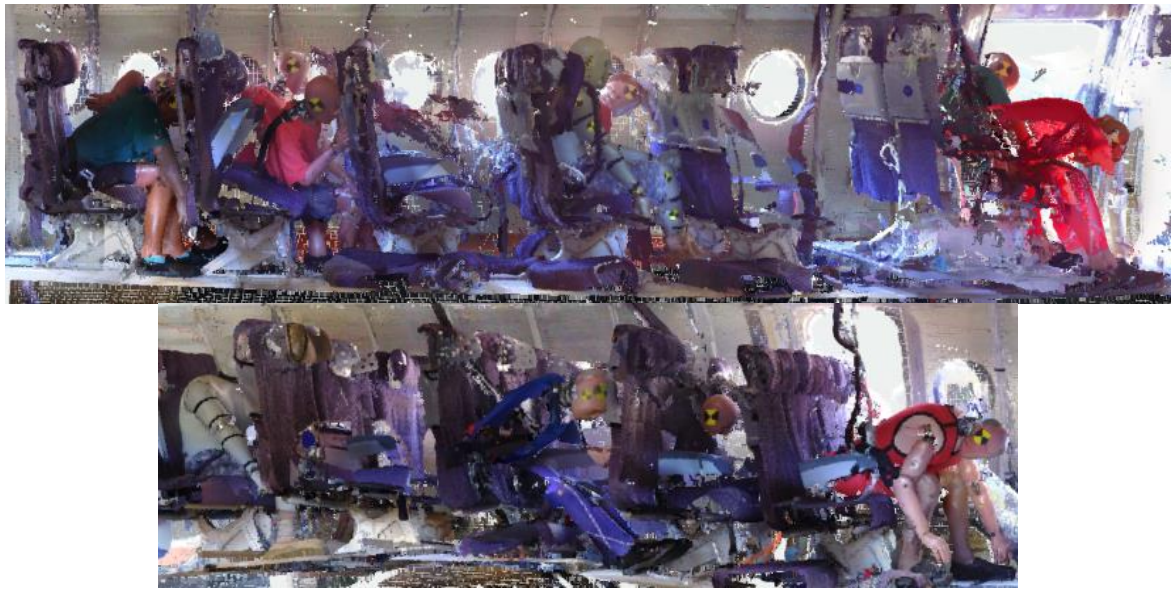

Figure 126. Post-test interior laser scan – Starboard side: Row 1–6 (Top) & 8–12 (Bottom)

As shown in the post-test scan, the majority of ATDs ended up in a forward slouched position, either resting against the forward seatback or completely folded forward in cases in which there was no forward seatback.

In the starboard side, the only ATDs that ended up in an upright posture were the two WIAMAN and the Hybrid III 95th. All seats remained intact on the starboard side of the aircraft. The interior post-test scan showing the port-side cabin section is shown in figure 127.

Figure 127. Post-test interior laser scan – Port side: Row 1–6 (Top) & 9–10 (Bottom)

The ATDs in the port side of the aircraft ended up slightly more upright than observed in the starboard-side, this difference may have been influenced by the slight yaw of the aircraft on impact. The laser scan shows the clear difference in post-test position between the Hybrid II and THOR seated in Row 3, with the Hybrid II ending in an upright posture while the THOR was folded under the forward seatback. The Seat 2E seatback in front of the Hybrid II can also be seen folded forward as the recline adjustment mechanism failed when the seatback was impacted by the ATD.

Conclusion

A full-scale crash test of an F28 MK1000 aircraft was conducted at NASA LaRC. This test was conducted in order to further understand TCA crashworthiness through the measurement of aircraft and occupant loads. Occupant loads were measured using a variety of 24 ATDs consisting of various makes, models, sizes, and types. Even though there was some data loss due to cabling and other issues, the vast amount of data collected allowed for many investigations and comparisons between the onboard ATDs.

When evaluating the kinematics of the ATDs within this test, generalized trends in response can be determined. The impact caused the ATDs initially to compress into their seats. Vertical acceleration of the ATD during this time generally matched the phase, magnitude, and shape of the seat base acceleration, though with a slight lag due to the interaction between the ATD and seat foam. Though the majority of ATDs measured similar peak vertical acceleration magnitude to the seat base, a few ATDs measured significant dynamic amplification with up to double the vertical acceleration measured in the ATD. It is difficult to attribute this to a specific ATD type or size as it was seen in both certification ATDs (FAA Hybrid III and Hybrid II) as well as the largest (THOR Obese) and smallest (Hybrid III 5th) adult ATDs

tested. Because the amplification does not follow established trends, it may be attributed to test variability such as the complex interaction between the ATD size, posture, and pelvis position to the seat foam. Each of these variables may affect the degree to which the seat foam compressed under vertical load which will lead to varied levels of amplification between the seat base and pelvis. Along the horizontal direction, larger differences were observed between seat base acceleration and pelvis response in all of the ATDs. In all ATDs there was a delay between the onset of seat horizontal acceleration and pelvis acceleration, and this result may be attributed to the distance between pelvis and lap belt restraint which were tightened using the two finger method. The variability in delay between pelvis horizontal acceleration and the seat is likely driven by the imprecise method to ensure belt tightness that results in variable gaps between the restraint and the pelvis. In certain cases, the ATD pelvis moved in the opposite direction of the seat base prior to the lap belt engaging; this may be attributed to the ATD sliding forward in the seat as it was accelerated downward. After the initial downward motion, the general motion of the ATDs was a rebound upward while beginning torso rotation about the lap belt. This motion ultimately led to all adult ATDs striking the adjacent forward seatback, if present, and in one case, the ATDs knees. In the non-forward seatback cases, higher lumbar tension and moment values were measured as the ATD torsos were able to undergo larger forward rotations. Although head strike increased head acceleration values, no indication of head injury risk due to acceleration, calculated using HIC 36, was measured. After head strike the majority of ATDs rebounded back into their own seatback as the aircraft continued through the impact event.

Occupant injury risk to the lumbar spine was assessed throughout all sections of the aircraft within this test. Each of the Hybrid II and FAA Hybrid III ATDs, defined for use in current TCA certification tests, measured compressive lumbar load values greater than the certification limit for safety of 1,500 lb. The only certification type ATD to measure a peak lumbar load value below this limit was oriented in a braced position, which would not meet the ATD position requirements defined for TCA seat certification tests. In addition, no clear relationship between occupant location within the cabin and lumbar spine injury risk was identified. These findings were somewhat contradictory to the results of the vertical-only drop tests of Fokker F28 sections previously performed [3]. Although these tests were implemented with similar vertical impact velocity, the majority of certification ATDs exhibited lumbar load values below the 1,500 lb injury limit. In addition, much lower lumbar load values were measured in the front section of the aircraft compared to the Wingbox section. Differences in occupant injury risk predicted between the full vehicle test and subsection tests may be attributed to the increased structural stiffness provided by the full vehicle as well as the horizontal velocity component only achievable within the full vehicle test. The effect of these differences should be kept in mind when considering the use of lower fidelity tests to quantify TCA crashworthiness.

The effect of occupant size on injury risk was evaluated within this crash test by comparing the responses of the 5th and 95th percentile Hybrid III ATDs. Much larger lumbar load and head acceleration values were measured in the 95th ATD. This was expected as the larger ATD torso resulted in more mass acting on the lumbar spine in compression and also caused head strike to occur earlier in the impact event then other ATDs. Although the lumbar load was higher in the 95th than the 5th percentile ATD, it wasn't higher than what was measured in the 50th percentile ATDs. This was attributed to the fact that the 95th Hybrid III has a curved lumbar spine compared to the Hybrid II and FAA Hybrid III ATDs tested. When accounting for reduced injury risk thresholds for the smaller anthropometry the results do not conclude one anthropometry being at greater risk than the other within the crash environment tested.

Differences in injury risk and occupant kinematics as predicted by ATD type were also evaluated. The legacy Hybrid II ATD was compared to the more recently developed THOR. Though the THOR is the more advanced ATD and has been developed to be more biofidelic than the Hybrid ATD, it was developed for automotive use and its potential use within aerospace applications is under evaluation. The kinematics of the ATDs within the crash event were shown to significantly diverge. Where the Hybrid ATD rotated forward like a hinge about its lap belt, the THOR folded downward about the additional flex joints contained

within its spine. This resulted in the Hybrid ATD impacting the top of the forward seat back while the THOR folded downward first and then forward, ultimately becoming stuck under the forward seat. The THOR also exhibited a different lumbar load response, with a much lower peak compressive load and almost no lumbar spine flexion moment. These results indicate a clear difference in prediction of occupant response by these ATDs. Any future inclusion of THOR within TCA certification requirements would require additional research into how these responses correspond with the human body within this environment as well as changes to current injury metrics in order to account for the change in measurements that are produced by THOR.

The responses measured within the child ATDs were similar throughout the aircraft cabin. This was true across ATD types and restraint systems implemented. Comparison between the CARES restraint system and standard lap belt showed little difference in head kinematic response, though peak acceleration magnitude was slightly higher in the standard lap belt. Lap belt forces were higher in the standard restraint, but this is to be expected as the lap belt in the standard restraint carried all of the ATD mass opposed to the CARES restraint which was also supported by shoulder belts. Minimal difference was also identified between the LODC and Hybrid III 10 YO ATDs. Though there are significant geometric and material differences in the design of these two ATDs, these differences were not shown to have a significant effect on response within the tested environment

All data presented in this report represented the culmination of a multi-year test program between NASA and the FAA in order to study the crashworthiness of TCA aircraft. With newer aircraft under design which contain novel design features such as composite materials and advanced manufacturing methods, it was important to be able to expand the knowledge base on TCA aircraft such that crashworthiness and occupant safety is improved.

The test was successful with the extensive data collected from a variety of ATD sizes, shapes, builds, and types, and will further understanding of occupant response within TCA crash conditions. In addition, the test brought together collaboration between various government organizations, commercial companies, and a host of NASA and FAA disciplines. It is expected that the successful nature of the test will serve as a guide in how to conduct large complex experiments that will ultimately expand the knowledge base of crashworthiness and improve public safety.

References

[1] Federal Register. Federal Aviation Administration, Aviation Rulemaking Advisory Committee, Transport Airplane and Engine Issues, Vol 80. 2015.

[2] Transport Aircraft Crashworthiess and Ditching Working Group. “Transport Aircraft Crashworthiness and Ditching Working Group Report to FAA” September 20, 2018, Rev B. https://www.faa.gov/regulations_policies/rulemaking/committees/documents/media/arac-tacdwg_faa_report-final_september20_2018ARAC%20w%20afa%20dissent.pdf

[3] Littell, J.D. “A Summary of Results from Two Full-Scale Fokker F28 Fuselage Section Drop Tests.” NASA TM 2018-219829. 2018.

[4] Hayduk, R.J. “Full-Scale Trasport Controlled Impact Demonstration.” Proceedings of a workshop sponsored by NASA Langley Research Center and FAA Technical Center. NASA CP-2395. 1985.

[5] Fasanella, E.L. et al. “Impact Data from a Transport Aircraft During a Controlled Impact Demonstration.” NASA-TP-2589. 1986.

[6] Barth, T.H. “Discovery Channel Plane Crash.” Proceedings from the Seventh Triennial Fire and Cabin Safety Conference. December 3, 2016.

[7] Federal Aviation Administration. “Emergency Landing Dynamic Conditions.” 14 CFR § 25.562. Amended May 17, 1988.

[8] Taylor, A. “Response from a Range of Occupants in Fokker F28 Full-Scale Crash Test.” Ninth Triennial FAA Fire and Ccabin Safety Research Conference, October 28–31, 2019. Atlantic City, NJ.

[9] Jackson, K.E. and Putnam, J.B., “Simulation of a Full-Scale Crash Test of A Fokker F28 Fellowship Aircraft.” NASA TM-2020-220435, 2020.

[10] Putnam, J.B., “Occupant Response Analysis of a Full-Scale Crash Test of a Fokker F28 Fellowship Aircraft.” NASA TM-2020-220571, 2020.

[11] Littell, J.D. “A Summary of Airframe Results from a Fokker F28 Full-Scale Crash Test.” NASA TM-2020-220572, 2020.

[12] Fokker. “Fokker Fellowship F28 Weight and Balance Manual.” Revised January 1, 1999.

[13] Pellettiere, J. and Moorcroft, D. “Anthropomorphic Test Dummy Lumbar Load Variation,” 22nd Enhanced Safety of Vehicles Conference, Washington, DC, Paper (No. 11-0157). 2011.

[14] NHTSA. “THOR – Test Device for Human Occupant Restraint.” https://www.nhtsa.gov/biomechanics-trauma/thor. Accessed December 2, 2019

[15] Littell, J.D. and Annett, M.S. “The Evaluation of a Test Device for Human Occupant Restraint (THOR) under Vertical Loading Conditions: Part 1 – Experimental Setup and Results.” Proceedings from the 69th Annual American Helicopter Society’s Forum and Technology Display. Phoeniz Az, May 21–23, 2013.

[16] Putnam, J.B. et al. “A Finite Element Model of the THOR-K Dummy for Aerospace and Aircraft Impact Simulations.” Proceedings from the 7th Triennial Fire and Cabin Safety Research Conference. December 2–5, 2013. Philadelphia PA.

[17] Humanetics. “Obese ATD.” ttps://humanetics.humaneticsgroup.com/products/anthropomorphic-test-devices/vulnerable/obese-atd. Accessed January 4, 2021.

[18] U.S. Army. “WIAMan Warrior Injury Assessment Manikin Project.” https://www.army.mil/article/111105/wiaman_warrior_injury_assessment_manikin_project. September 11, 2013.

[19] Federal Aviation Administration. “Flying with children.” https://www.faa.gov/travelers/fly_children/ Accessed January 4, 2021.

[20] Stammen, J. et al. “The Large Omnidirection Child (LODC) ATD: BIofidelity Comparison with the Hybrid III 10 Year Old.” Stapp Car Crash Journal, Vol 60. November 2016

[21] Society of Automotive Engineering. “J211-1 Instrumetation for Impact Test – Part 1 – Electroinc Instrumentation.” SAE International, 400 Commonwealth Drive, Warrendale, PA. 1995.

[22] M. Kleinberger, E. Sun, R. Eppinger, S. Kuppa, and R. Saul, "Development of Improved Injury Criteria for the Assessment of Advanced Automotive Restraint Systems," National Highway Traffic Safety Administration, Washington, DC, 1998.

[23] Bolukbasi, A. et al., "Full Spectrum Crashworthiness Criteria for Rotorcraft," U.S. Army Research, Development and Engineering Command, Ft. Eustis, VA RDECOM TR 12-D-12, 2011.

REPORT DOCUMENTATION PAGE

Form Approved
OMB No. 0704-0188

1. REPORT DATE *(DD-MM-YYYY)*	2. REPORT TYPE	3. DATES COVERED *(From - To)*
06/01/2021	TECHNICAL MEMORANDUM	

4. TITLE AND SUBTITLE
A Summary of ATD Results from a Full-Scale F28 Crash Test

5a. CONTRACT NUMBER

5b. GRANT NUMBER

5c. PROGRAM ELEMENT NUMBER

6. AUTHOR(S)
Littell, Justin D., Putnam, Jacob B.

5d. PROJECT NUMBER

5e. TASK NUMBER

5f. WORK UNIT NUMBER
664817.02.07.03.03

7. PERFORMING ORGANIZATION NAME(S) AND ADDRESS(ES)
NASA Langley Research Center
Hampton, VA 23681-2199

8. PERFORMING ORGANIZATION REPORT NUMBER

9. SPONSORING/MONITORING AGENCY NAME(S) AND ADDRESS(ES)
National Aeronautics and Space Administration
Washington, DC 20546-001

10. SPONSOR/MONITOR'S ACRONYM(S)
NASA

11. SPONSOR/MONITOR'S REPORT NUMBER(S)
NASA/TM-20210017474

12. DISTRIBUTION/AVAILABILITY STATEMENT
Unclassified - Unlimited
Subject Category
Availability: NASA STI Program (757) 864-9658

13. SUPPLEMENTARY NOTES

14. ABSTRACT

This report covers Anthropomorphic Test Device (ATD) data measured during a full-scale crash test performed on a Fokker F28 aircraft on June 20, 2019. The test was performed as part of a joint National Aeronautics and Space Administration (NASA) / Federal Aviation Administration (FAA) effort to investigate crashworthiness of transport category aircraft. A total of 24 ATDs of various sizes and configurations were included within the test. This report contains a summary of the data measured on the ATDs. In addition differences in predicted occupant injury risk, measured across the various ATD's throughout the vehicle cabin, are examined.

15. SUBJECT TERMS
airplane testing; full scale crash testing; crashworthiness; ATD; safety

16. SECURITY CLASSIFICATION OF:			17. LIMITATION OF ABSTRACT	18. NUMBER OF PAGES	19a. NAME OF RESPONSIBLE PERSON
a. REPORT	b. ABSTRACT	c. THIS PAGE			HQ - STI-infodesk@mail.nasa.gov
U	U	U	UU	106	19b. TELEPHONE NUMBER *(Include area code)* 757-864-9658